TABLE OF CONTENTS

ABSTRACT

Little effort has been made to apply the Critical State Soil Mechanics concept to the prediction of pavement response. The aim of this research is to apply soil mechanics principles, particularly the kinematic hardening concept, to the prediction of the response of lightly trafficked pavements to repeated loading. For this purpose, the finite element critical state program CRISP is used.

A comparison is made between the predictions given by the three-surface kinematic hardening (3-SKH) model and a layered elastic analysis BISAR for the resilient deformation produced by repeated loading of a thinly surfaced pavement, and the models are found to be in good agreement. The ability of the 3-SKH model to predict soil behaviour under cyclic loading, and under one-dimensional loading, unloading and reloading is also evaluated. A comparison between model predictions and experimental data obtained by other researchers shows that the 3-SKH model over-predicts the value of $K_{0,nc}$ and hence shear strain during monotonic loading. This problem is magnified when the model is applied to cyclic loading behaviour where large numbers of cycles are involved. The model also predicts an accumulation of negative shear strain with increasing number of cycles under some stress conditions. This will lead to unrealistic predictions of rutting in pavements. However, the model is suitable for obtaining resilient parameters for input to a layered elastic analysis program.

A new model, which is a modified version of the 3-SKH model, is therefore proposed by modifying the flow rule and the hardening moduli. This model can correctly predict the value of $K_{0,nc}$ and reduce the amount of shear strain predicted. The model also eliminates the problem of accumulation of negative shear strain with increasing number of cycles. The new model introduces two additional parameters, one of which can be determined by one-dimensional normal compression test, and the other by fitting a set of cyclic loading data. The new model is used to design the required thickness of granular material using the permissible resilient subgrade strain and permanent rut depth criteria during construction. It is found that the new model predicts a realistic granular layer thickness required to prevent excessive rutting, thus showing much promise for use in design of thinly surfaced pavements.

ACKNOWLEDGEMENTS

I would like to thank my supervisor, Dr. Glenn McDowell, for his excellent guidance and patient supervision throughout the last three years; without whose support and assistance this thesis would not have been possible.

I would also like to express my gratitude to the following people for their advice and help:

Professor Stephen Brown, co-supervisor, for his help in securing financial support for this research, and for his invaluable advice.

Dr. Guoping Zhang, co-supervisor, who helped with the triaxial testing.

Dr. Amir Rahim from the CRISP consortium, who provided technical support for the finite element program, CRISP.

Dr. Sarah Stallebrass from City University, who provided useful discussion of her model.

Mr. Karl Snelling from GDS Instruments Limited for his help with the triaxial equipment.

All colleagues in the Nottingham Centre for Geomechanics for their friendship, in particular Wee Loon Lim, Cuong Doan Khong and Jun Wang.

Rees Jeffreys Road Fund, Worshipful Company of Paviours, and University of Nottingham for funding this research project.

Finally, I would like to thank my parents, brother and Huei Ling Yeoh for their constant support and encouragement.

LIST OF TABLES

LIST OF FIGURES

LIST OF SYMBOLS

ϕ' – Angle of friction

μ' – Poisson's ratio

$-\lambda$ – Slope of the critical state line in v – ln p' space

$-\kappa$ – Slope of the swelling line in v – ln p' space

χ – Vector joining conjugate points on the history surface and bounding surface

$\underline{\beta}$ – Vector joining current stress on the yield surface and its corresponding conjugate point on the history surface

φ – Angle of stress path rotation

ψ – Exponent of hardening modulus

θ – Lode angle

η – Stress ratio

$-\lambda^*$ – Slope of the critical state line in ln v – ln p' space

$-\kappa^*$ – Initial slope of the swelling lines in ln v – ln p' space

ε_a – Axial strain

ε_{ap} – Permanent axial strain

ε_{qp} – Permanent triaxial shear strain

ε_o – Engineering strain

ε_p – Volumetric strain

ε_p^e – Elastic volumetric strain

ε_q^e – Elastic shear strain

ε_p^p – Plastic volumetric strain

ε_q^p – Plastic shear strain

ε_{pr} – Resilient volumetric strain

ε_{qr} – Resilient shear strain

ε_q – Shear strain

ε_r – Radial strain

σ'_v – Effective vertical stress

σ'_h – Effective horizontal stress

σ'_a – Effective axial stress

σ'_r – Effective radial stress

b_1 – Scalar measure of degree of approach of history surface to bounding surface

b_{1max} – Maximum value b_1

b_2 – Scalar measure of degree of approach of yield surface to history surface

b_{2max} – Maximum value b_2

E' – Young's modulus

e_{cs} – Voids ratio at critical state when $p' = 1$kPa

F – Scalar multiplier of the hardening modulus as a function of Lode angle

f – Yield function

F_e – The value of the multiplier in the hardening modulus in triaxial extension

g – Plastic potential function

G' – Shear modulus

G'_e – Elastic shear modulus

G_u – Undrained shear modulus

H_1, H_2 – Hardening moduli

h_o – Hardening modulus when the current stress state lies on the bounding surface

K' – Bulk modulus

k – New model parameter that controls the shape of the plastic potential

K_0 – Coefficient of lateral earth pressure at rest

$K_{0,nc}$ – K_0 during one-dimensional normal compression

$K_{0,r}$ – K_0 during one-dimensional reloading

$K_{0,u}$ – K_0 during one-dimensional unloading

K_a – Rankine active earth pressure coefficient

k_e – Value of k in triaxial extension

k_c – Value of k in triaxial compression

l – Current height of sample

L – Stress path length

l_g – Granular material thickness

l_o – Initial height of sample

M – Slope of the critical state line in $q - p'$ space

M_c – Value of M in triaxial compression

M_e – Value of M in triaxial extension

M_r – Resilient Modulus

N – Number of cycles

N – Specific volume of isotropically normal consolidated soil when $p' = 1$kPa

OCR – Overconsolidation ratio defined as the maximum previous vertical effective stress divided by the current vertical effective stress

PI – Plasticity index

p' – Mean effective pressure

p'_a – Mean effective pressure at the centre of the history surface

p'_b – Mean effective pressure at the centre of the yield surface

p'_c – Isotropic pre-consolidation pressure

p'_e – Equivalent stress

p'_m – The maximum mean effective pressure to which the soil has been loaded

p'_o – Mean effective pressure at the centre of the bounding surface

p'_p – Hardening parameter for plastic potential

q – Deviatoric stress

q_a – Deviatoric stress at the centre of the history surface

q_b – Deviatoric stress at the centre of the yield surface

S – Ratio of size of yield surface to history surface

s_{ij} – Deviatoric stress tensor

T – Ratio of size of history surface to bounding surface

u – Pore pressure

u_b – Back pressure

v – Specific volume

W_{frac} – Plastic work dissipated in fracture of particles

W_{fric} – Plastic work dissipated in friction caused by particle arrangement

1 INTRODUCTION

1.1 BACKGROUND

Most of the research and developmental work on pavements in the U.K. over recent years has focused on the needs of the motorway and trunk road systems, which constitute only a small proportion of the national highway system in the U.K. The design standards and material specifications developed by the Highways Agency for heavily-trafficked roads have, generally, also been adopted by the local authorities responsible for the lightly trafficked system. This has resulted in inappropriate and uneconomical standards for this sector, for which maintenance funds have always been restricted. Therefore, the need for the development of more appropriate evaluation, designs and material standards for lightly trafficked roads is clear and essential.

Pavement soil mechanics and traditional soil mechanics have developed as two separate disciplines. As a result, current pavement design methods are mainly based on empirical results, whereas constitutive modelling in traditional soil mechanics is based on fundamental elasticity and plasticity theory. As yet, there is no known single model in pavement engineering that can predict both the resilient (quasi-elastic) response of a pavement over one application of wheel load, and the accumulation of permanent deformation over many cycles. The aim of this project is to apply the principles of soil mechanics, in particular the kinematic hardening concept, to modelling the behaviour of lightly trafficked (or low volume) roads under repeated loading. Since lightly trafficked roads require relatively thin layers of bituminous material when compared with motorways, the granular material and soil subgrade are subjected to larger stresses, so their mechanical properties need to be taken carefully into account when predicting performance, conducting structural evaluation, and in the design of new pavements or rehabilitation of existing ones. The design concepts needed for heavily trafficked roads have not accommodated the understanding of soils that has resulted from research over the past 20 years. At present, a pavement foundation is designed according to the Design Manual for

Roads and Bridges: Volume 7 (Highways Agency, 1994) which is based on the California Bearing Ratio concept developed by the California Division of Highways in 1938 (Porter, 1938). This method helps to determine the thickness of the capping and sub-base required to protect the subgrade from excessive stress during construction that might lead to excessive rutting, and is largely based on experience from the performance of existing roads and full-scale pavement experiments performed by the Transport and Road Research Laboratory. Such empirical data can only be applied for instances where the materials used and loading conditions are similar to those used for the studies, but provide no confidence when other materials are used or under different loading conditions.

The application of fundamental soil mechanics principles to pavement design is needed and is particularly important if economies are to be introduced for lightly trafficked road design and maintenance. In the 36th Rankine Lecture to the British Geotechnical Society, Brown (1996) emphasized the need for theoretical models for pavement foundations, highlighting the complexity of pavement problems and the fact that the current practice of pavement engineering is lagging behind knowledge that has been accumulated through research.

With the advent of increasingly more powerful computer technology, pavement design procedures based on linear elastic analysis have become popular, the most common method being the Shell pavement design method (Shell International Petroleum Company, 1978). This requires the provision of a constant elastic modulus and a Poisson's ratio for each pavement layer including granular material and clay. Linear elastic analysis can be used with reasonable confidence for pavements with thick bituminous or concrete layers due to the relatively low stresses induced in the pavement foundations. However, for unsurfaced or thinly surfaced pavements where stresses are higher in the foundation layers, the non-linear and inelastic properties become crucial and elastic theory will not be able to give correct predictions for these types of pavements. Pavement failure occurs by gradual deterioration of the pavement and not by sudden collapse, as permanent deformation accumulates gradually with traffic loading, leading to progressive failure of the pavement. In an elastic analysis, no permanent deformation is predicted and hence no failure occurs. Nevertheless, most design methods are based on the assumption

that failure can occur under cyclic loading and use the vertical strain at the top of the subgrade as the design parameter. This vertical strain is calculated from a multi-layered elastic analysis, which requires the input of material stiffnesses. Hence, most of the constitutive models for pavement foundations were developed for better prediction of elastic or resilient strains. Permanent deformation models were also developed by curve-fitting a set of cyclic triaxial data and relating permanent strains to the number of cycles of load but fewer permanent deformation models were developed in the past compared to those for resilient deformation, due to the time needed to perform a test with a large number of cycles. These models are described in detail later in the dissertation. Finite element analysis has been found to be the most suitable method to analyse pavement response (Pappin, 1979), and several finite element programs have been developed especially for pavement analysis over the past few decades such as SENOL (Brown and Pappin, 1981) and FENLAP (Almeida, 1993). CRISP (CRItical State Program) (Britto & Gunn, 1987), a finite element program for modelling soil, is used in this research.

In order to predict the response of a soil, a suitable constitutive model has to be chosen. The three-surface kinematic hardening model (3-SKH) developed by Stallebrass (1990) was chosen for this research to predict the response of pavement subgrades. This model can account for the effect of recent stress history, which is important in pavements because stress history influences subgrade stiffness and therefore deformation. A series of triaxial tests were performed to determine the necessary parameters for input into the 3-SKH model in CRISP. The model was validated by performing cyclic triaxial tests on Speswhite kaolin and comparing the results with those predicted by the 3-SKH model. The model was then used to predict the behaviour of a real pavement geometry under repeated wheel loading.

The main aims of the research reported in this thesis are as follows:

(1) To evaluate the 3-SKH model in the prediction of the repeated loading behaviour of clay.
(2) To study the behaviour of pavement subgrades under repeated loading using kinematic hardening.

(3) To modify the 3-SKH model to better predict the behaviour of soil under repeated loading.
(4) To apply the new constitutive model to the prediction of resilient and permanent deformation of pavement subgrades under repeated loading using the finite element method.

1.2 RESEARCH METHODOLOGY

To achieve the objectives outlined in the previous section, the constitutive models used in the prediction of cyclic behaviour of soil were reviewed. A suitable model was then chosen and the model's ability to predict the cyclic loading behaviour of soil was investigated by comparing the model predictions with existing test data. In this way, the advantages and disadvantages of the model could be determined and necessary modifications to the model could be established in order to improve prediction. The model was then modified and the necessary model parameters were determined. Triaxial tests were then conducted to validate the prediction of the model. Finally, the model was used to make predictions of the response of a full-scale pavement under repeated loading.

1.3 STRUCTURE OF THESIS

This thesis is divided into seven chapters. A brief outline of this dissertation is given below.

Following the current introductory chapter, Chapter 2 presents a literature review, consisting of three parts: soil mechanics, pavement engineering and numerical modelling. Part one briefly describes theories of elasticity and plasticity, followed by the critical state concept. The Cam clay and Modified Cam clay models and their deficiencies are also studied. Various cyclic loading models for soil, based on fundamental plasticity theory are discussed, and the behaviour of soil under one-dimensional loading, unloading and reloading are also investigated. The one-

dimensional loading and unloading of soil are important since most soils have a one-dimensional history. Part two of the second Chapter examines the failure mechanisms in flexible pavements and the various models developed for pavement foundations, followed by a description of current UK pavement foundation design methods. The basic finite element method is described in part three followed by a brief description of the finite element program – CRISP. The preliminary study of the 'Bubble' model (Al-Tabbaa, 1987) and the 3-SKH model (Stallebrass, 1990) is presented in Chapter 3. This chapter examines the ability of these models to predict soil behaviour under cyclic loading, and under one-dimensional normal compression, unloading and reloading. A comparison is also made of the predictions made by the 3-SKH model and a layered elastic analysis program BISAR of the resilient response of a pavement.

A new non-associated three-surface kinematic hardening model is proposed and evaluated in Chapter 4. Chapter 5 consists of a description of the triaxial apparatus and test procedure used during the test programme, together with a presentation of the experimental results. The required model parameters are determined in this chapter and a parametric study to determine an optimum choice of parameters is performed. The model predictions for drained cyclic triaxial tests are then compared to the experimental results. Chapter 6 presents the analysis of a full-scale pavement problem using the new model. Two loading conditions are investigated: that due to the construction stage and that resulting from traffic once the pavement is complete and open to traffic. The new model is used to design the required thickness of granular material to prevent excessive rutting, using the permissible resilient subgrade strain and rut depth criteria during construction. The effect of the asphalt thickness and the granular layer thickness is also studied. Finally, Chapter 7 presents the conclusions of this research and gives suggestions for future work.

2 LITERATURE REVIEW

2.1 INTRODUCTION

This literature review comprises of three parts: (1) Soil Mechanics, (2) Pavement Engineering and (3) Numerical modelling. In Part one, basic elasticity and plasticity theory are briefly described followed by the concept of Critical State Soil Mechanics (CSSM). After the description of the Cam clay and the Modified Cam clay models, their shortcomings are briefly discussed. Various cyclic loading models based on the CSSM concept are reviewed, and the different existing empirical relationships between earth pressure coefficient at rest, K_0, and OCR during one-dimensional loading, unloading and reloading are briefly described since these relate to the plastic strains which occur during one-dimensional deformation, and are used later to improve an existing model. In Part two, the failure mechanisms of flexible pavements, and different models used in the prediction of resilient and permanent deformations of pavement foundations are briefly reviewed. Finally, the current UK flexible pavement design standards are presented. In Part three, basic finite element concepts are briefly described followed by a brief description of the finite element program CRISP.

2.2 SOIL MECHANICS

2.2.1 Elasticity

Soil is, unlike other materials such as metals, complex due to its multi-phase nature. Since elastic response is often easier to describe and comprehend than plastic response, the behaviour of soil is often idealised, for simplicity, as an elastic material, whether linear or non-linear. Hence, the stresses are uniquely determined by strains: that is, there is a one-to-one relationship between stress and strain.

The basic elastic model governing soil behaviour before yielding is given by Hooke's laws of elasticity. In elasticity theory, two parameters, Young's modulus E' and Poisson's ratio μ', are needed to describe the response of an isotropic homogeneous soil specimen to a general change of effective stress. The stress-strain relationships for isotropic, homogeneous, linear elastic materials are as follows:

$$\delta\varepsilon_a = \frac{1}{E'} \cdot \left(\delta\sigma'_a - 2\mu' \delta\sigma'_r \right) \tag{2.1}$$

$$\delta\varepsilon_r = \frac{1}{E'} \cdot \left[-\mu' \delta\sigma'_a + \left(1 - \mu'\right) \delta\sigma'_r \right] \tag{2.2}$$

where $\delta\varepsilon_a$ is the axial strain increment, $\delta\varepsilon_r$ is the radial strain increment, $\delta\sigma'_a$ is the effective axial stress increment and $\delta\sigma'_r$ is the effective radial stress increment. Equations (2.1) and (2.2) assume axisymmetry.

For soil, it is preferable to use the two more fundamental parameters: shear modulus G' and bulk modulus K' to describe elastic behaviour, so that the effects of changing size and changing shape can be uncoupled. The value of shear modulus is not affected by drainage conditions, as the water within the soil skeleton has zero shear stiffness, so that

$$G_u = G' \tag{2.3}$$

where G_u is undrained shear modulus and G' is effective shear modulus. The relationship between effective bulk modulus and shear modulus K' and G' and effective Young's modulus E' and Poisson's ratio μ' are as follows:

$$K' = \frac{E'}{3\left(1 - 2\mu'\right)} \tag{2.4}$$

$$G' = \frac{E'}{2\left(1 + \mu'\right)} \tag{2.5}$$

From equations 2.1 and 2.2, the elastic response can then be written using bulk modulus and shear modulus as:

$$\begin{bmatrix} \delta\varepsilon_p^e \\ \delta\varepsilon_q^e \end{bmatrix} = \begin{bmatrix} \frac{1}{K'} & 0 \\ 0 & \frac{1}{3G'} \end{bmatrix} \begin{bmatrix} \delta p' \\ \delta q \end{bmatrix} \tag{2.6}$$

where:

$$p' = \frac{(\sigma'_a + 2\sigma'_r)}{3} \tag{2.7}$$

$$q = \sigma'_a - \sigma'_r \tag{2.8}$$

$$\delta\varepsilon_p = \delta\varepsilon'_a + 2\delta\varepsilon'_r \tag{2.9}$$

$$\delta\varepsilon_q = \frac{2}{3}(\delta\varepsilon'_a - \delta\varepsilon'_r) \tag{2.10}$$

p' is the mean effective stress, q is the deviator stress, $\delta\varepsilon_p$ is the volumetric strain increment and $\delta\varepsilon_q$ is the deviator strain increment, and the superscript e denotes elastic component.

2.2.2 Plasticity

Soil rarely behaves entirely elastically, and can only be described by elasticity theory within a certain region of stress space. Beyond this region of stress space, plastic deformation occurs. Hence, an understanding of plasticity theory is essential. It is thought that soil only behaves elastically for shear strains approximately less than 10^{-5} (Clayton et al., 1995).

The plastic behaviour of an ideal elastic-plastic material is specified by a yield surface, a flow rule, and a hardening law. The yield surface separates states of stress

which cause only elastic strain from states of stress which cause both plastic and elastic strains. Strain increments are plotted on the same axes as associated stresses, and the normal to the plastic potential gives the plastic strain increment vector and the flow rule relates the direction of the plastic strain increment vector to the stress state. When the flow rule is associated the plastic strain increment vector is normal to the yield surface. If the plastic strain increment vector is not normal to the yield surface, then the flow is said to be non-associated. However, for any flow rule, a plastic potential can be drawn through a point in stress space. The plastic potential is drawn so as to be perpendicular to the plastic strain increment vector, as shown in Figure 2.1. Thus for associated flow, the yield surface and plastic potential coincide.

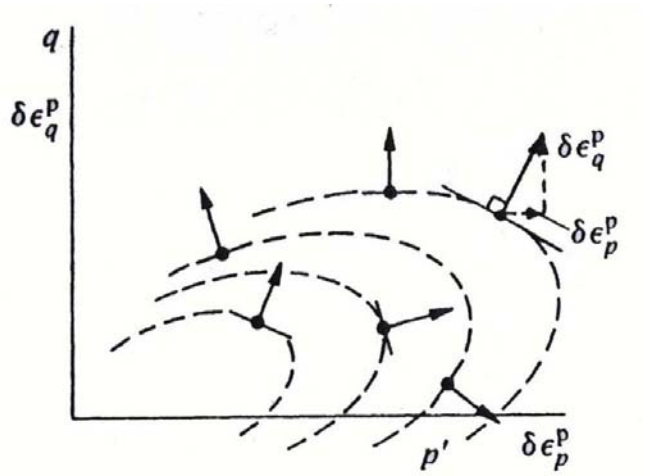

Figure 2.1. Plastic potentials and plastic increment strain vectors (Wood, 1990).

The hardening law relates the magnitude of a plastic strain increment to the magnitude of an increment of stress, as the state of stress causes plastic deformation and the material strain hardens. If the shape of the yield surface is assumed to be constant, and its size is assumed to be a function of plastic volumetric strain only (as is usually the case), then the model is said to be a 'volumetric hardening' model.

2.2.3 Critical State

The critical state concept is based on the consideration that, when a soil sample is sheared, it will eventually reach an ultimate or critical state at which plastic shearing

can continue indefinitely without changes in volume or effective stresses. This condition can be expressed by:

$$\frac{\partial p'}{\partial \varepsilon_q} = \frac{\partial q}{\partial \varepsilon_q} = \frac{\partial v}{\partial \varepsilon_q} = 0 \tag{2.11}$$

where v is the specific volume.

When the critical state is reached, critical states for a given soil form a unique line in $q - p' - v$ space referred to as the critical state line (CSL), which has the following equations in $q - p' - v$ space:

$$q = \mathrm{M}p' \tag{2.12}$$

$$v = \Gamma - \lambda \ln p' \tag{2.13}$$

where Γ, and λ are soil constants. For sands, the CSL may be curved in $v - p'$ space, so that equation 2.13 would not apply.

For isotropic stress conditions (i.e. $q = 0$), the plastic compression of a normally consolidated soil can be represented in $v - p'$ space by a unique line called the isotropic normal compression line (NCL), which can be expressed as:

$$v = \mathrm{N} - \lambda \ln p' \tag{2.14}$$

where N is the specific volume when $p' = 1$kPa or 1MPa, depending on the chosen units. If the soil is unloaded and reloaded, the path in $v - \ln p'$ is quasi-elastic (i.e. hysteretic), as shown in Figure 2.2a. However, the behaviour is often idealised as perfectly elastic, as shown in Figure 2.2b, so that the equation of a typical unload-reload line is:

$$v = v_\kappa - \kappa \ln p' \tag{2.15}$$

where v_κ and κ are soil constants. For this reason, unload-reload lines are known as 'κ-lines', as used in critical state soil models such as Cam clay. Models which do not assume perfectly elastic unload-reload behaviour are discussed later.

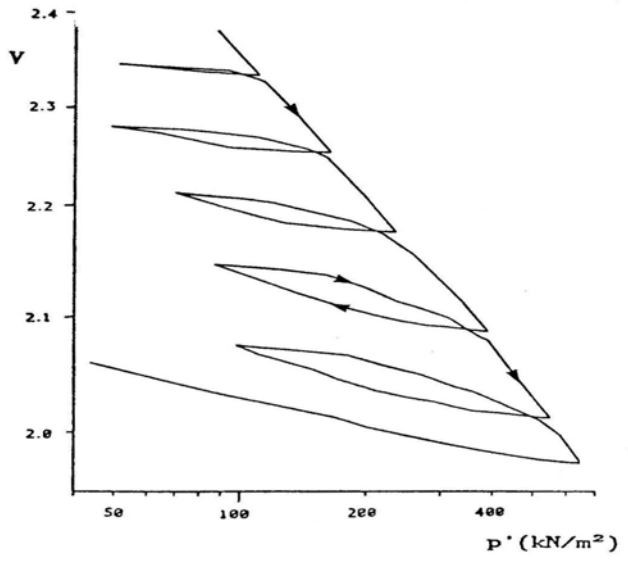

(a)

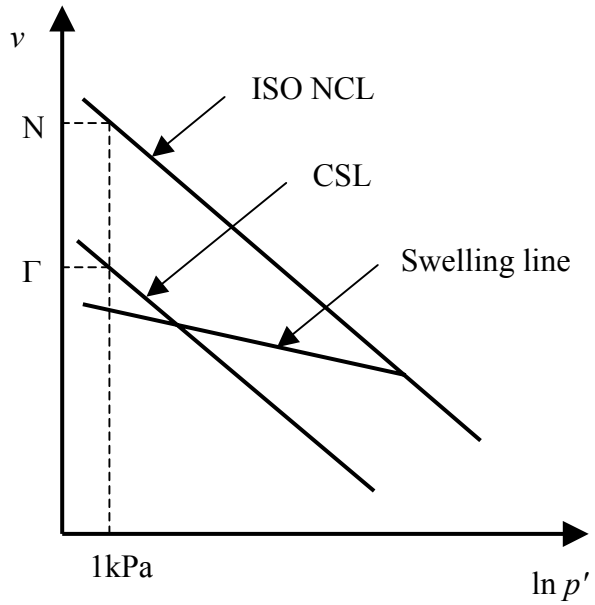

(b)

Figure 2.2. (a) True unload-reload behaviour and (b) idealised unload-reload behaviour of speswhite kaolin in v – ln p' space (Al-Tabbaa, 1987).

2.2.4 Cam clay

In this section, an elastic-plastic model, Cam clay, developed by Roscoe, Schofield and Thurairajah (1963) at the University of Cambridge is briefly described. This model is the basis for several more advanced models. In recent times, this classical critical state model has been modified in various ways by many researchers to model different soil types and loading conditions in an attempt to achieve a better understanding of soil behaviour and therefore a better prediction of soil response.

The Cam clay model is based on the concept of the critical state which says that soil, when sheared, will eventually come into a critical state at which unlimited shear strains take place without further change in effective stresses or volume.

The Cam clay yield surface is derived from the work equation as follows:

$$p'\delta\varepsilon_p^p + q\delta\varepsilon_q^p = \mathrm{M}p'\delta\varepsilon_q^p \tag{2.16}$$

Since the direction of the strain increment vector, $\delta\varepsilon_p^p/\delta\varepsilon_q^p$, is assumed to be normal to the yield locus (i.e. the yield locus and plastic potential coincide):

$$\frac{\delta\varepsilon_p^p}{\delta\varepsilon_q^p} = -\frac{\delta p'}{\delta q} \tag{2.17}$$

The corresponding plastic potential and yield surface in the $q - p'$ space are given by combining equations 2.16 and 2.17 and integrating, as:

$$\frac{q}{p'} = \eta = M \ln \frac{p'_c}{p'} \tag{2.18}$$

where p'_c is the isotropic pre-consolidation pressure, which is the value of p' when $\eta = 0$. The curve is plotted in Fig. 2.3.

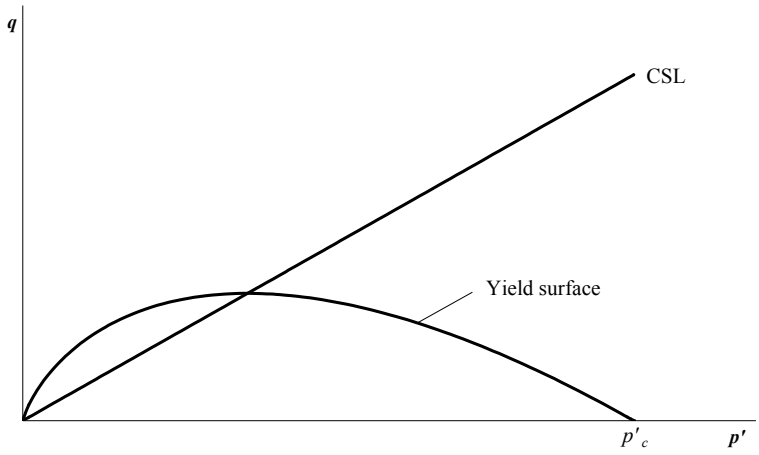

Figure 2.3. Cam clay yield surface.

In Cam clay, it is assumed that the plastic flow obeys the principle of normality or has an associated flow rule: that is, the plastic potential and the yield surface coincide. This is convenient when implementing the model in finite element calculations because the constitutive matrix, $[D^{ep}]$, is symmetric if the plastic potential, g, is equal to the yield surface, f.

The yield surface is assumed to expand at a constant shape, and the size of the yield surface is assumed to be related to changes in volume only, according to the equation:

$$\delta\varepsilon_p^p = \frac{\lambda - \kappa}{v} \frac{\delta p'_c}{p'_c} \tag{2.19}$$

This is known as volumetric hardening.

2.2.5 Modified Cam clay

Modified Cam clay was developed by Roscoe and Burland (1968) as a modification of the original Cam clay model developed by Roscoe, Schofield and Thurairajah (1963). This model successfully reproduces the major deformation characteristics of soft clay, and is more widely used for numerical predictions than the original Cam

clay model. It has been used successfully in several applications, as summarised by Wroth and Houlsby (1985).

One of the main improvements of the Modified Cam clay model from the Cam clay model is the prediction of the coefficient of earth pressure at rest, $K_{o,nc}$, for one-dimensional normal compression. For one-dimensional normal compression, original Cam clay predicts a value of zero for $\eta_{o,nc}$ so original Cam clay cannot distinguish between isotropic and one-dimensional normal compression. Furthermore, the discontinuity of the original Cam clay yield surface at $q = 0$ causes difficulties, as the associated flow rule will predict an infinite number of possible strain increment vectors for isotropic compression, and this causes difficulties in finite element formulations. Modified Cam clay model overcomes these problems by adopting an elliptical-shaped yield surface, as shown in Figure 2.4, and which has the following expression,

$$q^2 = \mathrm{M}^2 \left(p' p'_c - p'^2 \right) \tag{2.20}$$

or

$$\frac{p'}{p'_c} = \frac{\mathrm{M}^2}{\mathrm{M}^2 + \eta^2} \tag{2.21}$$

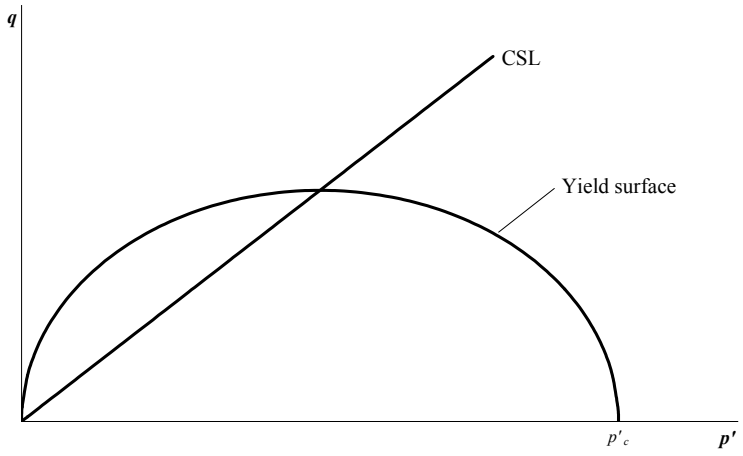

Figure 2.4 Modified Cam clay yield surface.

When the stress states are within the current yield surface, the elastic properties of Modified Cam clay are the same as those in the Cam clay model as described in section 2.2.4.

Since it is assumed that the soil obeys the normality condition, the plastic potential, *g*, is the same as the yield surface, *f*:

$$g = f = q^2 - \mathrm{M}^2\left[p'\left(p'_c - p'\right)\right] = 0 \tag{2.22}$$

where *g* and *f* are the plastic potential and yield surface functions respectively.

The flow rule for Modified Cam clay is then calculated by application of the normality condition:

$$\frac{\delta\varepsilon_p^p}{\delta\varepsilon_q^p} = \frac{\mathrm{M}^2 - \eta^2}{2\eta} \tag{2.23}$$

The yield surface is assumed to expand at a constant shape, and the size is controlled by the isotropic pre-consolidation pressure, p'_c. The hardening relationship for Modified Cam clay is:

$$\delta\varepsilon_p^p = \frac{(\lambda - \kappa)}{v}\frac{\delta p_c'}{p_c'} \tag{2.24}$$

The elastic and plastic stress-strain responses can be written in matrix form as:

$$\begin{bmatrix}\delta\varepsilon_p^e \\ \delta\varepsilon_q^e\end{bmatrix} = \begin{bmatrix}\kappa/vp' & 0 \\ 0 & 1/3G'\end{bmatrix}\begin{bmatrix}\delta p' \\ \delta q\end{bmatrix} \tag{2.25}$$

$$\begin{bmatrix}\delta\varepsilon_p^p \\ \delta\varepsilon_q^p\end{bmatrix} = \frac{(\lambda - \kappa)}{vp'\left(\mathrm{M}^2 + \eta^2\right)}\begin{bmatrix}\left(\mathrm{M}^2 - \eta^2\right) & 2\eta \\ 2\eta & 4\eta^2/\left(\mathrm{M}^2 - \eta^2\right)\end{bmatrix}\begin{bmatrix}\delta p' \\ \delta q\end{bmatrix} \tag{2.26}$$

2.2.6 Shortcomings of Cam clay and Modified Cam clay

Cam clay and Modified Cam clay are known to be able to predict the behaviour of normally and lightly overconsolidated clays reasonably well, but there are several shortcomings in the Cam clay models, which are discussed briefly in this section.

1. The Cam clay model cannot distinguish between isotropic and one-dimensional compression. For one-dimensional compression, it can be shown that, empirically (see Section 4.3.7),

$$\eta_{0,nc} \approx 0.6\mathrm{M} \tag{2.27}$$

and

$$\frac{\mathrm{d}\varepsilon_p^p}{\mathrm{d}\varepsilon_q^p} = \frac{3}{2}\frac{(\lambda-\kappa)}{\lambda} \approx 1.2 \tag{2.28}$$

if elastic shear strains are neglected, and assuming $\frac{(\lambda-\kappa)}{\lambda} \approx 0.8$, which is typical (Bolton, 1991a). However, the Cam clay stress-dilatancy equation gives:

$$\frac{\mathrm{d}\varepsilon_p^p}{\mathrm{d}\varepsilon_q^p} = \mathrm{M} - \eta \tag{2.29}$$

Thus the only way equation 2.28 can be satisfied by Cam clay for one-dimensional compression is if $\eta = 0$. This is because plasticity theory says that where there is a corner on a yield locus, the plastic strain increment vector can lie in any direction within the fan bounded by the two normals at that corner — see Figure 2.5.

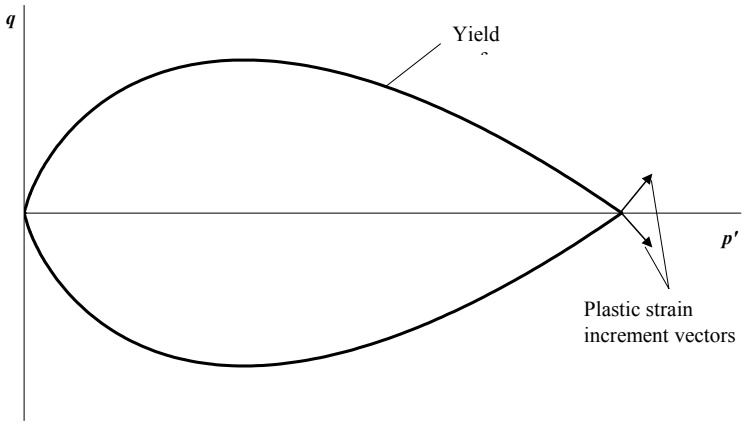

Figure 2.5. Plastic strain increment vector at the corner.

For modified Cam clay, the stress-dilatancy equation is:

$$\frac{\mathrm{d}\varepsilon_p^p}{\mathrm{d}\varepsilon_q^p} = \frac{\mathrm{M}^2 - \eta^2}{2\eta} \tag{2.30}$$

From equation 2.30 with $\mathrm{d}\varepsilon_p^p/\mathrm{d}\varepsilon_q^p = 1.2$, $\eta_{0,nc} \approx 0.4$ assuming $\mathrm{M} \approx 1$, which is better than the result predicted by Cam clay. But the predicted $\eta_{0,nc}$ is still too low, which implies that at most stress ratios, the predicted plastic shear strain is too high.

2. The Cam clay model was developed based on the assumption that soils are isotropic. It is well known that natural soils are anisotropic due to the mode of deposition. Many soils have been deposited over areas of large lateral extent, and the deformations they have experienced during and after deposition have been essentially one-dimensional.

The deviation of the predictions from experimental measurements on natural clays is due to the position rather than the shape of the yield loci (Wroth and Houlsby, 1985). Wroth and Houlsby (1985) summarised the tests carried out by Graham et al. (1983) on specimens of undisturbed Winnipeg clay. Yield points of the specimen were identified and plotted in Figure 2.6.

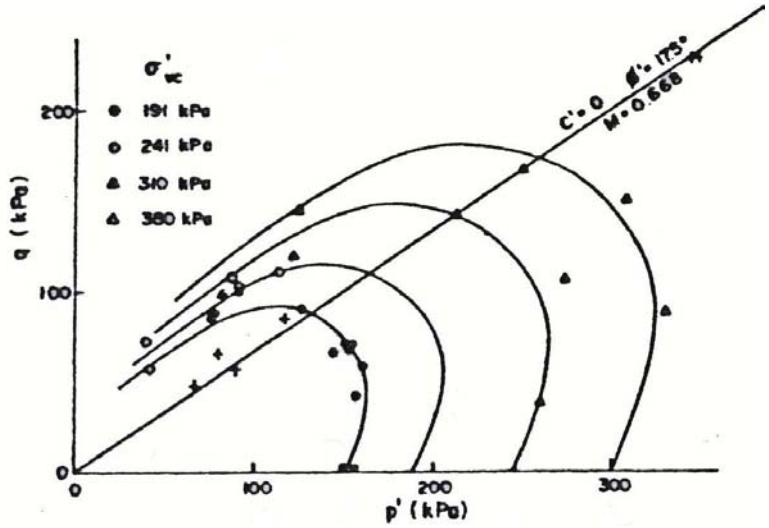

Figure 2.6. Yield surface observed in triaxial tests on undisturbed Winnipeg clay (Graham et al., 1983).

Figure 2.6 clearly indicates that its shape is approximately elliptical, but instead of being symmetrical about the p'-axis, the major axis of the yield locus seems to coincide approximately with the K_0-line. This is why Cam clay models were often validated using reconstituted isotropic clays. These models are attractive because of their simplicity, where only two independent parameters, bulk and shear modulus, are required to describe the elastic behaviour. On the other hand, 21 elastic constants are required to completely describe the anisotropic elastic behaviour. However, for a soil which is cross-anisotropic (i.e. has the same properties in horizontal directions but different properties in the vertical direction) only five parameters are required to describe its behaviour. Kinematic hardening models are capable of predicting much of the anisotropic behaviour of soil using an isotropic state boundary surface.

3. Cam clay and Modified Cam clay overestimate the failure stresses on the 'dry side' of critical i.e. states to the left of the CSL in $q - p'$ and $v - p'$. These models predict a peak strength in undrained, heavily overconsolidated clay which is not usually observed in experiments. This is due to the yield surfaces adopted in these models. Figure 2.7 shows the prediction by Modified Cam clay of the stress-strain response for an undrained test on heavily overconsolidated clay, together with an experimental result (Bishop and Henkel, 1957).

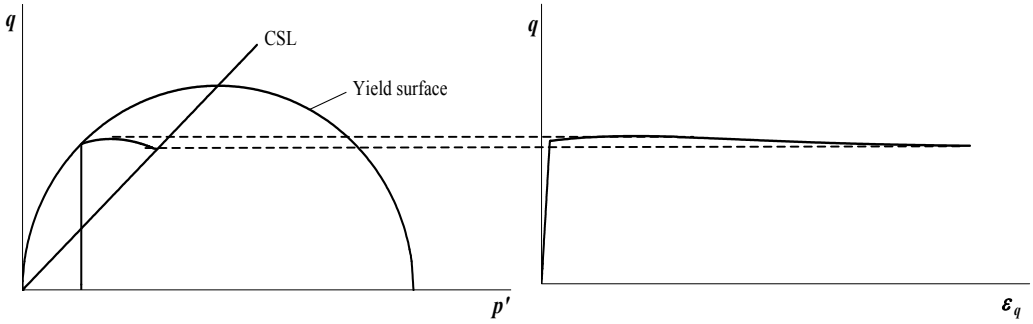

(a) *(b)*

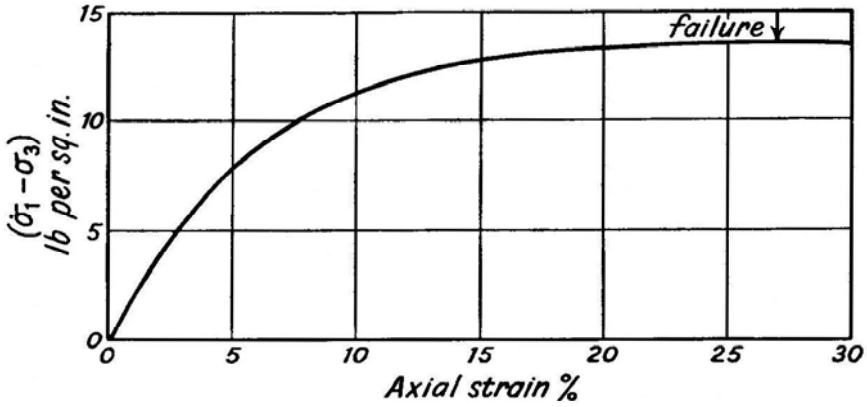

(c)

Figure 2.7. (a) Undrained stress path for heavily overconsolidated soil predicted by Modified Cam clay, (b) predicted stress – strain response, and (c) experimental result (Bishop and Henkel, 1957).

This deficiency can be overcome by using the Hvorslev surface in this region. Figure 2.8 shows the Hvorslev surface plotted in q/p'_e : p'/p'_e space where p'_e is the equivalent stress on the normal consolidation line associated with each value of specific volume. However, this will cause significant numerical difficulties due to the fact that there are two separate yield surfaces. Alternatively, kinematic hardening models can automatically generate a Hvorslev-type surface for peak strengths – see Al-Tabbaa (1987).

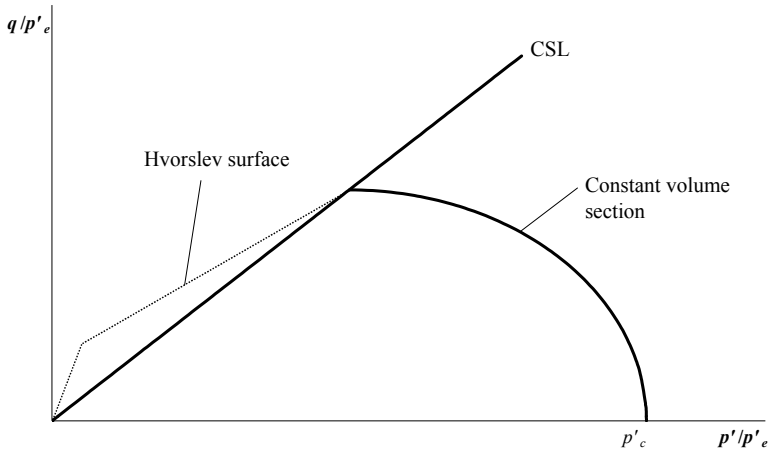

Figure 2.8. The Hvorslev surface.

4. Another main problem with modified Cam clay is its poor prediction of shear strains within the yield surface (Wroth and Houlsby, 1985), which is caused by non-linear behaviour or by using elastic model. Figure 2.9 shows the variation of Young's modulus with strain. It is thought that soil only behaves elastically for $\varepsilon < \varepsilon_o \approx 10^{-5}$ (Clayton et al., 1995).

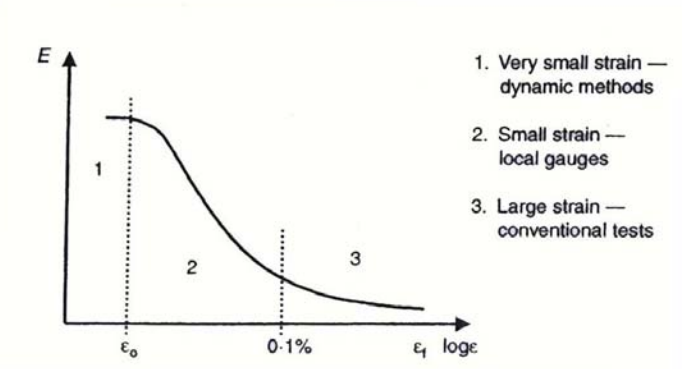

Figure 2.9. Secant Young's modulus against strain (Atkinson, 2000).

Yielding of soil is usually a much more gradual process compared with that of metal. Hence, the change of stiffness is much more gradual than that for annealed copper for example, and the stress-strain response on unloading and reloading is hysteretic. This implies that there is no one-to-one stress-strain relationship in the supposedly elastic region.

Various approaches have been suggested to account for the non-linearity and the gradual change in stiffness within the yield surface. These include the bounding

surface plasticity models in which the stiffness is dependent on the distance between the yield surface and the current effective stress state (Dafalias and Herrmann, 1982), and the inclusion of smaller inner or true kinematic yield surfaces inside the state boundary surface, to produce what are known as kinematic hardening models (e.g. Al-Tabbaa, 1987).

5. Cam clay and Modified Cam clay models cannot successfully model the behaviour of sand. The main problems lie in the fact that sand does not obey normality well, and experimental data shows that the critical state point does not lie at the top of the yield locus but lies to the left of the apex. This implies that undrained tests on normally consolidated sands can exhibit a peak value of q before the critical state is approached — see Figure 2.10, which cannot be predicted by these models.

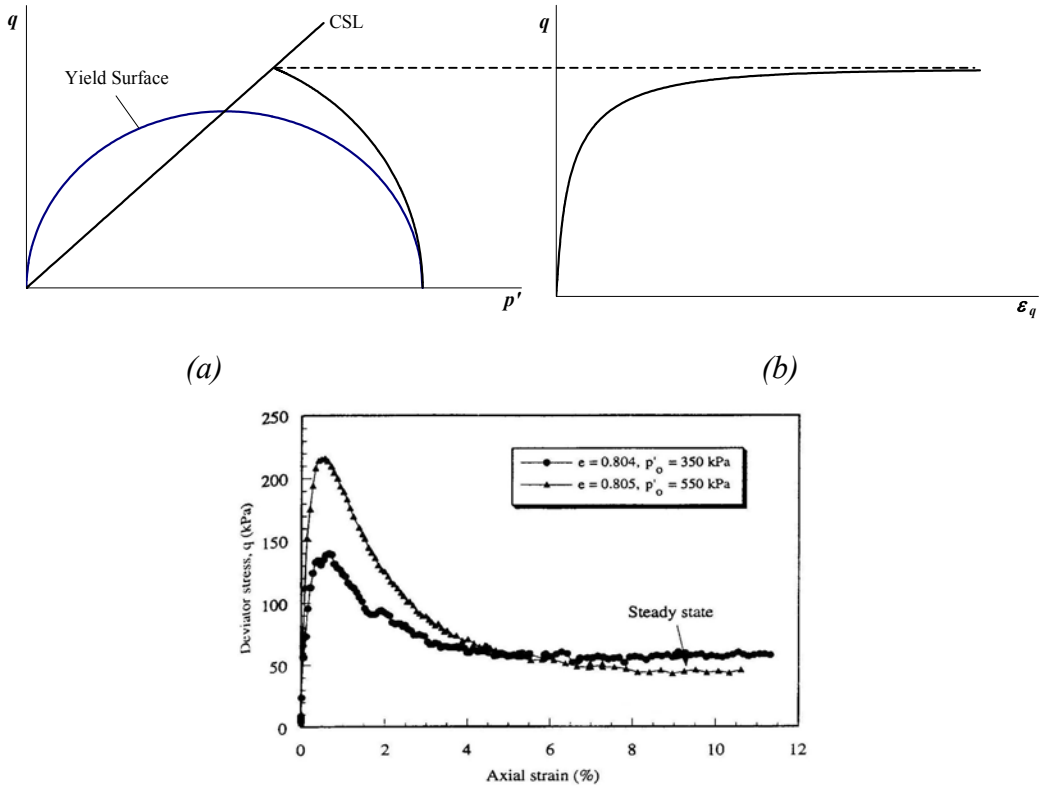

Figure 2.10. (a) Modified Cam clay undrained stress path, (b) Modified Cam clay predicted stress-strain response and (c) experimental undrained test results for very loose sand (Sasitharan, 1994).

6. The modelling of soils under cyclic loading is another deficiency in these elasto-plastic models. The essential features of the Cam clay model are that, on primary loading, large plastic strains occur, but on subsequent unload-reload cycles within the yield surface, only purely elastic strains are produced. This is not suitable for modelling the behaviour of soil under cyclic loading as, in reality, unload-reload cycles result in the gradual accumulation of permanent strain and/or pore pressure, and hysteretic behaviour occurs. The response of soil to undrained cyclic loading, according to the Cam clay model, is shown in Figure 2.11 (Wood, 1990), whereas the typical response of soil observed in cyclic loading is shown in Figure 2.12 (Wood, 1990).

Various models, such as the Bounding Surface model developed by Dafalias and Herrmann (1982) and the 'Bubble' model by Al-Tabbaa (1987), can produce some of the essential features of soil under cyclic loading.

7. Cam clay and Modified Cam clay do not take into account the effect of time on soil deformation i.e. soil deforms at constant effective stress (known as creep).

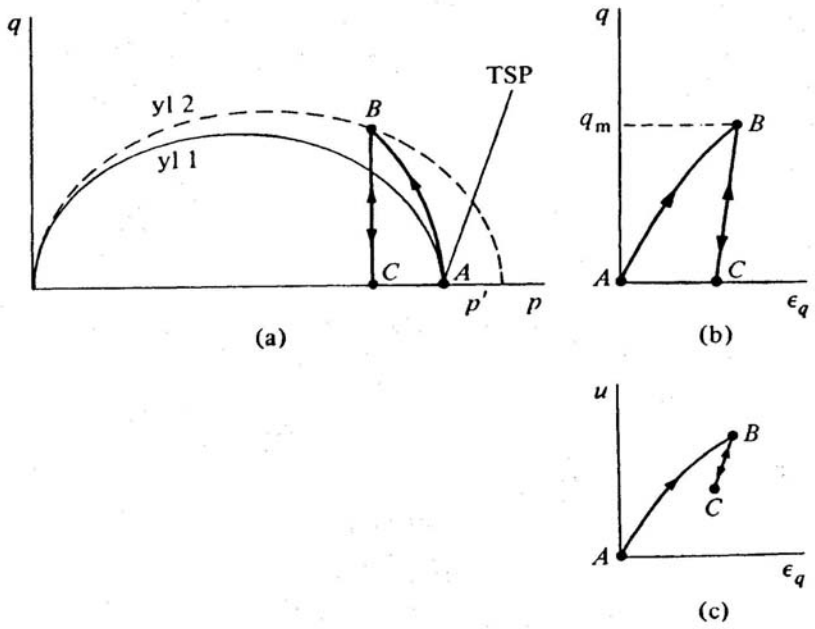

Figure 2.11. Modified Cam clay predictions of undrained cyclic loading: (a) effective stress path, (b) stress-strain response and (c) pore pressure-strain response (Wood, 1990).

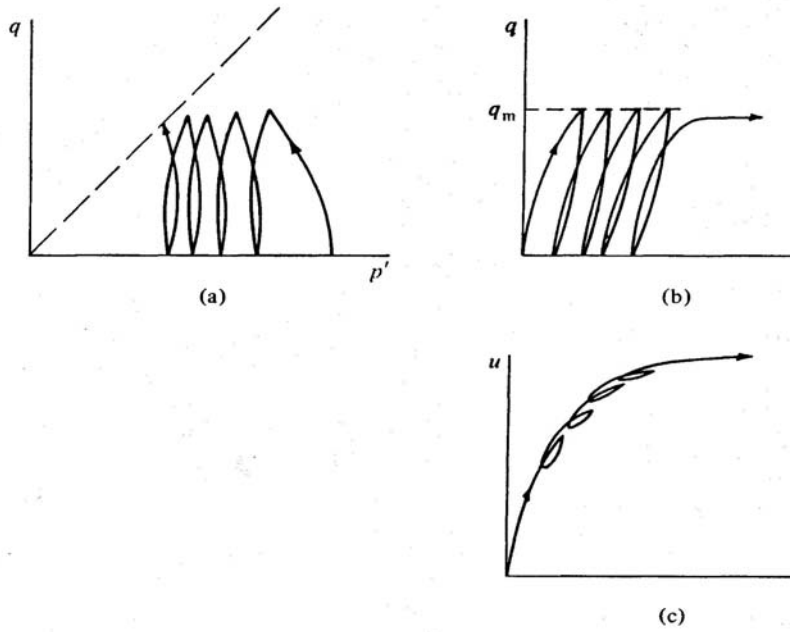

Figure 2.12. Typical response of soil under cyclic loading: (a) effective stress path, (b) stress-strain response and (c) pore pressure-strain response (Wood, 1990).

2.2.7 Advanced Models

Various more advanced models which are based on the Cam clay and the Modified Cam clay models have been proposed in the past to make better predictions of soil behaviour. These models are briefly described in this section.

The yield surfaces and plastic potentials of real soils appear to exhibit a variety of shapes and it is therefore desirable to adopt an expression which has flexibility. Lagioia et al. (1996) developed mathematical expressions for the plastic potential and yield surface, which not only eliminate the limitations of the original Cam clay model, but also produce a wide range of shapes. Some of the shapes currently found to exist empirically in the literature can be reproduced by means of an appropriate choice of parameters. The stress-dilatancy relation proposed by Lagioia et al. (1996) is:

$$\frac{\mathrm{d}\varepsilon_p^p}{\mathrm{d}\varepsilon_q^p} = c_1\left(\mathrm{M}-\eta\right)\left(\frac{c_2\mathrm{M}}{\eta}+1\right) \tag{2.31}$$

where c_1 and c_2 are material constants.

A family of yield surfaces was also developed by Yu (1998), which is suitable for both clay and sand. This model, Clay And Sand Model (CASM), requires two additional parameters to describe the yield surface. One of these parameters is used to specify the shape of the yield surface and the other is to control the position of the critical state on the yield surface (i.e. to control the separation of the isotropic normal and critical state lines in *e*-log *p′* space). One of the main features of this model is that the critical state in this model does not necessarily occur at the maximum deviatoric stress on the yield surface as opposed to the Original and Modified Cam clay models (see Section 2.2.6). This is observed experimentally for sands (e.g. Coop, 1990). However, the use of Rowe's stress-dilatancy relationship as the flow rule leads to non-associated flow at low stress ratios which is not observed experimentally (McDowell, 2002).

A family of yield loci was derived by McDowell (2000) based on the new work equation proposed by McDowell and Bolton (1998). The new work equation is given as:

$$q\delta\varepsilon_q + p'\delta\varepsilon_p = \delta W_{fric} + \delta W_{frac} \tag{2.32}$$

The left hand side is the plastic work done by the boundary stresses, which is assumed to be dissipated in friction caused by particle arrangement and in the fracture of particles. The first and second terms on the right are the energy dissipated in friction and in fracture respectively. If the ratio of the work dissipated in fracture to the work dissipated in friction is assumed to be a simple function of stress ratio, McDowell (2000) showed that a simple stress-dilatancy relation could be developed with the equation:

$$\frac{d\varepsilon_p^p}{d\varepsilon_q^p} = \frac{\mathrm{M}^{a+1} - \eta^{a+1}}{\eta^a} \tag{2.33}$$

where $\eta = q/p'$, M is the critical state dissipation constant, and a is constant.

This stress-dilatancy rule generates a yield surface whose equation is:

$$q = \mathrm{M}p'\left((a+1)\ln\left(\frac{p'_c}{p'}\right)\right)^{\frac{1}{a+1}} \tag{2.34}$$

where p'_c is the isotropic pre-consolidation pressure.

By changing the parameter a, different shapes of yield loci can be obtained, consistent with those commonly encountered for isotropically consolidated clays and sands.

2.2.8 Cyclic Loading Models

Various models have been developed for cyclic loading. Iwan (1967) and Mróz (1967) independently formulated the first kinematic hardening model for metals which was later applied to soils by Prévost (1977, 1978). Mróz et al. (1979) described a two-surface kinematic hardening model which has a kinematic yield surface inside the consolidation surface. If the current stress state reaches the yield surface, plastic deformations occur and the yield surface translates. Hashiguchi (1985) described a model which is similar to the model described by Mróz et al. (1979) and introduced an extra surface in order to obtain a smooth stress-strain curve beyond yield. Hashiguchi (1993) also describes in detail how the kinematic hardening concept may be applied to generate multi-surface and infinite surface models.

Dafalias and Herrman (1982) the bounding surface model, which can produce an accumulation of permanent strain with increasing number of cycles. This model is

based on the concept of Critical State Soil Mechanics. The yield surface of a conventional elastic-plastic model is now termed the bounding surface; it is no longer the boundary between elastic and plastic deformations. In this model, the sudden change of stiffness associated with the passage of the stress state through a yield surface is eliminated by making the stiffness fall steadily from the high (elastic) value at a point in the interior of the bounding surface to the low (plastic) value when stress state reaches the bounding surface. For a stress state A, an image point on the bounding surface B is defined by a radial mapping rule from a projection origin O (Figure 2.13). The stiffness is made to be a function of the distance between the stress state and the image stress. The salient feature of the bounding surface model is the occurrence of plastic deformation for stress states inside the bounding surface, and the possibility of having a very flexible variation of the plastic modulus with changing stress states.

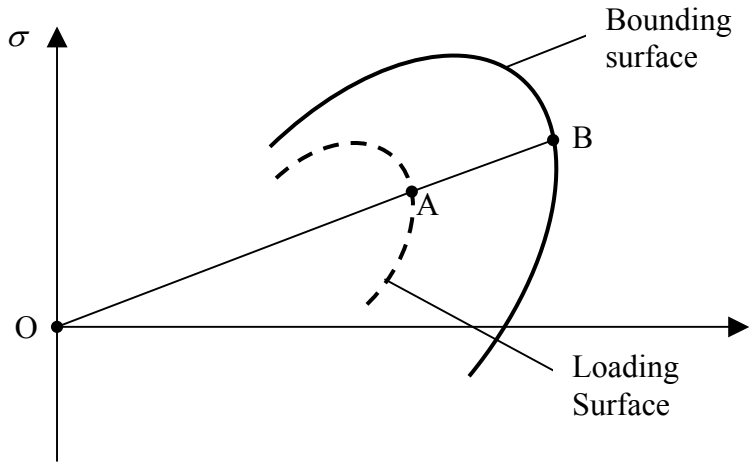

Figure 2.13. Schematic diagram showing the bounding surface concept.

Another simple way of modelling cyclic loading behaviour using the critical state soil model is by reducing the size of the yield surface in an isotropic manner on unloading. This model, developed by Carter et al. (1982) assumes that the form of the yield surface remains unchanged but that its size has been reduced in an isotropic manner by the elastic unloading. This model is based on the Modified Cam clay model with one important modification: the size of the yield surface shrinks during unloading, with the left apex always passing through the origin. The resulting model allows for accumulating plastic strain and pore pressure but not for hysteresis. Only

one additional parameter is needed which can be determined by performing cyclic triaxial tests under undrained conditions.

Pender (1982) proposed a cyclic loading model based on the Critical State Soil Mechanics framework. The initial version of the model predicted a rapid accumulation of strains with increasing number of cycles. This is contrary to observed behaviour where a state of equilibrium will be reached if the stress level is less than a critical stress level (Sangrey et al., 1969; Brown, Lashine and Hyde, 1975). To remedy this defect Pender (1982) modified the hardening function of the model by introducing a cyclic hardening index that depends on the number of cycles. This allows the stiffness to increase with number of cycles, so that the material gets progressively stiffer. However this does not solve the dilemma of how to model monotonic behaviour following a history of cyclic loading.

Ghaboussi et al. (1982) proposed a cyclic model for sand using isotropic and kinematic hardening for the yield surface. A hardening modulus is assumed and volumetric strain is computed based on a semi-empirical relationship and the plastic deviatoric strain is computed from a non-associated flow rule. The model underestimates the amount of accumulated irreversible shear strain whereas the predicted volumetric strain is reasonably accurate.

Nova (1982) described a model, which is suitable for both granular material and clay. The model uses two different flow rules for high stress ratio and low stress ratio such that non-associated flow is observed at high stress ratios whereas associated flow is observed at low stress ratios. A smooth transition is ensured between these flow rules. To model cyclic loading, Nova (1982) suggested that during unloading the bulk and shear compliance varied and at the start of reloading the bulk and shear compliance were restored to the initial values.

Al-Tabbaa (1987) developed a two-surface kinematic hardening model, known as the ‘Bubble’ model, based on the Modified Cam clay model, which enables more accurate predictions of the stress-strain behaviour of kaolin in overconsolidated states. This two-surface bubble model is similar to the models described by Mróz et al. (1979) and Hashiguchi (1985). A small inner true yield surface, which bounds a

small truly elastic region, was introduced – see Figure 2.14. This inner yield surface stores some information concerning past stress changes, and a function is used to produce a steadily decreasing stiffness as the outer yield surface, now termed 'bounding surface', is approached. Only two additional parameters are introduced. Later, Stallebrass (1990) extended the 'Bubble' model by introducing an extra kinematic surface to account for the effect of recent stress history. This model is discussed extensively in Chapter 3.

Ramsamooj and Alwash (1990) and Ramsamooj and Piper (1992) developed a multi-surface elasto-plastic model which was applied to the prediction of rutting in pavements. This model adopts different hardening rules for drained and undrained loading; for drained loading only volumetric hardening is applied, and for undrained loading, both volumetric and kinematic hardening rules are applied.

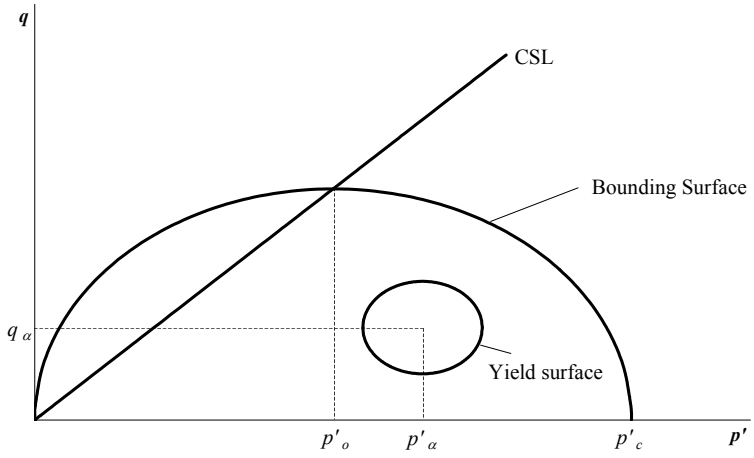

Figure 2.14. Diagram showing the yield and bounding surfaces and the symbols used for their centres (Al-Tabbaa, 1987).

More recently, Li and Meissner (2002) proposed a two-surface plasticity model based on a new type of kinematic hardening rule, which can model the cyclic undrained behaviour of clay. The model is based on the concept of 'memory centre'. The 'memory centre' is defined as the point where the stress path changes its direction and is directed into the interior of a loading surface. When the 'memory centre' gets its new position, a new bounding surface and loading surface passing through the 'memory centre' are formed. A total of 11 parameters are required to define the model.

2.2.9 Earth Pressure Coefficient at Rest

One-dimensional Loading

The prediction of the in-situ stress state in soil is of major importance in geotechnical problems. Vertical stresses can be determined easily, but the determination of horizontal stresses are more difficult. Many soils have a one-dimensional stress history and in the analysis of any pavement subgrade, it will be necessary to consider the stress history. This section therefore reviews literature on the one-dimensional history of soils.

The ratio of the horizontal to vertical effective stresses in soil is called the coefficient of earth pressure at rest, K_0:

$$K_0 = \frac{\sigma'_h}{\sigma'_v} \tag{2.35}$$

The value of K_0 during one-dimensional normal compression, $K_{0,nc}$, is known empirically to be constant for a given soil. Numerous relationships between $K_{0,nc}$ and angle of shearing resistance, ϕ', have been proposed over the past based on experimental data. The most widely used is that proposed by Jâky (1944):

$$K_{0,nc} = \left(1 + \frac{2}{3}\sin\phi'\right)\left(\frac{1-\sin\phi'}{1+\sin\phi'}\right) \tag{2.36}$$

This equation is approximated to:

$$K_{0,nc} = 1 - \sin\phi' \tag{2.37}$$

For clays, it is found that the value of ϕ' in equation 2.37 is the critical state angle of friction, ϕ'_{crit}. For sand, the value of ϕ' in equation 2.37 is less certain. According to Wood (1990), for sand the value of $K_{0,nc}$ will depend on the initial structure of the sand, and is therefore likely to depend on the maximum angle of shearing resistance

(Wood, 1990). However, for a sand which has yielded and is deforming plastically under one-dimensional normal compression (i.e. the state lies on the state boundary surface), it would be expected that the initial structure will have been eliminated, so that the value of ϕ' in equation 2.37 will be ϕ'_{crit} as for clay.

Brooker and Ireland (1965) proposed a modified form of Jâky's equation for cohesive soil:

$$K_{0,nc} = 0.95 - \sin\phi' \tag{2.38}$$

Bolton (1991b) suggested a relationship for sand:

$$K_{0,nc} = \frac{1-\sin\left(\phi'_c - 11.5^\circ\right)}{1+\sin\left(\phi'_c - 11.5^\circ\right)} \tag{2.39}$$

Simpson (1992) proposed a relationship for $K_{0,nc}$ based on the 'BRICK' model:

$$K_{0,nc} = \frac{\sqrt{2}-\sin\phi'}{\sqrt{2}+\sin\phi'} \tag{2.40}$$

One-dimensional Unloading

The effective horizontal stresses reduce more slowly than vertical effective stresses during one-dimensional unloading. Therefore the K_0 value for overconsolidated clay increases with overconsolidation ratio (OCR). Wroth (1975) derived an expression for K_0 on unloading for lightly overconsolidated soil based on the assumption that on unloading the soil is linear elastic.

$$K_0 = \mathrm{OCR} \cdot K_{0,nc} - \frac{\mu'}{1-\mu'}\left(\mathrm{OCR} - 1\right) \tag{2.41}$$

This relationship is only suitable for soil with OCR of not more than four where the unloading line in $q - p'$ space is approximately linear. Numerous researchers have

proposed empirical relationships for K_0 on unloading which can fit experimental data well. A simple expression was given by Schmidt (1966) for clays for K_0 on unloading as a function of $K_{0,nc}$ and OCR:

$$K_{0,u} = K_{0,nc}\left[\mathrm{OCR}\right]^{\alpha} \tag{2.42}$$

where:

$$\alpha = \sin 1.2\phi'_{crit} \tag{2.43}$$

Meyerhof (1976) suggested that $\alpha = 0.5$ is suitable for most soils for most practical purposes. Based on the study of experimental data on 170 different soils, Mayne & Kulhawy (1982) suggested that:

$$\alpha = \sin \phi'_{crit} \tag{2.44}$$

Al-Tabbaa (1987) performed oedometer tests on Speswhite kaolin and found that $\alpha = 0.464$, which agrees well with equation 2.43 with $\phi'_{crit} = 23°$.

Pruska (1973) proposed an expression for the variation of K_0 with OCR:

$$K_{0,u} = \frac{\sqrt{K_a}\cdot \mathrm{OCR}}{1 - K_a \cdot \left(1 - \mathrm{OCR}\right)} \tag{2.45}$$

where K_a is the Rankine active earth pressure coefficient:

$$K_a = \frac{1 - \sin\phi'}{1 + \sin\phi'} \tag{2.46}$$

One-dimensional Reloading

Very little data has been published for one-dimensional reloading. Based on the data available, Mayne & Kulhawy (1982) proposed a relationship for K_0 during reloading,

$K_{0,r}$ which will reduce to equation 2.37 for normally consolidated soils, i.e. OCR_{max} = OCR = 1, where OCR is the overconsolidation ratio. Equation 2.47 suggests that $K_{0,r}$ would not join the virgin curve at OCR = 1:

$$K_{0,r} = 1 - \sin\phi' \left(\left(\frac{OCR}{OCR_{max}^{1-\sin\phi'}} \right) + \frac{3}{4} \left(1 - \frac{OCR}{OCR_{max}} \right) \right) \tag{2.47}$$

Schmidt (1983) suggested that for reloading, $K_{0,r}$ would return to $K_{0,nc}$ at OCR = 1 and proposed an expression for $K_{0,r}$:

$$K_{0,r} = \frac{1 - \sin\phi'}{OCR_{max} - 1} \left(OCR_{max} - OCR + (OCR - 1) OCR_{max}^{\alpha} \right) \tag{2.48}$$

These equations suggest that $K_{0,r}$ varies linearly with OCR. Al-Tabbaa (1987) found that Schmidt's equation 2.48 fitted her data exactly with α = 0.464 for Speswhite kaolin.

Since the stresses which occur during one-dimensional history will be related to the strains via a flow rule, the above data can be used to test the validity of any new model which may be developed for clays. This is discussed in Chapters 3 and 4.

2.3 PAVEMENT ENGINEERING

2.3.1 Pavement Types and Failure Modes

The purpose of a pavement is to support the loads induced by traffic and to distribute these loads safely to the foundation. There are several different types of pavement but this project is concerned specifically with lightly trafficked (or low volume) flexible pavements, and hence other types of pavement are not in the scope of this research. Behrens (1999) defines low volume roads as those in a rural environment that enable automobile operation and account for less than 500 vehicles per day. Since lightly trafficked roads require relatively thin layers of bituminous material

compared with motorways, the pavement foundation properties assume greater significance since they are more highly stressed. The main objective of this research is the application of the principles of soil mechanics to the pavement foundation.

Figure 2.15 shows a typical cross-section of a flexible pavement. This pavement comprises a number of bituminous layers placed over road base (unbound or bound material) over crushed stone or a similar unbound sub-base material placed on the natural subgrade. This pavement is referred to as 'flexible' because the bituminous materials are capable of flexing slightly under traffic loading. For thinly surfaced pavements, the road base is often unbound material and not formally part of the foundation. However, for the purposes of this work it can be regarded as part of the foundation.

The pavement foundation is defined as the granular layer or layers placed over the subgrade and the subgrade itself — see Figure 2.15. The reason for considering all the unbound granular material is that the principles of soil mechanics apply to the sub-base, capping and subgrade. These principles have not been effectively applied in pavement engineering. Capping is a relatively cheap material placed between the subgrade and the sub-base to protect weak subgrades.

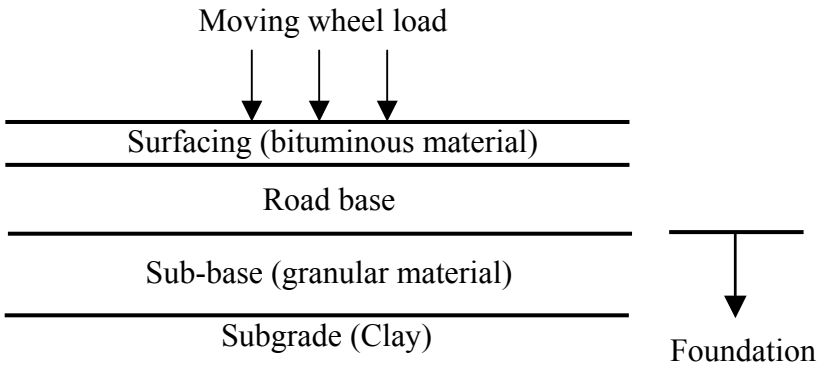

Figure 2.15. Cross-section of pavement.

In order to design a flexible pavement, the failure mechanisms must be adequately understood. Pavements do not fail suddenly but gradually deteriorate with time to a terminal level, which may be defined as failure. When a vehicle trafficks a road, it induces a stress pulse in the subgrade and granular layer. Figure 2.16 shows the

stresses in a pavement under a wheel load (Lekarp et al., 2000). This stress pulse causes strain and this strain can be divided into two parts: recoverable and permanent strain — see Figure 2.17.

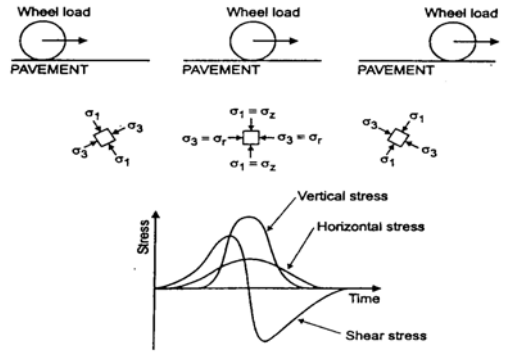

Figure 2.16. Stress pulse induced by a wheel load in a pavement foundation (Lekarp et al., 2000).

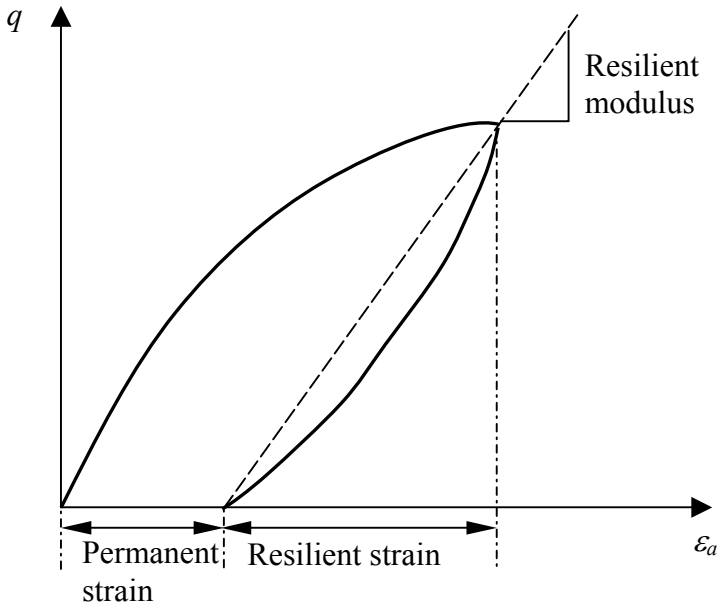

Figure 2.17. Diagram showing recoverable and permanent strains and definition of resilient modulus.

The two main structural failure mechanisms for flexible pavements are permanent deformation (rutting) and fatigue cracking. These two failure modes are shown in Figure 2.18. Rutting is the result of an accumulation of irrecoverable strains in the various pavement layers. In the U.K., a pavement is assumed to have reached 'critical' conditions when the rut depth reaches 10mm and failure is assumed to have

occurred when 20mm rut depth is reached. For a lightly trafficked pavement, subgrade and granular layer contribute most to rutting of a pavement. Fatigue cracking has been defined as the phenomenon of fracture under repeated or fluctuating stress having a maximum value generally less than the tensile strength of the material (Ashby and Jones, 1980). In the U.K., a pavement is usually assumed to have reached 'critical' conditions at the onset of fatigue cracking in the wheel path. Failure conditions have been reached when there is evidence of extensive cracking in the wheel path.

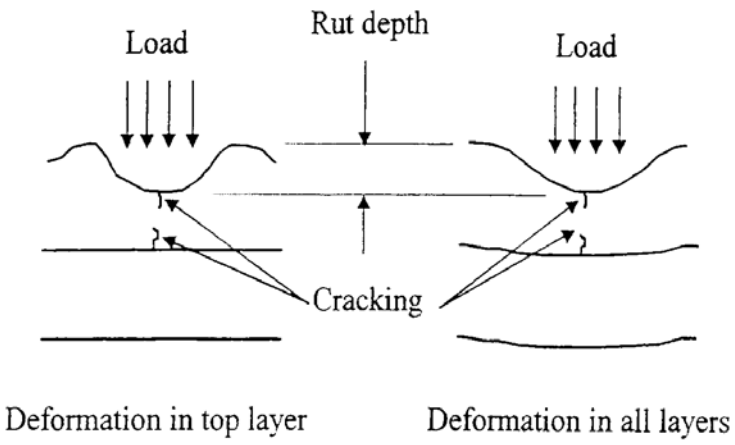

Figure 2.18. Diagrams showing the two types of failure mechanisms in pavements.

2.3.2 Resilient Deformation Models

The concept of resilient behaviour of pavements was introduced by Hveem & Carmany (1948) and Hveem (1955). In the 1950s, Seed et al. (1955) at the University of California at Berkeley followed the lead established by Hveem, who had developed the repeated load test. They introduced the term 'modulus of resilience', which they later changed to 'resilient modulus' (Seed et al., 1962) — see Figure 2.17. The definition of resilient modulus is the ratio of the repeated deviator stress to the recoverable (resilient) axial strain in the triaxial test (Seed et al., 1962). This concept has gained recognition by the pavement community as a good property to describe the resilient behaviour of granular materials and subgrade soils.

The resilient response of the soil plays an important role in pavement design, as this is the factor, which determines the thickness and stiffness of higher layers so that adequate load spreading takes place. During pavement construction, if the resilient deformations are too high, the paving plant will not be able to satisfactorily compact the bituminous layers of the pavement. The resilient response of unbound aggregates has been found to be influenced by many factors. An extensive literature review on the effect of different factors affecting the resilient response of unbound aggregates was performed by Lekarp et al. (2000), who describe the available modelling techniques. The factors affecting the resilient behaviour of unbound aggregates are stress level, density, grading, fines content, maximum grain size, moisture content, stress history, number of load cycles, aggregate type and particle shape, load duration and sequence. Among these, Lekarp et al. (2000) found that the effect of stress level on the resilient behaviour is the most significant factor. Resilient modulus increases greatly with confining pressure, and decreases with increasing deviator stress q.

The model most widely used for resilient deformations of unbound granular materials is the so-called K-θ model, which expresses the resilient modulus, M_r as a function of the sum of principal total stresses, θ:

$$M_r = k_1 \theta^{k_2} \tag{2.49}$$

where k_1 and k_2 are the constants and $\theta = 3p_{max}$ and p_{max} is the maximum mean stress during the load cycle. This model was developed by Hicks et al. (1971) based on repeated load conventional triaxial tests (constant radial stress σ_r) performed on two types of aggregate, namely crushed gravel and crushed rock.

Later Boyce (1980) developed a non-linear purely elastic model, G-K model based on the theorem of reciprocity (the proof of which was given by Boyce (1980)):

$$\frac{\partial \varepsilon_p}{\partial q} = \frac{\partial \varepsilon_q}{\partial p} \tag{2.50}$$

In this model Boyce expressed the bulk modulus K and shear modulus G as a function of mean normal stress p to a power less than one:

$$K = K_1 p^{(1-t)} \tag{2.51}$$

$$G = G_1 p^{(1-t)} \tag{2.52}$$

where K_1, G_1 and t are material constants. This model is similar to the K-θ model described above.

Since equations 2.51 and 2.52 do not satisfy the reciprocity theorem (equation 2.50), Boyce suggested a more complicated approach which satisfies this. The resilient volumetric strain, ε_{pr} and the resilient shear strain ε_{qr} proposed by Boyce have the following expressions:

$$\varepsilon_{pr} = \frac{1}{K_1} p^t \left(1 - \omega \frac{q^2}{p^2} \right) \tag{2.53}$$

$$\varepsilon_{qr} = \frac{1}{3G_1} p^t \frac{q}{p} \tag{2.54}$$

where

$$\omega = \left(1-t\right) K_1 / 6G_1 \tag{2.55}$$

This G-K model contains only three parameters, K_1, G_1, and t, to describe the resilient deformation of the material. The constant K_1 is the bulk modulus when the mean normal stress is 1kPa and the deviatoric stress is zero, and G_1 is the shear modulus when the mean normal stress is 1kPa. The parameter t is a measure of stress dependency, and varies between 0 and 1. For t = 1, a linear elastic relationship is obtained. This model was later modified by others such as Sweere (1990) to improve predictive capability.

In order to incorporate the resilient modulus, M_r, into the pavement design methods, some empirical correlations based on California Bearing Ratio (CBR) are widely used, such as:

$$M_r = 10CBR \text{ [MPa]} \tag{2.56}$$

proposed by Heukelom & Klomp (1962), and:

$$M_r = 17.6CBR^{0.64} \text{ [MPa]} \tag{2.57}$$

proposed by Powell et al. (1984). CBR is the average ratio, expressed as a percentage, of the loads required to penetrate a given material and a standard material by 2.5mm and 5mm. The CBR test is briefly described in Section 2.3.5.

Brown et al. (1987) demonstrated that the resilient modulus is stress dependent and non-linear and checked the validity of equations 2.56 and 2.57; the results are shown in Figure 2.19. It was found that the resilient modulus is not a simple function of CBR; it depends on stress level and material type.

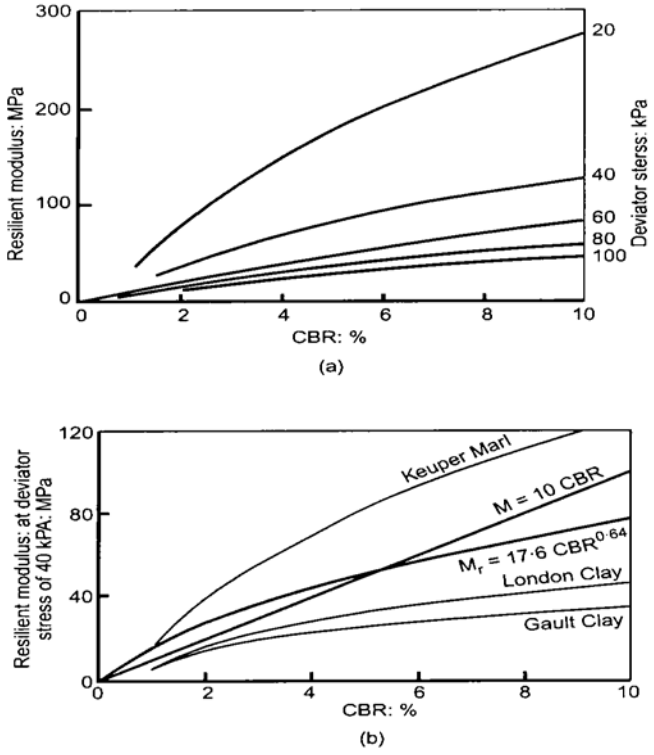

Figure 2.19. Relationships between resilient modulus and CBR (Brown et al., 1987).

2.3.3 Permanent Deformation Models

Fewer permanent deformation models have been proposed compared to those for resilient deformation because permanent deformation tests are time consuming and destructive. Models for permanent deformation are based on repeated load triaxial tests with a large number of cycles and the permanent strain is related to the number of load applications. Barksdale (1972) performed a series of repeated load triaxial tests with 10^5 cycles on different granular materials, and found that the accumulation of permanent axial strain was proportional to the logarithm of number of load cycles. Barksdale (1972) suggested the following expression:

$$\varepsilon_{ap} = a_1 + a_2 \log N \tag{2.58}$$

where ε_{ap} = permanent axial strain, N = number of load cycles and, a_1 and a_2 are constants for a given stress level.

Later, Sweere (1990) showed that, after applying 10^6 cycles, a log-log approach is more appropriate for large numbers of cycles:

$$\log \varepsilon_{ap} = a_1 + a_2 \log N \tag{2.59}$$

Other approaches relate the permanent strain to the length of the stress path and stress ratio such as Pappin (1979) and Lekarp et al. (1998).

A full range of repeated load triaxial tests was carried out by Pappin (1979) on a well-graded crushed limestone with a maximum particle size of 38mm, which is commonly used in pavements in the U.K. The objective of these tests was to investigate the permanent strain behaviour and to formulate a predictive model. In each test an attempt was made to apply at least 100,000 cycles of load at a frequency of 1Hz. From these results Pappin derived an expression for permanent shear strain:

$$\varepsilon_{qp} = b \times L \times \left(\sqrt{2} / 3 \right)^{2.8} \left(q / p \right)_{\max}^{2.8} \times 10^{-4} \tag{2.60}$$

where ε_{qp} is permanent shear strain in %, b is the shape factor, which is calculated for different numbers of cycles, and L is the stress path length in kPa.

Lekarp et al. (1998) used the repeated load triaxial equipment and hollow cylinder apparatus at Nottingham to test five different granular materials, which are commonly used as sub-base materials in pavement structures. The objective was to study the development of permanent strain with increasing number of load cycles and as a function of stress level. A relationship that takes account of stress path length and stress level was proposed by Lekarp et al. (1998) for permanent axial strain:

$$\frac{\varepsilon_{ap}\left(N_{ref}\right)}{L/p_r} = a_1\left(\frac{q}{p}\right)_{\max}^{a_2} \tag{2.61}$$

where $\varepsilon_{a,p}(N_{ref})$ is the accumulated permanent axial strain at a given number of cycles, L is the length of the stress path in kPa, a_1 and a_2 are regression parameters and p_r is a reference stress, taken to be 1kPa. Lekarp et al. (1998) found that the growth of permanent strain would eventually reach an equilibrium condition, at which the rate of growth of permanent strain was zero, if the stress ratio was low. However, at high stress ratios the accumulation of permanent strain was more progressive, indicating that a threshold stress ratio must exist above which accumulation of permanent strain will cause progressive failure. This threshold stress ratio is called the shakedown limit.

2.3.4 Stress History of a Pavement

The response of an element of soil to applied load depends crucially on its stress history and current stress state. The soil beneath a pavement may be in its natural undisturbed state or be remoulded depending on whether the section of pavement is in a ‘cut’ or ‘fill’ area (Brown, 1996), and these two situations have to be treated separately. Brown (1996) illustrated the typical stress history for an element in a ‘cut’ condition and in a ‘fill’ condition. For the cut or undisturbed condition, the

typical stress history is shown in Figure 2.20 (Brown, 1996). The stress path from point O to point C and to point A in Figure 2.20 represents the natural stress history of soil due to one-dimensional compression and subsequent unloading due to erosion. This historical sequence generates an overconsolidated soil. Subsequent pavement construction operations will bring the soil to the final state P. The construction operation of a pavement involves three processes, which will influence the stress state of soil. These are:

1. Removal of overburden during earthworks construction
2. Lowering of the water table
3. Addition of overburden due to the pavement construction.

Figure 2.21 (Brown, 1996) shows the effects of construction operations on stress conditions in a ‘cut’ condition. The path AB is due to the removal of overburden, and as time passes, pore pressure will reach equilibrium as the effective stress moves from B to P'. The path P'D results from lowering the water table. Construction of the pavement will take place before point D is reached and therefore the increase of overburden due to construction will cause the effective stress to move from E to F. After the dissipation of pore pressure, the effective stress will move towards equilibrium at P. In reality, the actual stress path is likely to be represented by the curve BGEP due to the time needed for the dissipation of pore pressure.

For soil which is cut, transported and compacted as fill in an embankment, the effective stress regime is rather different and less well understood. Brown (1996) suggested a possible stress regime for construction in the ‘fill’ condition, shown in Figure 2.22. The soil is first brought to failure in an undrained condition due to the scraper operation – represented by AB in Figure 2.22. The stress state will then move to Q or Q′, depending on the environment and weather conditions. The effective stress state will move to Q if conditions are dry and the soil is placed above the water table at which suctions will be high and tend to increase the effective stress. If conditions are wet, the soil will move to a lower effective stress state such as Q′. The stress state at Q′ will move to Q after equilibrium conditions have been reached. The net effect on soil due to the 'fill' condition is then a reduced overconsolidation ratio after excavation, transportation and compaction as fill.

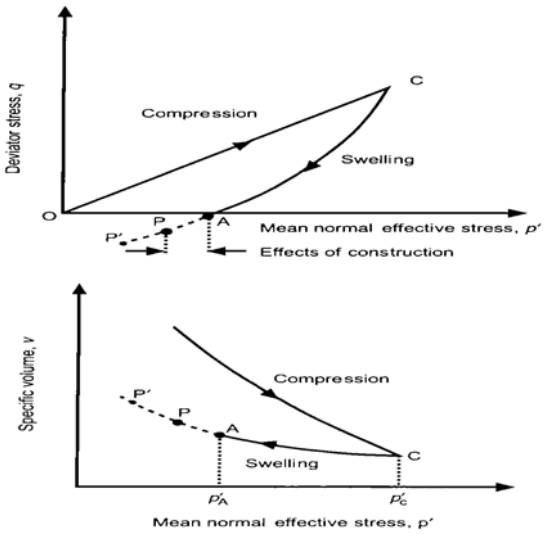

Figure 2.20. Typical stress history in a 'cut' condition (Brown, 1996).

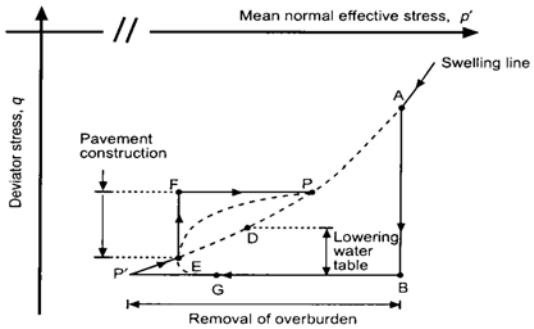

Figure 2.21. Effect of construction operations (Brown, 1996).

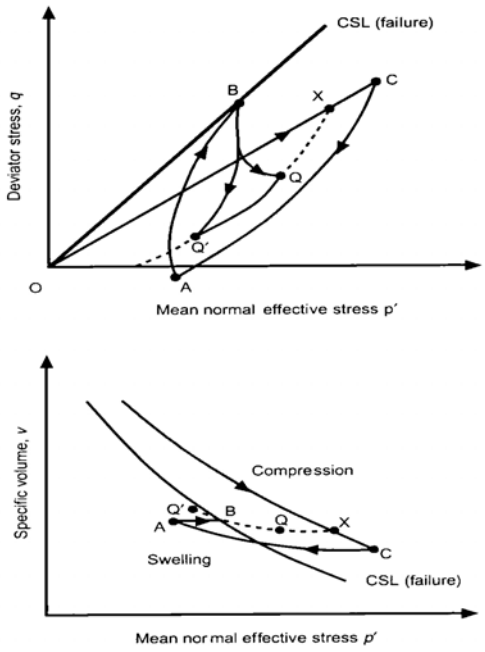

Figure 2.22. Stress history in a 'fill' condition (Brown, 1996).

2.3.5 Current UK Flexible Pavement Design Methods

The current UK practice of flexible pavement design is based on the Design Manual of Roads and Bridges (DMRB), Volume 7 (Highways Agency, 1994). This method was established by considering the performance of a number of experimental roads and is essentially empirical. The subgrade of a pavement is characterised by the California Bearing Ratio (CBR) concept developed in the US by the California Division of Highways in 1938. The CBR test involves the insertion of a plunger into the soil sample which is constrained within a small mould; the test procedure can be found in BS1377:1990 Part 4 (British Standards Institution, 1990). The load and the penetration are recorded while the plunger penetrates the sample. The loads at a penetration of 2.5mm and 5mm are compared with the result for a standard sample and the ratio expressed as a percentage is the CBR of the soil. The CBR of a pavement subgrade determines the thickness of the sub-base required using the empirical charts in DMRB Volume 7. This empirical design method provides no confidence when different types of material are used.

Some other design methods based on linear elastic theory were also proposed; the Shell design method (Shell, 1978) is the most common procedure using this theory. In this method, the pavement structure is represented by a three-layer system comprising an asphalt layer over a granular sub-base over the subgrade. This system is analysed using a multi-layered elastic theory with a program such as BISAR. The design criteria are to limit the maximum tensile strain at the bottom of the asphalt layer so that fatigue cracking of the asphalt layer will not occur, whilst the rutting of a pavement is related to the maximum compressive strain at the top of the subgrade. The non-linear properties of soil are not taken into account by this method. Brown and Dawson (1992) proposed a design method for asphalt pavements, which allows for the non-linear resilient behaviour of soils by using an equivalent resilient modulus. The design process is divided into two stages. The first involves the determination of the thickness of granular material required to protect the subgrade from being excessively stressed during the construction stage, and the second stage involves the design of the thickness of the asphaltic material required to prevent rutting and fatigue cracking when the pavement is opened to traffic. The thickness of

the granular material is chosen such that the deviatoric stress at the top of the subgrade does not exceed a certain value.

Brown and Brunton (1986) proposed a simplified approach to the design of flexible pavements, which assumes a standard 200mm layer of granular material with a resilient modulus of 100MPa. The subgrade is characterised by a single resilient modulus of value between 20 and 100MPa, which in the absence of better information, can be estimated from some empirical relationships between resilient modulus and CBR as described in Section 2.3.2. The design process involves the determination of an appropriate thickness of asphalt layer to ensure that the resilient tensile strain at the bottom of the asphalt layer and the resilient compressive strain at the top of the subgrade are below their maximum allowable values.

All of these design methods are either empirical or based on linear elastic theory, with little or no input from conventional Critical State Soil Mechanics.

2.4 NUMERICAL MODELLING

2.4.1 Introduction

The theory of elasticity has been extensively applied to the analysis of layered pavement systems. Various computer programs have been developed to analyse pavements. The most widely used layered elastic program in pavement engineering is BISAR, developed by Shell (Shell International Petroleum Company, 1978). Pavement layers are assumed to be linear elastic. A constant value of Young's modulus E' and Poisson's ratio μ', is assigned to each layer. The use of constant values for E' and μ' is a simplification, made to allow the use of a relatively simple computer program based on linear elastic theory. Linear elastic analysis can be used with reasonable confidence for pavements where the main structural element is formed by the asphalt layer (thick asphalt). However, for thinly surfaced (low volume) or unsurfaced pavements the simplification to a linear elastic system is no longer justified due to the fact that pavement foundations have markedly non-linear

and inelastic stress-strain relationships. This non-linearity and inelasticity must be properly taken into account in theoretical analysis. To accommodate this non-linearity, the granular layer and soil can be subdivided into sub-layers. Stress-dependency of the stiffness can then be taken into account by assigning a higher stiffness to the deeper sub-layers. The problem of obtaining a correct stiffness for each sub-layer remains. To accommodate the accumulation of permanent deformation, however, any kind of layered elastic approach is useless. It has to be used in conjunction with other empirical relationships which relate the permanent deformation to stresses computed from layered elastic analysis, and the number of load applications (Barksdale, 1972).

Most of the pavement analysis accommodating non-linear behaviour, has used the finite element approach. Several finite element packages specially developed for the pavement problem such as SENOL (Brown and Pappin, 1981) and FENLAP (Almeida, 1993) have been developed at the University of Nottingham. These programs use empirical stress-strain relationships to model the material behaviour.

2.4.2 Basic Finite Element Concepts

The basic steps involved in the formulation and application of the finite element method are:

- Step 1: Element Discretization

This step involves subdividing the structure into a number of small regions, termed finite elements. These elements have nodes or nodal points, which are the intersections of the sides of the elements.

- Step 2: Select Approximate Models or Functions

In this step, the primary unknown quantity must be selected such as displacement or stress. This variable is expressed in terms of nodal values by mathematical functions such as polynomials.

- Step 3: Define Stress-strain Relationships

  A constitutive relationship which describes the stress-strain behaviour is defined:

$$\{\Delta\sigma\} = [D]\{\Delta\varepsilon\} \tag{2.62}$$

  where [D] is the constitutive matrix relating the change in stress to the change in strain.

- Step 4: Derive Element Equations

  Energy methods and residual methods are the two methods commonly used in the derivation of element equations (Desai, 1979). The element equations are commonly expressed as:

$$[K_E]\{\Delta d_E\} = \{\Delta R_E\} \tag{2.63}$$

  where $[K_E]$ is the element stiffness matrix, $\{\Delta d_E\}$, is the vector of increment element nodal displacements and $\{\Delta R_E\}$ is the vector of element incremental nodal forces.

- Step 5: Assemble element equations to obtain global equations and introduce boundary conditions.

  In this step, element equations are combined to form global equations for the entire structure, which define approximately the behaviour of the structure as a whole. The global equations are expressed as:

$$[K_G]\{\Delta d_G\} = \{\Delta R_G\} \tag{2.64}$$

  where $[K_G]$ is the global stiffness matrix, $\{\Delta d_G\}$, is the vector of all incremental nodal displacements and $\{\Delta R_G\}$ is the vector of all incremental nodal forces. Boundary conditions are the physical constraints or supports that exist so that the structure can stand in space uniquely. These conditions are known values.

- Step 6: Solve for the Primary Unknowns

  Equation 2.64 is a set of simultaneous equations. In this step, these simultaneous equations are solved to obtain $\{\Delta d_G\}$ using Gaussian elimination or iterative methods.

- Step 7: Solve for Derived or Secondary Quantities

  Once the primary quantities are obtained, secondary quantities such as stresses and strains can be evaluated.

If the material is linear elastic, the constitutive matrix [D] is constant. However, the behaviour of soil is highly non-linear, and if the soil is assumed to be non-linear elastic or elasto-plastic the constitutive matrix [D] is no longer constant but varies with stress or strain: it changes during a finite element analysis. The finite element method can be adapted to deal with non-linear constitutive relationships by applying the boundary conditions incrementally. This causes the governing finite element equations to be reduced to incremental form:

$$\left[K_G\right]^i \left\{\Delta d\right\}_{nG}^i = \left\{\Delta R_G\right\}^i \tag{2.65}$$

where $[K_G]^i$ is the incremental global system stiffness matrix, $\{\Delta d\}^i_{nG}$ is the vector of incremental nodal displacements, $\{\Delta R_G\}^i$ is the vector of incremental nodal forces and i is the increment number. Due to the non-linear constitutive relationships, the incremental global stiffness matrix $[K_G]^i$ varies during an increment, and hence the solution of equation 2.64 is not straightforward. There are three different methods used to solve these equations: (1) Tangent stiffness method (2) Visco-plastic method and (3) Modified Newton-Raphson (MNR) method. In principle, if the number of increments applied is sufficiently large, all methods should give similar results. However, an increase in the number of increments will increase the computational time. Hence the method used in non-linear finite element analysis plays an important role, as it can influence the amount of computational effort required to obtain the results and the accuracy of the results (Potts & Zdravković, 1999).

The tangent stiffness method is the simplest and most widely used method in engineering practice. This is the method used in the finite element program CRISP (Britto and Gunn, 1987). In this method, the total applied load is divided into a small number of increments and each increment is applied individually. During each increment, the stiffness properties appropriate for the current stress levels are used in the calculations. Provided the increments are small, the material behaviour may be assumed to be linear during the load increment. If only a few increments are used, this method produces a solution which tends to drift away from the exact solution – see Figure 2.23.

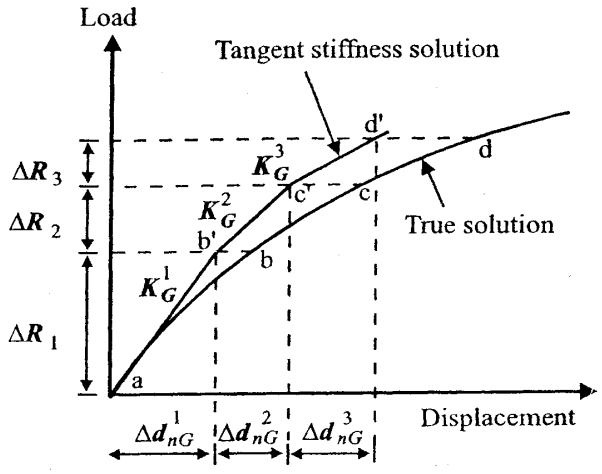

Figure 2.23. Tangent stiffness method (Potts & Zdravković, 1999).

2.4.3 Critical State Program (CRISP)

CRISP (Critical State Program) was developed by research workers in Cambridge University (Britto and Gunn, 1987). This is a finite element program which is able to perform drained, undrained and time dependent analysis of static problems under monotonic loading or unloading conditions. It is not suitable for cyclic loading in its currently commercially available form. Plane strain, axisymmetric and three-dimensional analysis can be carried out. Various constitutive models, from linear elastic models to advanced critical state models, are available in CRISP. However, the constitutive models currently available in CRISP are not suitable for analysing

partially saturated soils. Different types of finite element are available such as linear strain triangle and cubic strain triangle.

Modifications made to CRISP

In order to simulate the pavement subgrade under cyclic loading, thousands of cycles have to be applied. Without modification to the program, it is very tedious and time consuming to generate large numbers of cycles. A computer program, which is able to generate large numbers of cycles automatically, was written by the CRISP Technical Support for the purpose of this project. This greatly reduces the amount of time required to generate a large number of load cycles. This program was also modified by CRISP Technical Support so that a large number of cycles of multiple stress blocks can be applied automatically. This is important, because it makes it possible to calculate the stress distribution at the top of the subgrade clay in a three-layer pavement due to an applied wheel load. This stress distribution can be approximated by rectangular stress blocks applied repeatedly to the surface of the clay subgrade. This was found to be particularly helpful, because if a three-layer pavement is analysed directly in CRISP, and the nodes at the interfaces between layers are common to each of the two layers at an interface, then each time the pavement is unloaded, the upper elastic layers pull the subgrade soil into tension. Thus, the use of stress blocks applied to the clay directly eliminates this problem, with the assumption that the granular and bituminous layers will settle to follow the surface of the clay in the long term.

2.5 SUMMARY

The most commonly used type of analysis in pavement engineering makes use of multi-layered linear elastic theory. This requires the provision of a constant elastic modulus and a Poisson's ratio for each pavement layer including granular material and clay. In conditions where the asphalt layer is relatively thick and hence the pavement foundation is relatively insignificant due to the low stresses induced in this

layer, such analysis can give reasonable results. However, when the stresses in the foundation layers are high such as in unsurfaced and thinly surfaced pavements, the non-linear and inelastic properties become crucial and elastic theory will not be able to predict correctly the behaviour of these types of pavements. It is clear that the problem of analysis of pavements including soil is one that is still not completely solved. This is particularly true for unsurfaced and thinly surfaced conditions, where the rutting behaviour of the pavement under repeated loading will be largely determined by the subgrade properties.

The majority of models developed specifically for pavement problems are empirically based, and therefore provide no confidence when extrapolating to different materials or different loading conditions. For the past decades, various cyclic models for soil have been developed based on the CSSM concept, which have been shown to be able to predict some of the essential features of soil under cyclic loading. However, little effort has been put into applying these models to the prediction of pavement response. The design methods developed for motorways are generally adopted by the local authorities that are responsible for lightly trafficked roads, which leads to uneconomical design standards. It is clear that there is an urgent need to apply to pavement engineering the knowledge of soil mechanics that has been accumulated through research, if economical design methods are to be established, especially for thinly surfaced pavements where the behaviour of the foundation plays a very important role.

3 PRELIMINARY STUDY – EVALUATION OF THE TWO AND THREE-SURFACE KINEMATIC HARDENING MODELS

3.1 INTRODUCTION

In the previous chapter, various models used in pavement engineering and soil mechanics were briefly described. The existing models which can predict the essential features of soil behaviour under cyclic loading are those based on the kinematic hardening concept. In this chapter the formulation of the 3-SKH model is briefly described, and the predictions of the two-surface model and the 3-SKH model of the coefficient of earth pressure at rest and of soil behaviour under cyclic loading in triaxial tests are evaluated. The main objective of this chapter is to establish whether a kinematic hardening model is capable of predicting the response of a typical three-layer pavement under cyclic loading. The suitability of both the two-surface and the 3-SKH models for modelling the subgrade clay will be examined. In this way, the advantages and disadvantages of the models can be determined and necessary modifications to the models can be established in order to improve predictive capability.

3.2 MODEL DESCRIPTION

The detailed derivation of the two-surface model (or the 'Bubble' model) and the 3-SKH model are given in Al-Tabbaa (1987) and Stallebrass (1990) respectively. These models are an extension of the Modified Cam clay model, but these models are slightly different from the Modified Cam clay model in that the normal compression lines and the swelling lines are assumed to be linear in $\ln v - \ln p'$ space with slopes λ^* and κ^* respectively (Butterfield, 1979), whereas in Modified Cam clay these lines were assumed to be linear in $v - \ln p'$ space. In this section only the formulation of the 3-SKH model is described as this is very similar to the

formulation of the two-surface model, which is a special case of the 3-SKH model. The 3-SKH model is defined in triaxial stress space as shown in Figure 3.1. The model consists of two kinematic surfaces, namely the history surface and yield surface, lying within the Modified Cam clay state boundary surface, which will be called the bounding surface. All surfaces have the same shape and expand and contract according to a fixed ratio. These surfaces are defined by the following equations:

Bounding surface:

$$\left(p'-p'_o\right)^2+\frac{q^2}{\mathrm{M}^2}=p'^2_o \tag{3.1}$$

History surface:

$$\left(p'-p'_a\right)^2+\frac{\left(q-q_a\right)^2}{\mathrm{M}^2}=T^2p'^2_o \tag{3.2}$$

Yield surface:

$$\left(p'-p'_b\right)^2+\frac{\left(q-q_b\right)^2}{\mathrm{M}^2}=T^2S^2p'^2_o \tag{3.3}$$

The quantities p'_a and q_a represent the stress state at the centre of the history surface, and p'_b and q_b represent the stress state at the centre of the yield surface. The parameter T is the ratio between the size of the history surface and that of the bounding surface; S is the ratio between the size of the yield surface and that of the history surface. The parameter M is the critical state friction constant: i.e. the slope of the critical state line in q–p' space. The consistency condition, which ensures that the stress state always lies on or within the yield surface, is obtained by differentiating the equation of the yield surface, equation 3.3:

$$\left(p'-p'_b\right)\left(\delta p'-\delta p'_b\right)+\frac{\left(q-q_b\right)}{\mathrm{M}^2}\left(\delta q-\delta q_b\right)-T^2S\ \ p'_o\,\delta p'_o=0 \tag{3.4}$$

The consistency equation for the history surface is:

$$(p'-p'_a)(\delta p'-\delta p'_a)+\frac{(q-q_a)}{M^2}(\delta q-\delta q_a)-T^2 p'_o\,\delta p'_o=0 \tag{3.5}$$

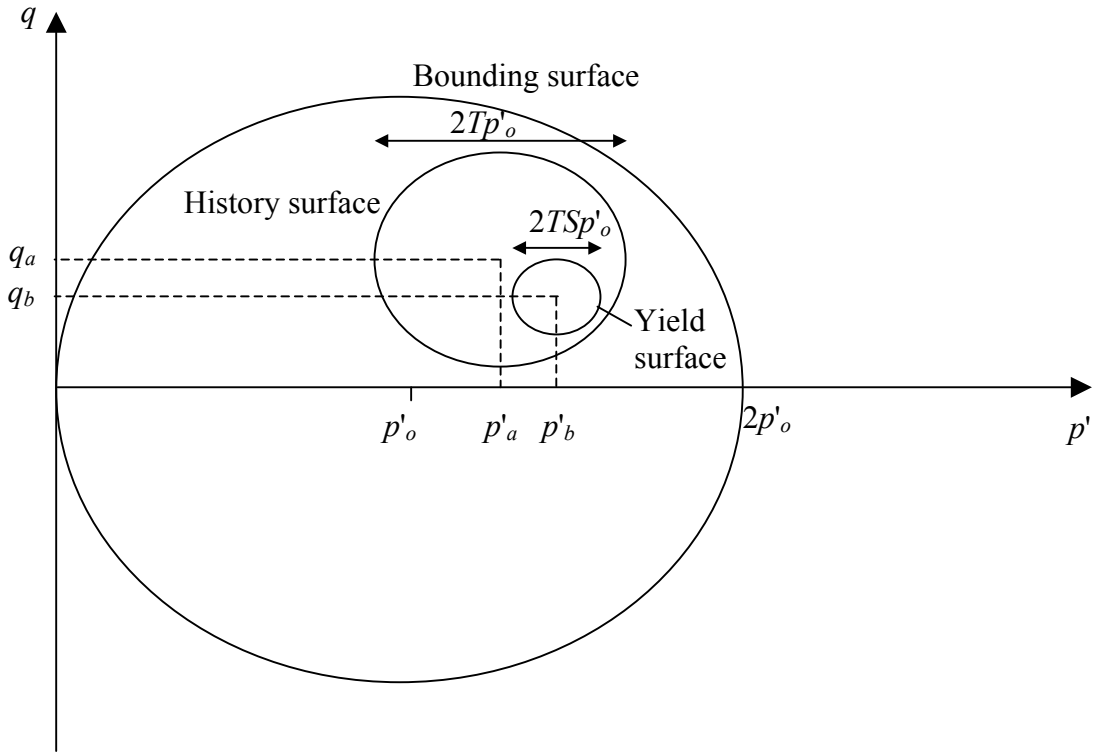

Figure 3.1. Diagram showing the 3-SKH model in triaxial stress space (Stallebrass, 1990).

When the stress state of the soil lies within the yield surface, the deformations of the soil are governed by isotropic elasticity:

$$\begin{bmatrix}\delta\varepsilon_p^e\\ \delta\varepsilon_q^e\end{bmatrix}=\begin{bmatrix}\kappa^*/p' & 0\\ 0 & 1/3G'_e\end{bmatrix}\begin{bmatrix}\delta p'\\ \delta q\end{bmatrix} \tag{3.6}$$

where G'_e is the elastic shear modulus: i.e. the shear modulus at very small strains and κ^* is the initial slope of the isotropic swelling line in ln v – ln p' space. The value of G'_e can be assumed to vary with p' and overconsolidation ratio, R_o according to

the relationship proposed by Viggiani and Atkinson (1995) (Stallebrass and Taylor, 1997):

$$G'_e = A\left(p'/p'_r\right)^n R_o^{\,m} \tag{3.7}$$

where p'_r is a reference pressure equal to 1kPa, R_o is the overconsolidation ratio (equal to p'_c/p'), and m and n are material constants.

3.2.1 Translation Rule

The translation laws used to control the movement of the kinematic surfaces have the same form as those used in the two-surface model developed by Mróz et al. (1979) and Al-Tabbaa (1987). These translation laws follow a rule which states that the centre of a surface should always move along a vector joining the current stress state to its conjugate point on the next surface, as shown in Figure 3.2. The conjugate point is defined as the point on the surface with the same outwards normal. When all the surfaces are in contact, this model reduces to Modified Cam clay.

The conjugate point corresponding to the current stress state can be calculated using the following equation:

$$\begin{pmatrix} \overline{p}' \\ \overline{q} \end{pmatrix} = \begin{pmatrix} \dfrac{p' - p'_b}{TS} \\ \dfrac{q - q_b}{TS} \end{pmatrix} + \begin{pmatrix} p'_o \\ 0 \end{pmatrix} \tag{3.8}$$

where $\overline{p}'$ and $\overline{q}$ are the conjugate stresses on the bounding surface.

The translation rules ensure that when the surfaces meet, they align gradually along the stress path direction and do not intersect. The translation rule for each kinematic surface consists of two components – the movement caused by the contraction and expansion of the surface, and the movement of the surface when it is dragged by the

current stress state. The size of the surface is related to the change in the plastic volumetric strain by the following relationship:

$$\delta p'_o = \frac{p'_o}{\lambda^* - \kappa^*} \delta \varepsilon_p^p \tag{3.9}$$

A – Current stress state
B and **C** – conjugate points with the same outward normal as **A**
γ – vector of movement of yield surface parallel to **AB** and of magnitude **AB**
β – vector of movement of yield surface parallel to **BC** and of magnitude **BC**

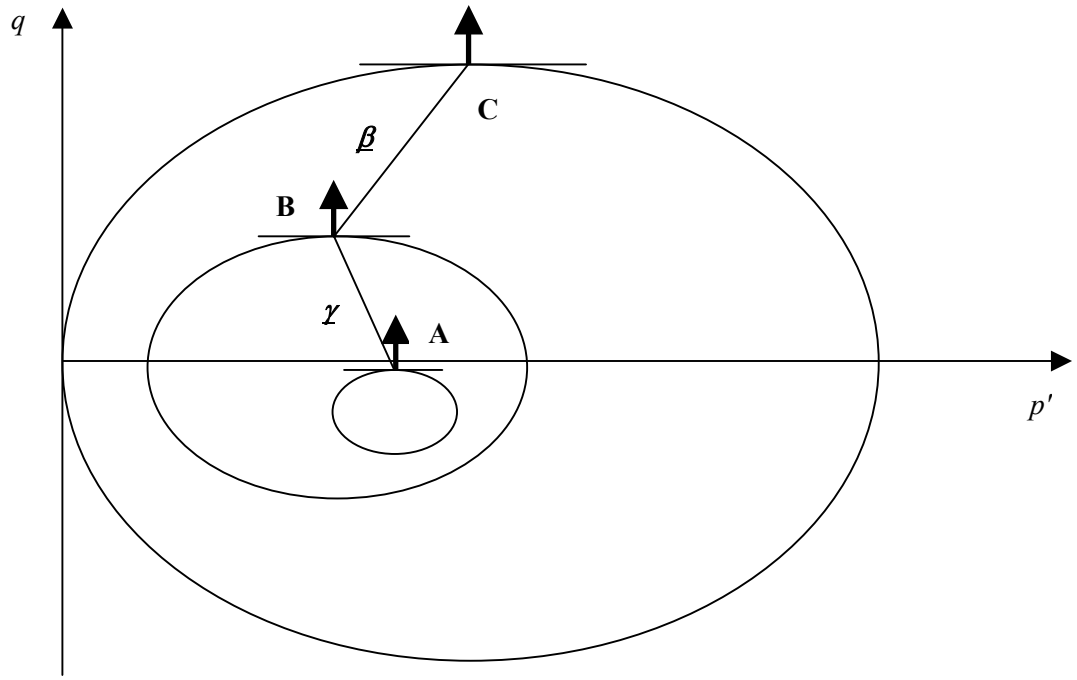

Figure 3.2. Conjugate stresses and vectors of movement of the kinematic surfaces (Stallebrass and Taylor, 1997).

Translation rules for history surface:

The first part of the translation rule is the change in size of the history surface due to the change in p'_o and can be obtained from the geometry of the surfaces:

$$\begin{bmatrix} \delta p'_a \\ \delta q_a \end{bmatrix} = \frac{\delta p'_o}{p'_o} \begin{bmatrix} p'_a \\ q_a \end{bmatrix} \tag{3.10}$$

For the second part of the translation rule, the history surface is assumed to translate along the vector $\underline{\beta}$ that connects the stress state on the history surface to the conjugate stress on the bounding surface as shown in Figure 3.2. The translation rule that controls the movement of the history surface is:

$$\begin{bmatrix} \delta p'_a \\ \delta q_a \end{bmatrix} = \mathrm{W}\underline{\beta} \tag{3.11}$$

where W is the scalar quantity to be obtained by substitution of the translation rule into the consistency equation of the history surface, equation 3.5.

From the geometry of the surfaces, the following expression for the vector $\underline{\beta}$ can be obtained when the stress state lies on the history surface:

$$\underline{\beta} = \begin{bmatrix} \dfrac{p'-p'_a}{T} - \left(p'-p'_o\right) \\ \dfrac{q-q_a}{T} - q \end{bmatrix} \tag{3.12}$$

The full expression for the translation of the history surface can be obtained by the addition of the translation rule that controls the change in the size of the history surface (equation 3.10) and the movement of the history surface (equation 3.11):

$$\begin{bmatrix} \delta p'_a \\ \delta q_a \end{bmatrix} = \frac{\delta p'_o}{p'_o}\begin{bmatrix} p'_a \\ q_a \end{bmatrix} + \mathrm{W}\begin{bmatrix} \dfrac{p'-p'_a}{T} - \left(p'-p'_o\right) \\ \dfrac{q-q_a}{T} - q \end{bmatrix} \tag{3.13}$$

By substituting equation 3.13 into the consistency equation of the history surface (equation 3.5), the scalar quantity W can be obtained:

$$W = \frac{\left(p' - p'_a\right)\left(\delta p' - \frac{\delta p'_o}{p'_o} p'\right) + \left(\frac{q - q_a}{M^2}\right)\left(\delta q - \frac{\delta p'_o}{p'_o} q\right)}{\left(p' - p'_a\right)\left[\frac{p' - p'_a}{T} - \left(p' - p'_o\right)\right] + \left(\frac{q - q_a}{M^2}\right)\left[\frac{q - q_a}{T} - q\right]} \tag{3.14}$$

When the history surface is in contact with the bounding surface and the loading path is such that the surfaces are expanding:

$$T\left(p' - p'_o\right) = p' - p'_a \text{ and } Tq = q - q_a \tag{3.15}$$

Differentiating equation 3.15 gives the translation rule for the history surface when the history surface is in contact with the bounding surface, and when the loading path is such that the surface is expanding:

$$\begin{bmatrix} \delta p'_a \\ \delta q_a \end{bmatrix} = (1 - T)\begin{bmatrix} \delta p' \\ \delta q \end{bmatrix} + T\begin{bmatrix} \delta p'_o \\ 0 \end{bmatrix} \tag{3.16}$$

Translation rules for yield surface:

The translation rule that controls the change in size of the yield surface is:

$$\begin{bmatrix} \delta p'_b \\ \delta q_b \end{bmatrix} = \frac{\delta p'_o}{p'_o}\begin{bmatrix} p'_b \\ q_b \end{bmatrix} \tag{3.17}$$

The translation of the yield surface is assumed to be along the vector $\underline{\gamma}$ which joins the stress state on the yield surface to the conjugate stress on the history surface as shown in Figure 3.2:

$$\underline{\gamma} = \begin{bmatrix} \frac{p' - p'_b}{S} - \left(p' - p'_a\right) \\ \frac{q - q_b}{S} - \left(q - q_a\right) \end{bmatrix} \tag{3.18}$$

The full expression for the translation of the yield surface, which is similar to the translation rule for the history surface, is:

$$\begin{bmatrix} \delta p'_a \\ \delta q_a \end{bmatrix} = \frac{\delta p'_o}{p'_o} \begin{bmatrix} p'_b \\ q_b \end{bmatrix} + Z \begin{bmatrix} \frac{p'-p'_b}{S} - (p'-p'_a) \\ \frac{q-q_b}{S} - (q-q_a) \end{bmatrix} \tag{3.19}$$

By substituting the above equation into the consistency equation of the yield surface (equation 3.4), the scalar quantity Z can be obtained:

$$Z = \frac{(p'-p'_b)\left(\delta p' - \frac{\delta p'_o}{p'_o} p'\right) + \left(\frac{q-q_b}{M^2}\right)\left(\delta q - \frac{\delta p'_o}{p'_o} q\right)}{(p'-p'_b)\left[\frac{p'-p'_b}{S} - (p'-p'_a)\right] + \left(\frac{q-q_b}{M^2}\right)\left[\frac{q-q_b}{S} - (q-q_a)\right]} \tag{3.20}$$

The translation rule for the yield surface when it is in contact with the history surface and when the loading path is such that the surface is expanding is:

$$\begin{bmatrix} \delta p'_b \\ \delta q_b \end{bmatrix} = (1-S) \begin{bmatrix} \delta p' \\ \delta q \end{bmatrix} + S \begin{bmatrix} \delta p'_a \\ \delta q_a \end{bmatrix} \tag{3.21}$$

3.2.2 Hardening Modulus

Plastic deformations are assumed to obey the associated flow rule so that the vector of plastic strain increments is always normal to the current yield surface. The flow rule adopted by the 3-SKH model is the same as that for Modified Cam clay, so that on the bounding surface:

$$\frac{d\varepsilon_p^p}{d\varepsilon_q^p} = \frac{M^2 - \eta^2}{2\eta} \tag{3.22}$$

In general, on the yield surface, the constitutive relationship for plastic strain increments is:

$$\begin{bmatrix} \delta\varepsilon_p^p \\ \delta\varepsilon_q^p \end{bmatrix} = \frac{1}{h_o} \begin{bmatrix} (p'-p'_b)^2 & (p'-p'_b)\dfrac{(q-q_b)}{\mathrm{M}^2} \\ (p'-p'_b)\dfrac{(q-q_b)}{\mathrm{M}^2} & \dfrac{(q-q_b)^2}{\mathrm{M}^4} \end{bmatrix} \begin{bmatrix} \delta p' \\ \delta q \end{bmatrix} \tag{3.23}$$

where:

$$h_o = \frac{(p'-p'_b)}{(\lambda^*-\kappa^*)} \left[p'(p'-p'_b) + \frac{q(q-q_b)}{\mathrm{M}^2} \right] \tag{3.24}$$

and λ^* and κ^* are the slopes of the isotropic normal compression line, and the initial slope of an unloading curve, in ln v – ln p' space respectively. Following Al-Tabbaa (1987), h_o cannot be used on its own because equation 3.23 will predict infinite strains at a number of singularity points. These occur when the stress state hits the top or bottom apex and the points where the dot product of the vector that joins the origin to the current stress state and the vector normal to the yield surface at that stress point is zero, as shown in Figure 3.3. Between the singularity points, there are unstable regions, where the hardening modulus h_o is less than zero and the direction of the plastic shear strain increment is opposite to the direction of the increment of shear stress.

Therefore h_o is replaced by:

$$h = h_o + H_1 + H_2 \tag{3.25}$$

where H_1 and H_2 are functions of the position of the history surface and the yield surface respectively:

$$H_1 = \frac{1}{\lambda^*-\kappa^*} \left(\frac{b_1}{b_{1\max}} \right)^{\psi} p'^3_o S^2 \tag{3.26}$$

$$H_2 = \frac{1}{\lambda^* - \kappa^*}\left(\frac{T \cdot b_2}{b_{2\max}}\right)^{\psi} p'^{\,3}_{o} \tag{3.27}$$

Equation 3.23 can be rewritten as:

$$\begin{bmatrix} \delta\varepsilon_p^p \\ \delta\varepsilon_q^p \end{bmatrix} = \frac{\lambda^* - \kappa^*}{(p' - p'_b)\left[p'(p' - p'_b) + \dfrac{q(q - q_b)}{\mathrm{M}^2}\right] + \left(\dfrac{b_1}{b_{1\max}}\right)^{\psi} p'^{3}_{o} S^2 + \left(\dfrac{T \cdot b_2}{b_{2\max}}\right)^{\psi} p'^{3}_{o}} \times$$
$$\begin{bmatrix} (p' - p'_b)^2 & (p' - p'_b)\dfrac{(q - q_b)}{\mathrm{M}^2} \\ (p' - p'_b)\dfrac{(q - q_b)}{\mathrm{M}^2} & \dfrac{(q - q_b)^2}{\mathrm{M}^4} \end{bmatrix} \begin{bmatrix} \delta p' \\ \delta q \end{bmatrix} \tag{3.28}$$

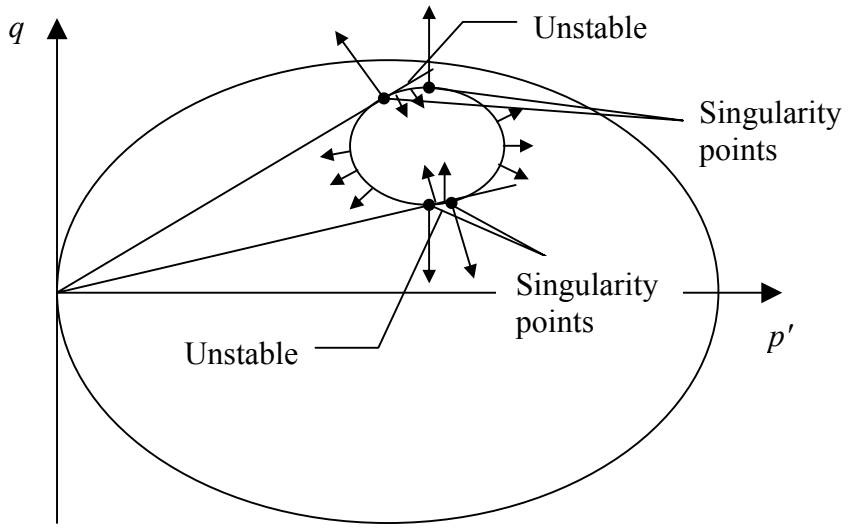

Figure 3.3. Schematic diagram showing the singularity points which divide the yield surface into two unstable regions (Al-Tabbaa, 1987).

The quantity b_1 is the scalar product of the outward normal at B (conjugate stresses on the history surface) and the vector $\underline{\beta}$, as shown in Figure 3.2, divided by the size of the history surface, and similarly, b_2 is the scalar product of the outward normal at A (current stress state) and the vector $\underline{\gamma}$ divided by the size of the yield surface:

$$b_1 = \left(\frac{\partial f_{hs}}{\partial \sigma} \cdot \underline{\beta}\right) \Big/ 2Tp'_o \tag{3.29}$$

$$b_2 = \left(\frac{\partial f_{ys}}{\partial \sigma} \cdot \underline{\gamma} \right) \Big/ 2TSp'_o \tag{3.30}$$

$$\frac{\partial f_{hs}}{\partial \sigma} = \begin{pmatrix} 2\left(\bar{p}' - p'_a\right) \\ \dfrac{2\left(\bar{q} - q_a\right)}{\mathrm{M}^2} \end{pmatrix} \tag{3.31}$$

$$\frac{\partial f_{ys}}{\partial \sigma} = \begin{pmatrix} 2\left(p' - p'_b\right) \\ \dfrac{2\left(q - q_b\right)}{\mathrm{M}^2} \end{pmatrix} \tag{3.32}$$

$$\bar{p}' = \frac{\left(p' - p'_b\right)}{S} + p'_a \text{ and } \bar{q} = \frac{\left(q - q_b\right)}{S} + q_a \tag{3.33}$$

where the subscripts *hs* and *ys* denote history surface and yield surface respectively for the yield functions, and $\bar{p}'$ and $\bar{q}$ are conjugate stresses at history surface (see Figure 3.2).

The vector $\underline{\beta}$ is the vector of movement of the history surface parallel to BC and has magnitude BC, and vector $\underline{\gamma}$ is the vector of movement of yield surface parallel to AB and has magnitude AB. The parameter ψ is a constant, which determines the rate at which stiffness deteriorates with strain. The functions b_1 and b_2 are normalised by their respective maximum possible values, $b_{1\max}$ and $b_{2\max}$ respectively, and these can be obtained from the geometry of the surfaces as shown in Figure 3.4. The functions b_1, b_2 can be obtained from equations 3.29 – 3.33:

$$\begin{aligned} b_1 = {} & \frac{1}{Tp'_o}\left[\frac{\left(p' - p'_b\right)}{S}\left(\frac{\left(p' - p'_b\right)}{TS} - \left[\frac{\left(p' - p'_b\right)}{S} + p'_a - p'_o\right]\right)\right] \\ & + \frac{\left(q - q_b\right)}{S\mathrm{M}^2}\left[\frac{\left(q - q_b\right)}{TS} - \left(\frac{\left(q - q_b\right)}{S} + q_a\right)\right] \end{aligned} \tag{3.34}$$

$$b_2 = \frac{1}{TSp'_o}\left[\left(p' - p'_b\right)\left(\frac{\left(p' - p'_b\right)}{S} - \left(p' - p'_a\right)\right)\right] + \frac{\left(q - q_b\right)}{\mathrm{M}^2}\left[\frac{\left(q - q_b\right)}{S} - \left(q - q_a\right)\right] \tag{3.35}$$

and their maximum values are:

$$b_{1\max} = 2p'_o\left(1 - T\right) \tag{3.36}$$

$$b_{2\max} = 2Tp'_o\left(1 - S\right) \tag{3.37}$$

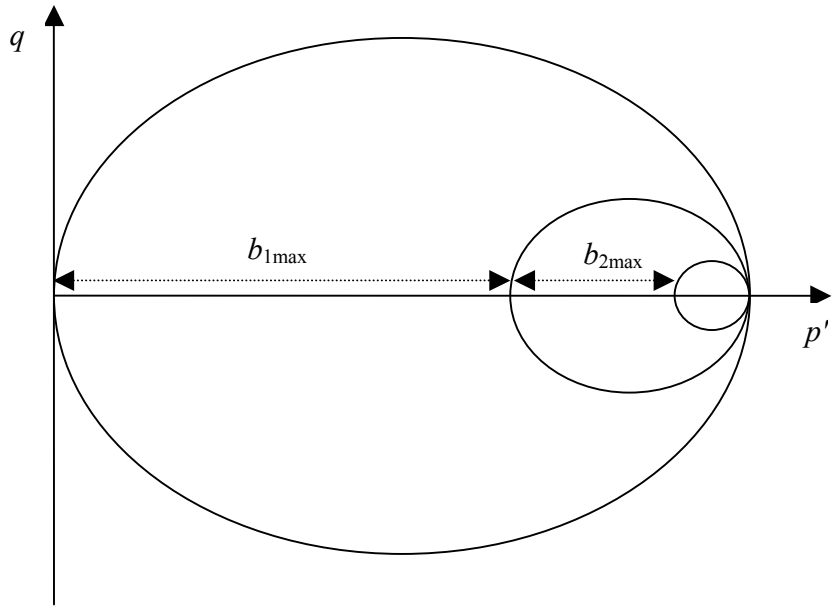

Figure 3.4. Position of the surfaces when b_1 and b_2 are maximum.

When the history and yield surfaces are in contact, i.e.b_2 = 0, the model reduces to the two-surface model developed by Al-Tabbaa (1987). The S^2 term in equation 3.26 is needed to ensure that Al-Tabbaa's model is reproduced when the history and yield surfaces are in contact and p'-p'_b is replaced by $S(p'$-$p'_a)$ in equation 3.28. The parameter T is introduced into equation 3.27 to reduce the value of H_2 in order to predict realistic strains when the stress state is inside the history surface.

3.2.3 Determination of Model Parameters

For the Modified Cam clay model, five parameters are required to define the model:

e_{cs} – The voids ratio on the critical state line when p' = 1kPa.
M – The slope of the critical state line in the $q - p'$ space.
$-\lambda^*$ – The slope of the normal compression line in $\ln v - \ln p'$ space.
$-\kappa^*$ – The initial slope of the swelling line defined in $\ln v - \ln p'$ space.
G_e – The elastic shear modulus.

For the 3-SKH model, three additional parameters are required:

T – The ratio of the size of the history surface to that of the bounding surface.
S – The ratio of the size of the yield surface to that of the history surface.
ψ – The exponent in the hardening function.

Instead of e_{cs}, any point on the isotropic normal compression line or the critical state line can be used to locate the model in $\ln v - \ln p'$ space.

Stallebrass (1997) described a method to determine all the model parameters using simple triaxial tests. All the model parameters, except parameter ψ, can be determined directly. The extra parameters T and S can be determined by isotropic swelling and recompression tests. Atkinson et al. (1990) defined recent stress history by a sudden change in the direction of the stress path or an extended period of rest, and used an angle φ to characterize the recent stress history of soil. The angle φ is the angle of rotation required to follow the new stress path, and is measured positive clockwise (see Figure 3.5), so in Figure 3.5, the angle φ would be negative. Figure 3.6 shows isotropic stress paths for two different stress histories, $\varphi = 0^o$ (O-B-A) and $\varphi = 180^o$ (O-B-A-B-A). The parameters T and S can be obtained by plotting a graph of K' against $\Delta p'$ graph as shown in Figure 3.7. The bulk modulus, K' is the tangent stiffness obtained from the graph of p' against ε_p. The initial stiffness of soil subjected to isotropic swelling ($\varphi = 180^o$) is used to estimate κ^* by plotting K'/p'

against p'/p'_m, where p'_m is the maximum mean effective pressure to which the soil has been loaded and $\kappa^* = p'/K'$. The parameter S is obtained by observing the stress change for which the strains become inelastic, and T is obtained by estimating the change in stress at which the two curves in Figure 3.7 converge.

The parameter ψ is the only parameter, which cannot be measured directly, and is obtained by parametric studies. A value of ψ is chosen such that the experimental results are best fitted.

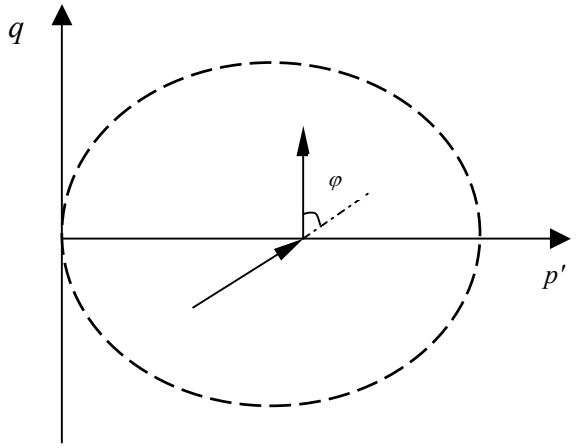

Figure 3.5. Definition of recent stress history (after Atkinson et al., 1990).

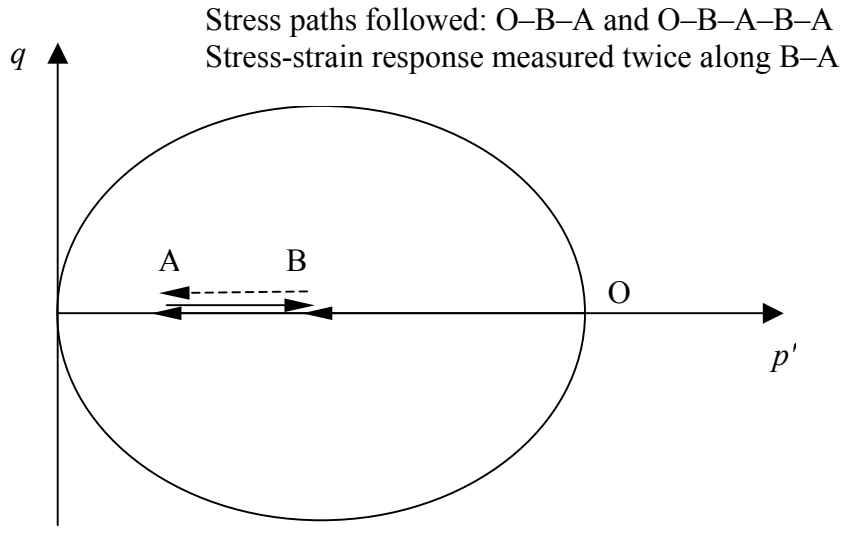

Figure 3.6. Stress paths required to determine parameters T and S (Stallebrass and Taylor, 1997).

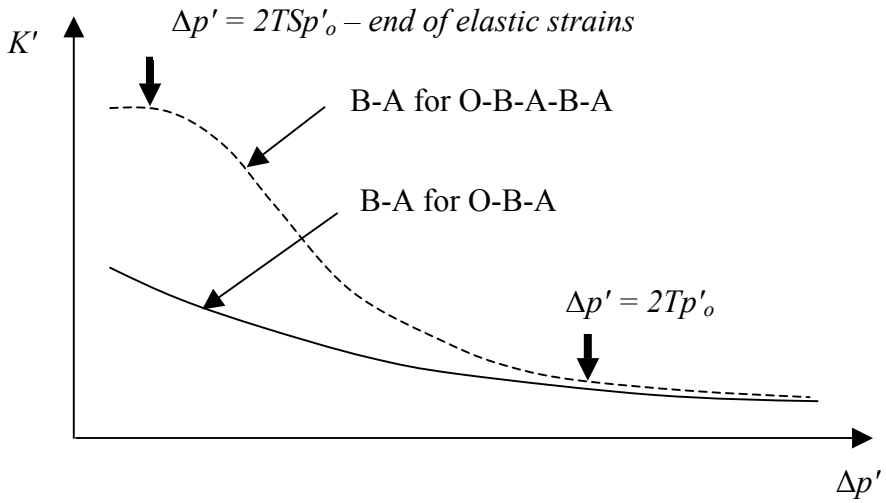

Figure 3.7. Stiffness plots from which T and S can be determined (Stallebrass and Taylor, 1997).

3.3 ONE-DIMENSIONAL LOADING, UNLOADING AND RELOADING

Since the 3-SKH model adopts the Modified Cam clay stress-dilatancy rule, the 3-SKH model will over-estimate the value of K_0 during normal compression and hence shear strain (this is shown in the next section). In this section the ability of the 3-SKH model to predict the earth pressure coefficient was investigated. The results were obtained using the CRISP finite element program with four cubic strain triangular elements and the parameters used in the simulation are those for kaolin from Stallebrass (1997) given in Table 3.1.

M	λ^*	κ^*	e_{cs}	T	S	ψ	G [kN/m^2]
0.89	0.073	0.005	1.994	0.25	0.08	2.5	$1964(p'/p'_r)^{0.65}(p'_c/p')^{0.2}$

Table 3.1. Model parameters for kaolin (Stallebrass and Taylor, 1997).

Figures 3.8 and 3.9 shows the prediction of the 'Bubble' model and the 3-SKH model for $K_{0,nc}$ and K_0 during unloading versus OCR compared to the empirical relationship proposed by Schmidt (1966). The 3-SKH model and the 'Bubble' model

predict a $K_{0,nc}$ value of 0.78 while the experimental value obtained by Al-Tabbaa is 0.69. These models will predict the same value of K_0 during normal compression because all the surfaces are in contact for normally consolidated states and therefore both models reduce to the Modified Cam clay model. The experimental value obtained by Al-Tabbaa is higher than that predicted by the empirical relationship proposed by Jâky (1944) in equation 2.37 with $\phi' = 23°$ for kaolin, which gives $K_{0,nc}$ = 0.61. For K_0 during unloading, Al-Tabbaa found that Schmidt's (1966) equation 2.42, with $\alpha = 0.464$, fitted her data well. It can be seen from Figure 3.8 that the two-surface model predicts a correct trend for K_0 during unloading, $K_{0,u}$ but the value is over-predicted significantly. The 3-SKH model gives a better prediction on unloading, but the value of $K_{0,u}$ is still over predicted (see Figure 3.9). If one-dimensional unloading is started from the correct in-situ stress state i.e. a correct $K_{0,nc}$, the 3-SKH model will give better results. The prediction of K_0 during unloading with a correct $K_{0,nc}$ is shown in Figure 3.10. This shows that a better prediction of K_0 during unloading can be obtained if the analysis starts from the correct $K_{0,nc}$.

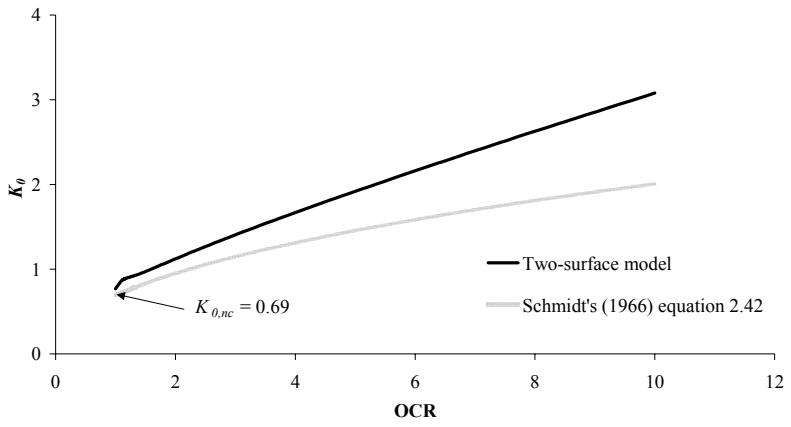

Figure 3.8. Comparison between the two-surface model prediction of K_0 and the empirical relation by Schmidt (1966).

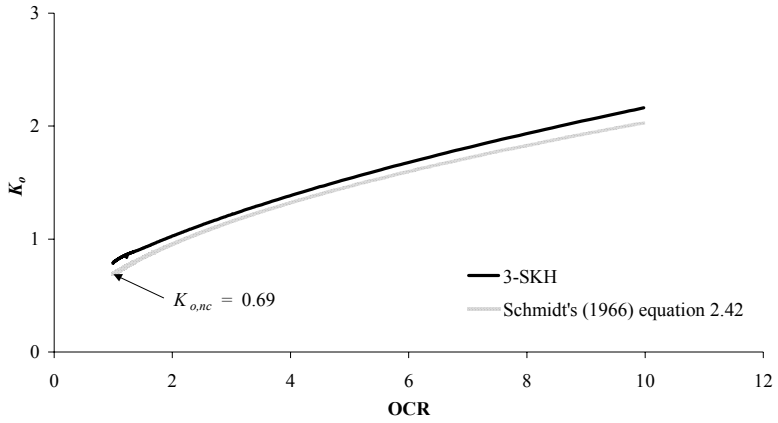

Figure 3.9. Comparison between the 3-SKH model prediction on K_0 and the empirical relation by Schmidt (1966).

Figure 3.10 also presents the predicted variation of K_0 with OCR during reloading for the 3-SKH model, compared with Schmidt's (1983) empirical relation in equation 2.48 with $\alpha = 0.464$. The prediction of K_0 on reloading is slightly overestimated by the 3-SKH model. Al-Tabbaa (1987) found that the variation of K_0 with OCR on reloading could be approximated by a linear relationship. Figure 3.11 shows the variation of K_0 with OCR on reloading predicted by the 3-SKH model for different maximum values of OCR. The model predicts that the slope of the reloading line increases as the maximum OCR decreases indicating that the variation of K_0 with OCR on reloading is dependent on the maximum OCR.

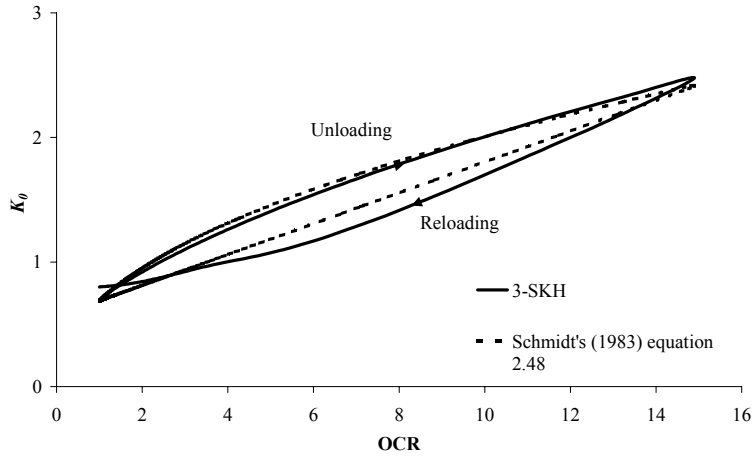

Figure 3.10. Comparison between the 3-SKH model prediction of K_0 using the correct $K_{0,nc}$ with the empirical relationship proposed by Schmidt (1983) during one-dimensional unloading and reloading.

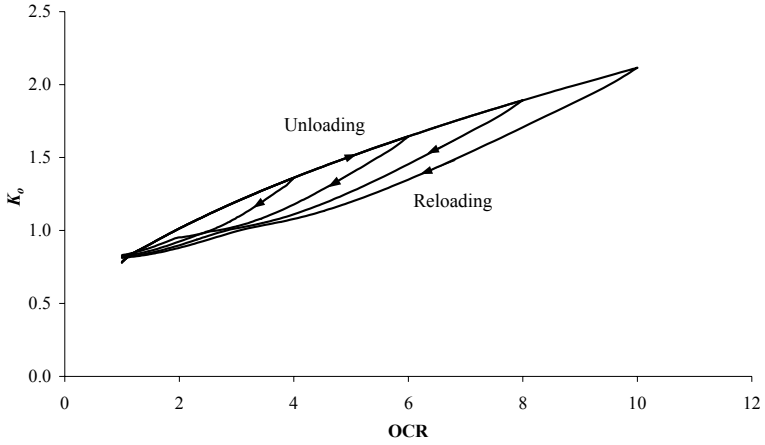

Figure 3.11. The 3-SKH model prediction of K_0 on reloading for different maximum values of OCR.

3.4 CYCLIC LOADING

The 3-SKH model has been shown to be able to predict the essential features of soil behaviour under monotonic loading (Stallebrass and Taylor, 1997). A preliminary evaluation of the model's ability to predict soil behaviour under cyclic loading was performed using the finite element program CRISP (Britto and Gunn, 1987). In this section, the ability of the 3-SKH model to predict soil behaviour under repeated loading is investigated for different stress histories.

In order to simulate the pavement subgrade under cyclic loading, thousands of cycles have to be applied. CRISP, as purchased, was not suitable for analysing cyclic loading with a large number of cycles because every applied load has to be generated manually. Without modification to the program, it is very tedious and time consuming to generate large numbers of cycles. A computer program, which is able to generate large numbers of cycles automatically by modifying the input file, was written by the CRISP Technical Support for the purpose of this project. This greatly reduces the amount of time required to generate a large number of load cycles.

3.4.1 Model Predictions for Repeated Loading

The model predictions for drained cyclic loading behaviour are investigated in this section. Some existing drained cyclic loading test data on kaolin performed by Al-Tabbaa (1987) was used to compare with the 3-SKH predictions for these tests. Figure 3.12a shows the data for a drained cyclic test on normally consolidated kaolin; the soil was consolidated isotropically to p' = 300kPa and then loaded cyclically between stress ratios η of 0 and 0.34 at constant cell pressure.

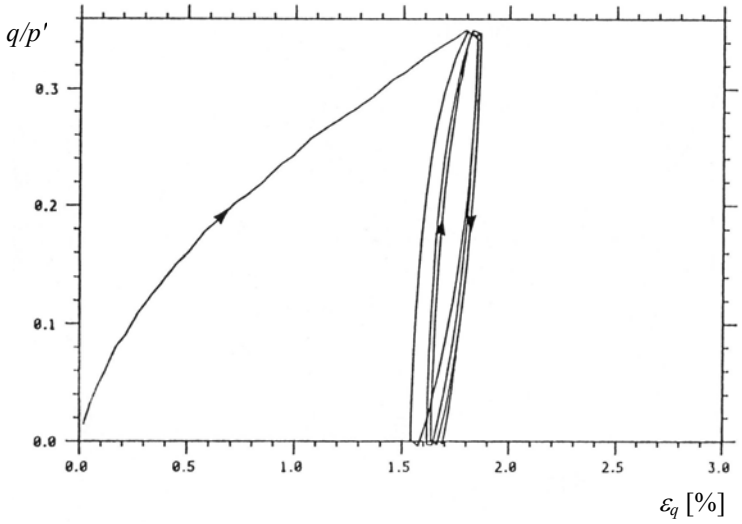

(a)

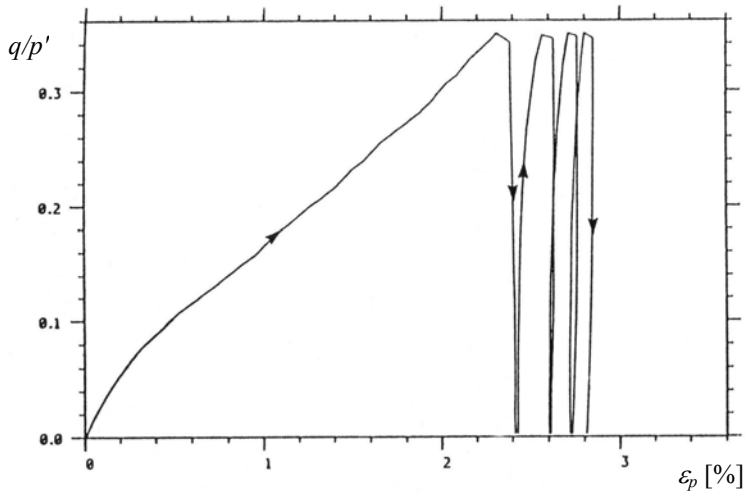

(b)

Figure 3.12. Drained cyclic triaxial test on normally consolidated kaolin (Al-Tabbaa, 1987) (a) q/p' versus ε_q and (b) q/p' versus ε_p.

Figures 3.13 and 3.14 show the predictions by Al-Tabbaa's model and the predictions by the 3-SKH model respectively. Both the models predict the right trend for shear strain and volumetric strain; however, the shear strain was greatly over predicted after four cycles. The shear strain predicted by the 3-SKH model is worse than that of Al-Tabbaa's model because of the smaller elastic region and different values of ψ used by Al-Tabbaa (1987) and Stallebrass (1990). The experimental result shows that the shear strain stabilized but both of these models cannot predict this. The volumetric strain predicted by the models is, however, reasonable. It should be noted that the parameters used in Figure 3.13 are those quoted by Al-Tabbaa (1987) for kaolin, whilst those used in Figure 3.14 are those quoted by Stallebrass (1990).

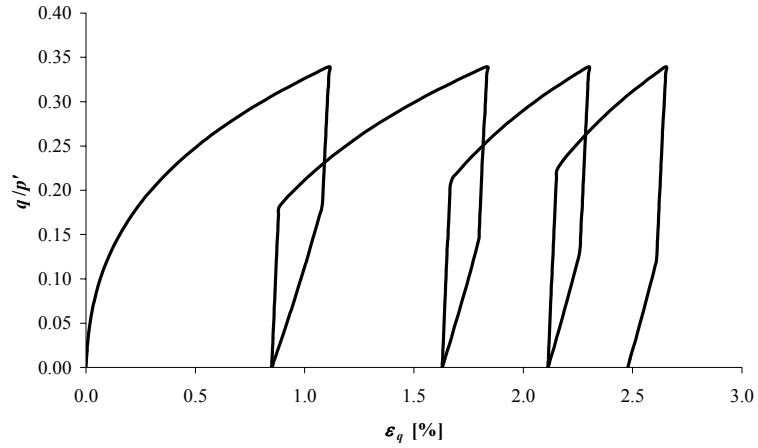

(a)

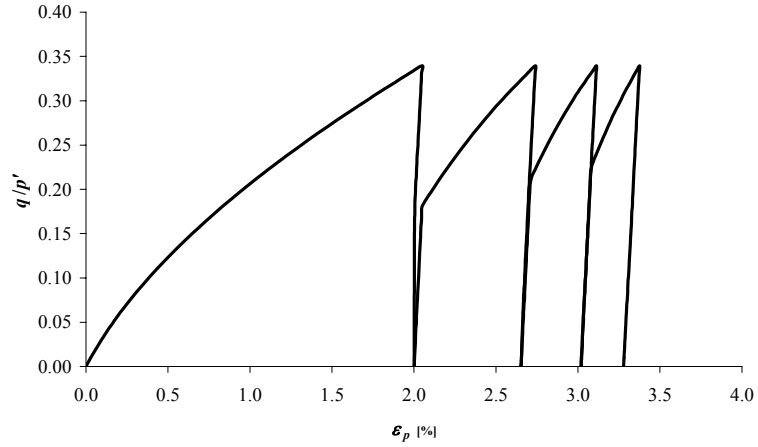

(b)

Figure 3.13. Two-surface model predictions for the test in Figure 3.12 (Al-Tabbaa, 1987), (a) q/p' versus ε_q and (b) q/p' versus ε_p.

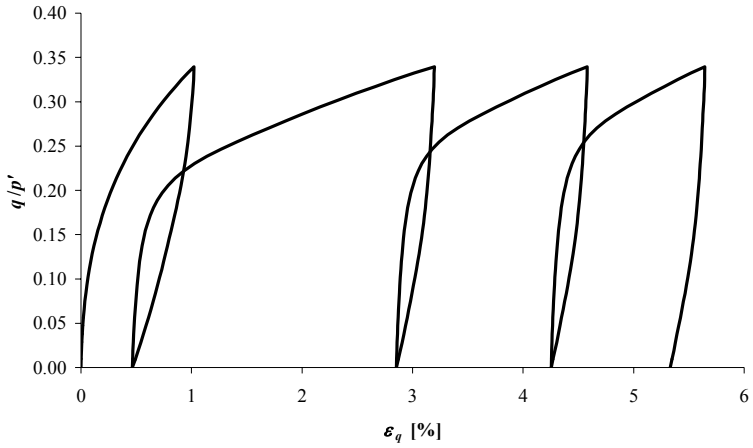

(a)

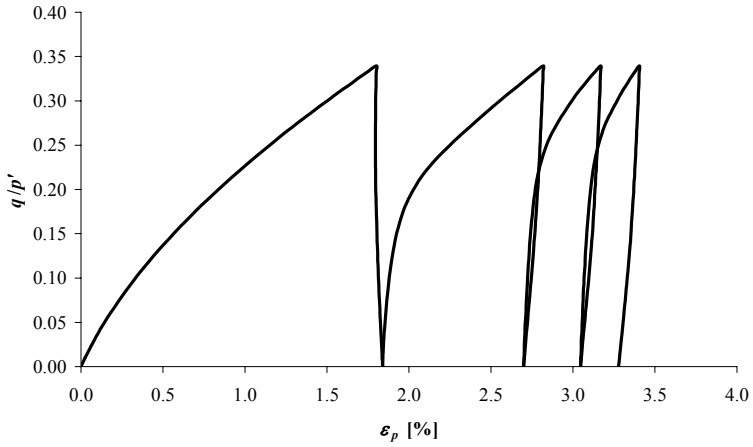

(b)

Figure 3.14. The 3-SKH model predictions for the test in Figure 3.12, (a) q/p′ versus ε_q and (b) q/p′ versus ε_p.

Figure 3.15 shows another drained cyclic test result from Al-Tabbaa (1987) on overconsolidated kaolin. The soil was unloaded isotropically to p' = 100kPa from p'_c = 300kPa and cyclically loaded between values of $\eta = 0$ and $\eta = 0.78$ (Al-Tabbaa, 1987). The predictions by Al-Tabbaa's model and the 3-SKH model are shown in Figures 3.16 and 3.17 respectively. Both Al-Tabbaa's model and the 3-SKH model over-predict the shear strain, but the prediction by the 3-SKH model is worse than that predicted by the two-surface model. This is because of the inclusion of a smaller yield surface, which causes the size of the bounding surface, p'_c to decrease significantly during isotropic unloading, and also because of the different values of ψ used by Stallebrass (1990) and Al-Tabbaa (1987). A value of ψ of 2.5 was found

from parametric studies to be suitable for reconstituted kaolin by Stallebrass (1990), whilst a ψ value of 1.5 was chosen by Al-Tabbaa (1987) to best fit data using her two-surface model. It should be noted that this curve-fitting parameter might need to be adjusted to better model the behaviour of soil under cyclic loading, especially if any further amendments to the model are made.

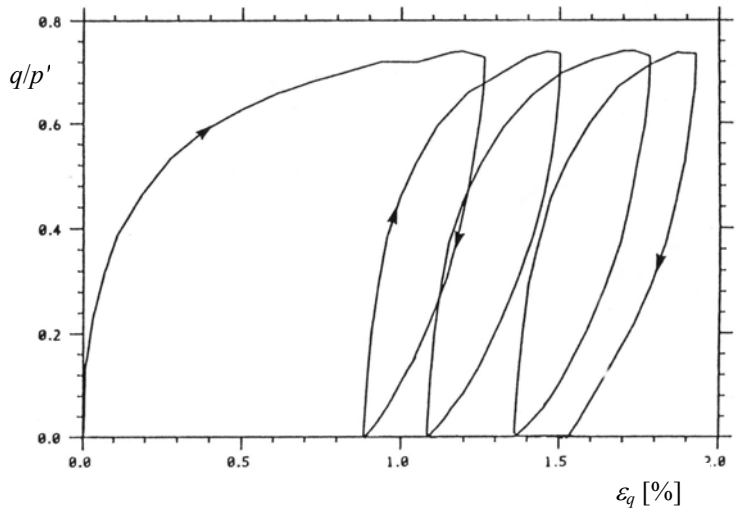

(a)

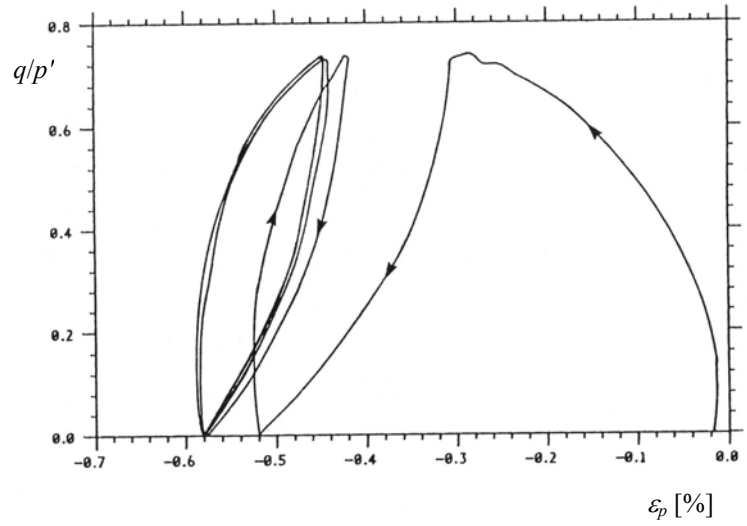

(b)

Figure 3.15. Drained cyclic test result on over consolidated kaolin (Al-Tabbaa, 1987), (a) q/p' versus ε_q and (b) q/p' versus ε_p.

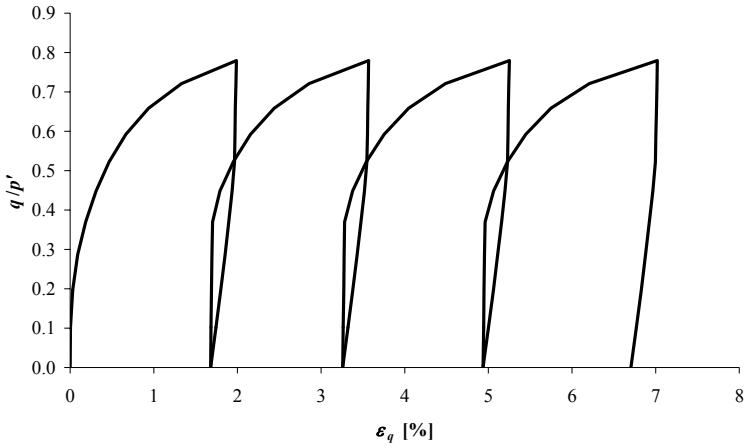

(a)

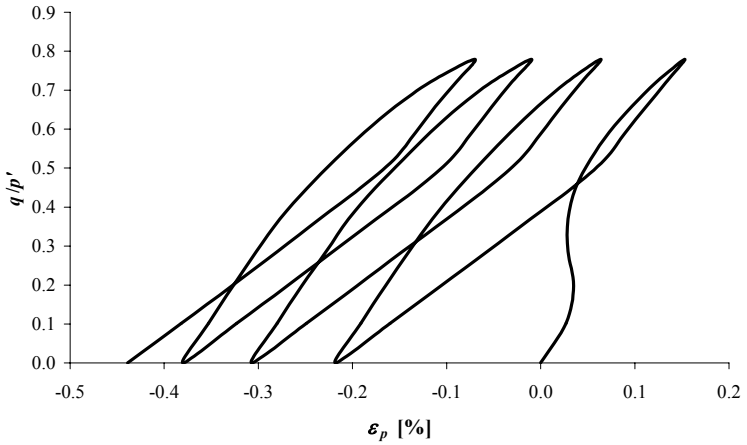

(b)

Figure 3.16. Two-surface model predictions for the test in Figure 3.15 (Al-Tabbaa, 1987), (a) q/p' versus ε_q and (b) q/p' versus ε_p.

Figure 3.18 shows the result of a drained cyclic load test at constant mean effective stress on kaolin, the details of which can be found in Stallebrass (1990), together with the prediction of the 3-SKH model. It can be seen that, again, the model over-predicts the shear strain produced on primary loading and reloading but the model appears to predict well the change in shear strain caused by unloading.

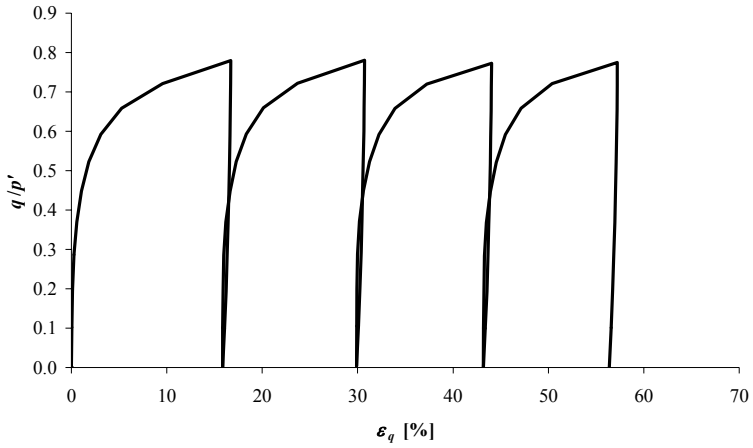

(a)

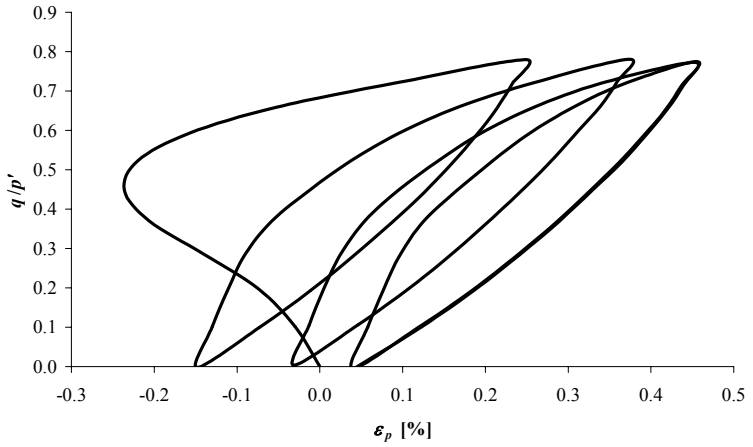

(b)

Figure 3.17. The 3-SKH model prediction for the test in Figure 3.15, (a) q/p' versus ε_q and (b) q/p' versus ε_p.

From the above comparisons of two-surface and 3-SKH model predictions of drained cyclic soil behaviour, it can be seen that both models over-predict shear strain. This problem is magnified when attempting to model cyclic loading behaviour over many cycles, where too much shear strain will accumulate. This will, of course, apply to the modelling of pavement subgrades: A typical three-layer pavement problem was analysed and too much permanent deformation was predicted using the 3-SKH model. The results of this analysis are presented in Section 3.5.

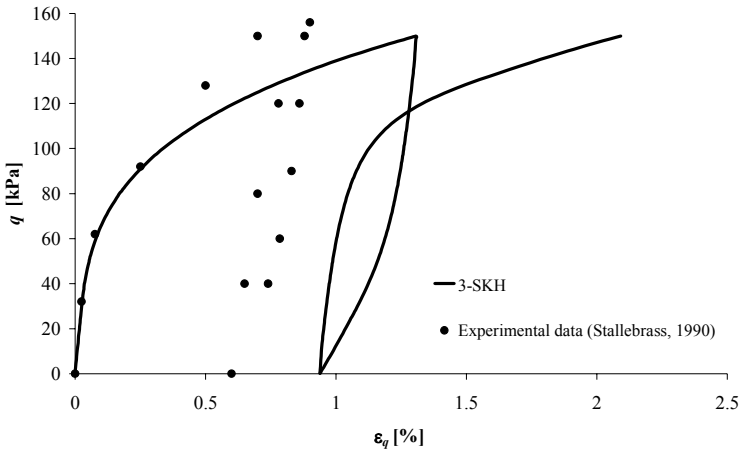

Figure 3.18. Constant p' test and prediction by the 3-SKH model (Stallebrass, 1990).

3.4.2 Accumulation of Negative Shear Strain

The 3-SKH model (in addition to the two-surface model) suffers a major drawback. It was found that the model would predict an accumulation of negative shear strain, which is not observed experimentally, under some stress conditions. To investigate this phenomenon, conventional drained cyclic triaxial simulations were performed on isotropically normally consolidated soil with a pre-consolidation pressure p'_c = 500kPa. A deviatoric stress q of 0–50kPa was applied for five cycles. Figure 3.19 shows the predicted result of deviatoric stress versus shear strain. It can be seen that the shear strain decrement during the unloading part of the cycle is greater than the increment during the loading part of the cycle, due to the sudden decrease of the stiffness on unloading, and for subsequent cycles the shear strain becomes more negative. The rate of increase of negative shear strain is most serious during first unloading.

The reason for the accumulation of negative shear strain is that the shear strain developed during unloading is larger than that developed during loading. This occurs when the stress state hits the bottom of the yield surface shown in Figure 3.20.

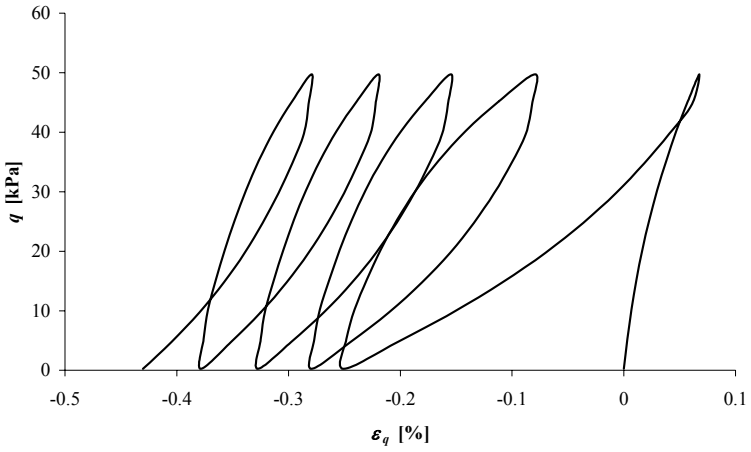

Figure 3.19. Stress-strain curve showing the accumulation of negative shear strain predicted by the 3-SKH model.

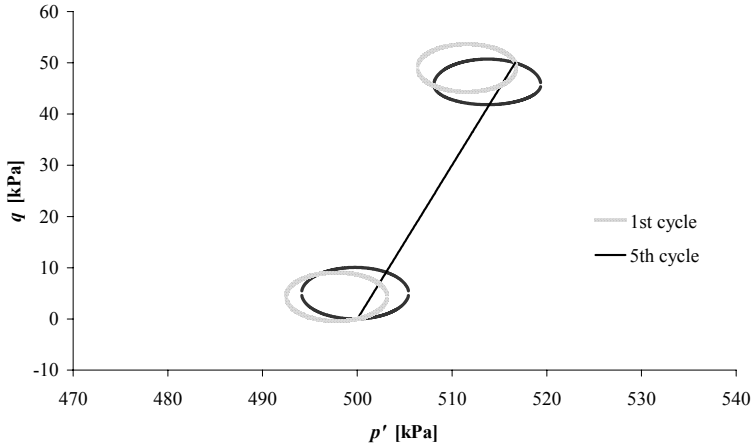

Figure 3.20. Positions of the yield surface during cyclic loading.

Figure 3.21 shows the plastic strain increment vector on the yield surface on loading and unloading when the stress pulse is cycling between two points, where the plastic increment strain ratio, $\delta\varepsilon_p^p/\delta\varepsilon_q^p$ is very large on loading compared to that on unloading. Since the model is a volumetric hardening model, volumetric strains tend to stabilise as p'_o stabilises, so the increase in shear strain is ultimately the same for each cycle. Hence the large value of $\delta\varepsilon_q^p/\delta\varepsilon_p^p$ on unloading means that the shear strain on unloading is greater than the shear strain on loading. The negative shear strain problem is the most significant during first unloading in this case. On first loading, because the applied stress ratio is small, the value of q-q_b (the vertical distance of the stress state to the centre of the yield surface in $q - p'$ space) is much

smaller than that on the subsequent unloading. Figure 3.20 shows the positions of the yield surface at the end of first loading and unloading. From this figure it can be seen that the stress state hits the yield surface at a point which would give a large negative value of q-q_b compared to that at the end of first loading. This will tend to generate large negative shear strain. The H_1 and H_2 terms would help to prevent this problem, but for small stress levels these two terms are not large enough to compensate the loss of stiffness when the stress state hits the yield surface on unloading. The variation of plastic hardening modulus during loading and unloading is shown in Figure 3.22. During loading, both H_1 and H_2 are zero because all the surfaces are in contact. During unloading, h_o decreases due to the smaller value of p'-p'_b and large negative value of q-q_b on unloading (see equation 3.24). The hardening modulus H_1 is increasing because of the increase of p'_o, and during unloading the stress state never reaches the history surface, so b_1 is increasing due to the increase of p'_o. During unloading, H_2 is increasing at the beginning and decreasing after a certain value. This is because of the decrease of b_2 and the increase of p'_o during unloading. The increase in p'_o is insufficient to overcome the decrease in b_2, hence H_2 increases and then decreases. For larger applied cyclic deviatoric stresses, the H_1 and H_2 terms are large enough to prevent the negative shear strain problem because the distance of the current stress point to its conjugate stress points at the bounding surface and history surface, b_1 and b_2 respectively, are larger and the size of the bounding surface, p'_o also increases. It should be noted that the increase in p'_o will also increase the values of $b_{1\max}$ and $b_{2\max}$. However, the rate of increase in b_1 and b_2 is larger than the rate of increase in $b_{1\max}$ and $b_{2\max}$, so there is an overall increase in the ratios of b_1 and b_2 to their maximum values.

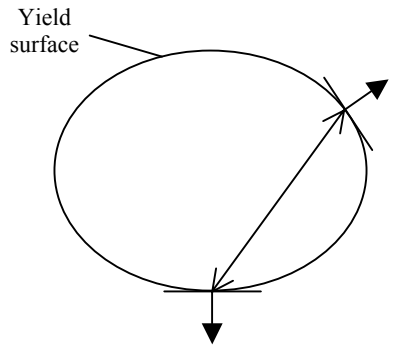

Figure 3.21. Schematic diagram showing the yield surface and the plastic strain increment vectors.

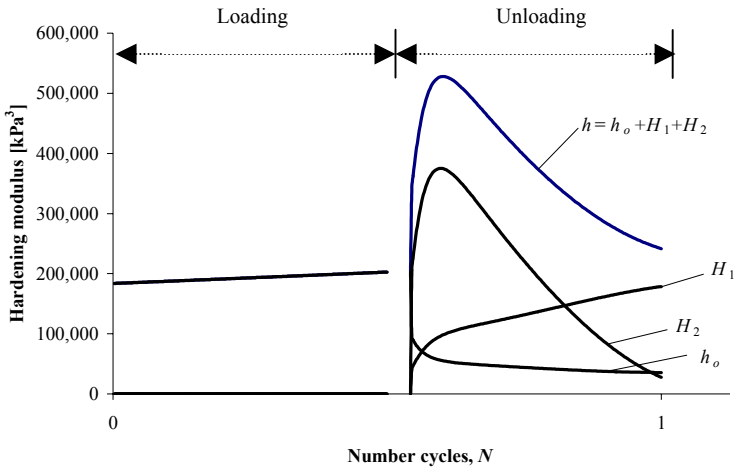

Figure 3.22. Plastic hardening modulus during loading and unloading.

The effect of the model parameters and stress level on the accumulation of negative shear strain was investigated by conducting a series of conventional drained cyclic triaxial simulations on normally consolidated soil. The graphs of shear strain versus number of cycles, N, are plotted in Figure 3.23-28. These graphs show the effects of stress level and model parameters, S, T, ψ, κ^*, λ^* on the accumulation of negative shear strain.

Figures 3.23 (a) and (b) shows the effect of the applied stress level on the generation of negative shear strain during unloading. There appears to be a stress level where the shear strain generated during loading is equal to that generated during unloading, and hence at this stress level, there is no accumulation of shear strain. Generally the negative shear strain problem vanishes when larger stresses are applied.

Figures 3.24–3.28 show the effect of varying model parameters. In general, for each simulation, the values of the parameters are those in Table 3.1, except for the parameter being varied. In Figure 3.27, S is allowed to vary so that TS is constant (i.e. constant size of elastic region relative to the bounding surface). It can be seen that the generation of negative shear strain is relatively insensitive to the parameters κ^* and λ^*. Changing the parameters T, S or ψ will have a more influential role on the shear strain.

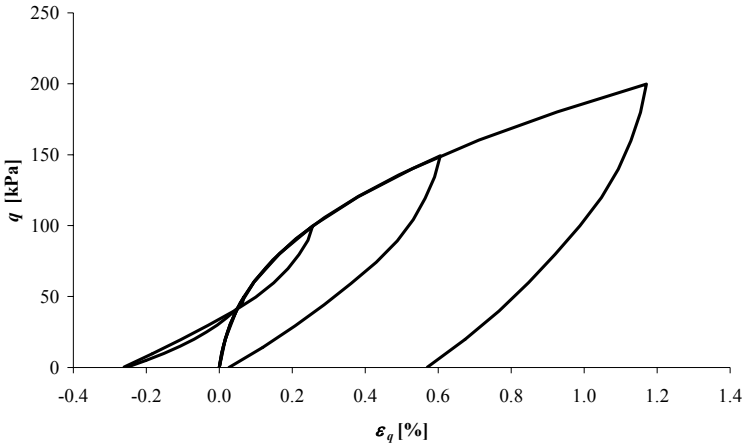

(a)

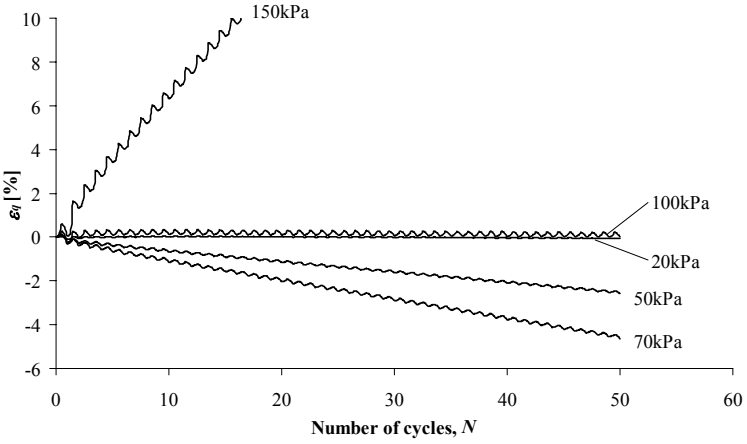

(b)

Figure 3.23. Effect of stress level on the generation of negative shear strain, (a) stress-strain response and (b) shear strain as a function of number of cycles.

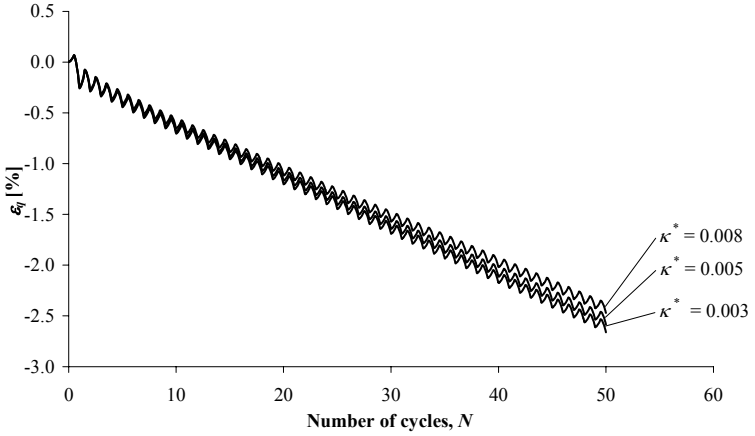

Figure 3.24. Shear strain versus number of cycles for different κ^*.

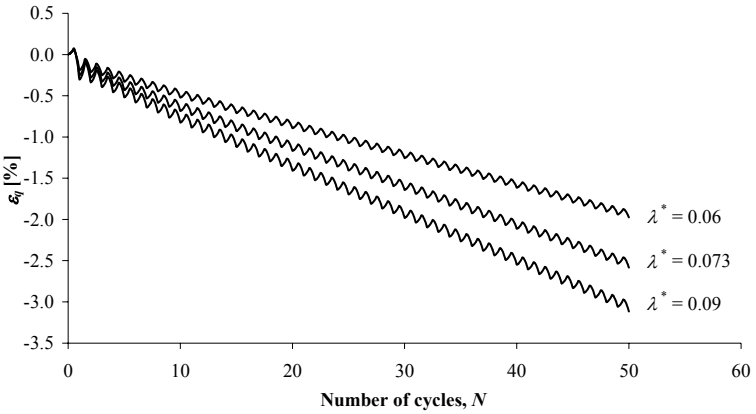

Figure 3.25. Shear strain versus number of cycles for different λ^*.

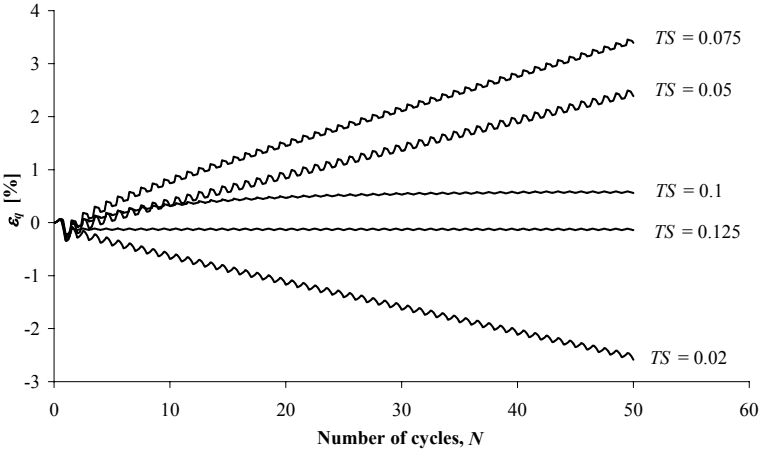

Figure 3.26. Shear strain versus number of cycles for different sizes of yield surface (for constant T = 0.25).

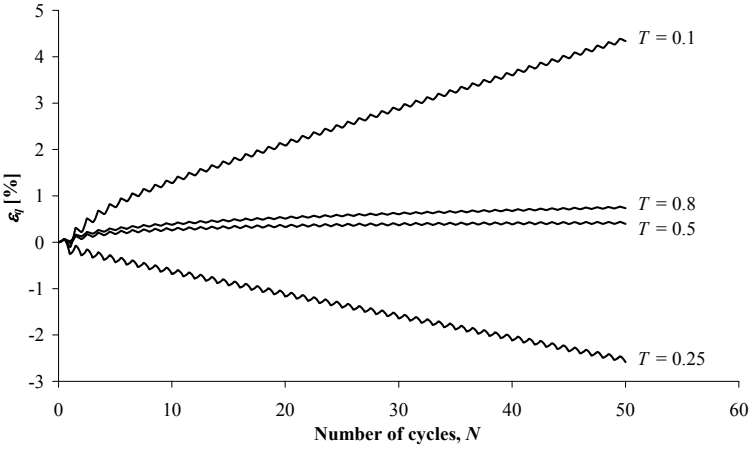

Figure 3.27. Shear strain versus number of cycles for different sizes of history surface (TS = 0.02).

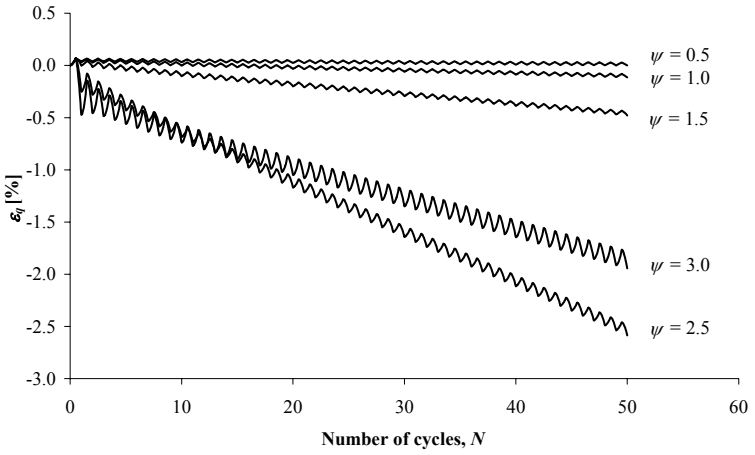

Figure 3.28. Shear strain versus number of cycles for different values ψ.

3.5 THREE-LAYER PAVEMENT: RESILIENT AND PERMANENT DEFORMATIONS

In this section the application of the 3-SKH model to the prediction of pavement deformation is presented. It will be shown that the 3-SKH model is capable of predicting both the resilient and permanent deformation of a pavement.

3.5.1 Resilient Deformation: BISAR vs CRISP

The theory of elasticity has been extensively applied to the analysis of layered pavement systems. Various computer programs have been developed to analyse pavements. The most widely used layered elastic program in pavement engineering is BISAR, developed by Shell (Shell International Petroleum Company, 1978) – see Section 2.4. Pavement layers are assumed to be linear elastic. A constant value of Young's modulus E' and Poisson's ratio μ', are assigned to each layer. The design criteria are to limit the maximum resilient tensile strain at the bottom of the asphalt layer and the maximum resillient compressive strain at the top of the subgrade. The stiffness of the subgrade is estimated from a purely empirical relationship based on CBR value of the subgrade. Brown et al. (1987), however, demonstrated that the stiffness is not a simple function of CBR.

An attempt was made to compare the results of the 3-SKH model in CRISP with results from the layered elastic program, BISAR, which required calculating typical vertical stress changes in the pavement using CRISP, and applying many cycles of these stress changes to triaxial samples of 3-SKH clay in order to obtain an equivalent stiffness for input to the elastic model.

A typical three-layer pavement was analysed using CRISP. The three-layer pavement consisted of 50mm of bituminous material over 200 – 600mm of granular material (sub-base) and 10m of clay (subgrade). The pavement was assumed to be constructed in a 'cut' condition with typical stress history as shown in Figure 3.29. The model subgrade was initially one-dimensionally swelled (due to erosion) from a normally consolidated state with a value of $K_{0,nc}$ of 0.69, and re-compressed to model re-deposition and construction of a pavement. This is a typical stress history for a pavement. The swelling and recompression stress paths were applied by removing and applying an overburden stress on the surface of the subgrade under drained conditions. The maximum effective vertical pressure, σ'_v, was assumed to be 500kPa and the change in effective vertical stress due to erosion and re-deposition, $\Delta\sigma'^{e}_{v}$ and $\Delta\sigma'^{r}_{v}$ are -450kPa and 70kPa respectively. No attempt was made to simulate a particular stress history for an existing real pavement.

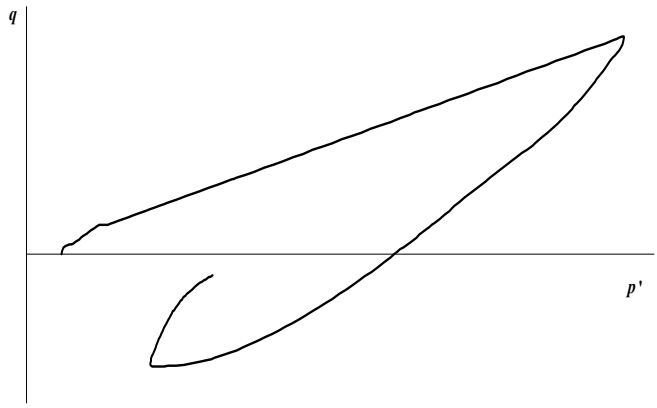

Figure 3.29. Typical stress history of a three-layer pavement.

Six-node linear strain triangular elements were used in the pavement analysis. For the vertical boundary, radial displacements were restrained and vertical displacements were allowed. For the horizontal boundary, both radial and vertical

displacements were restrained. The vertical boundaries were 5m from the axis of symmetry and the depth of the mesh was 10m. It was shown by Almeida (1993) that if the horizontal boundary is positioned at a distance away from the centreline of the load of 20 times the radius of the load and the vertical boundary is positioned at a distance away from the load of 50 times the radius of the load, then the boundary conditions will not significantly affect the results. The effect of boundary on the results for the pavement analyses performed in this research was found to be insignificant.

The 3-SKH model was used to model the subgrade layer, and isotropic homogenous linear elastic behaviour was assumed for the bituminous and granular layers. The bituminous layer was assumed to have a Young's modulus E' = 5,000MPa, Poisson's ratio μ' = 0.35 and for the granular material values of E' = 100MPa, μ' = 0.3 were assumed. These are the typical values used in pavement analysis (Brown & Pappin, 1981). The parameters used for the 3-SKH model are shown in Table 3.1.

A typical wheel load of 42.4kN and radius of 0.15m, giving an applied surcharge of 600kPa, was applied at the top of the bituminous layer. In the pavement analysis, it is difficult to know whether a drained or undrained analysis is appropriate. If the subgrade is fully saturated, then the application of a single wheel load would cause undrained deformation followed by consolidation. The passage of many wheel loads makes this process even more complicated. It was considered to be currently too time-consuming to perform a fully coupled consolidation analysis using CRISP with the 3-SKH model. Furthermore, most subgrades are likely to be partially saturated, in which case the behaviour may be more drained than undrained. In any case, it was considered that the fully drained analysis was more relevant to the long term behaviour of a pavement than an undrained analysis, and hence only drained analyses of the pavement problem have been examined.

The vertical effective stress changes during the first cycle at different depths in the subgrade were computed. The increase in effective vertical stress due to the first application of wheel load was then applied as a deviatoric stress increment to a triaxial sample in CRISP with a similar initial stress history for 50 cycles. Changes

in horizontal stress were not applied to the triaxial sample. The resilient bulk modulus K', and shear modulus G', for the 50th cycle were then computed for unloading. The parameters, E' and μ', needed in BISAR were then calculated. To accommodate the variation of stiffness with depth, the subgrade was sub-divided into three layers of thickness 0.26m, 0.9m and 8.84m, and the Young's modulus was calculated at the centre of each layer. Figure 3.30 shows the three-layer pavement and the locations where the Young's modulus were computed. The Young's moduli obtained for each sub-layer of subgrade with different thicknesses of granular material are shown in Table 3.2. It can be seen that the estimated Young's modulus for the clay increases with increasing granular layer thickness. This illustrates that the model is able to estimate the stiffness of the subgrade, which is stress-dependent. The stiffness at the top layer varies quite markedly with thickness of granular material compared to the lower layers as the vertical stresses in these two lower layers are very small and the soil at these depths is almost elastic except for the case where the granular material is 200mm thick, where the stiffness of the middle layer is about 20% lower.

Stallebrass (1990) found from her experimental data that the Poisson's ratio obtained using equation 2.4 and 2.5 is either extremely small or negative. However, this may be improved by adjusting the model parameter κ^* in the 3-SKH model. The parameter κ^* was determined from the initial stiffness of soil subjected to isotropic swelling with the stress path rotation of 180°. The initial stiffness is not very reliable because measuring stiffness at very small strains is difficult. Therefore the parameter κ^* can be adjusted, since it cannot easily be determined accurately by experiment. However, by adjusting the parameter κ^*, the Poisson's ratio obtained was still either extremely small or negative. A 'resilient Poisson's ratio' could be derived from resilient values of shear and bulk modulus after 50 cycles. However, the value of Poisson's ratio found in this way was found to be unrealistic. This is because it cannot be expected that the resilient values of G', K', E' and μ' will be consistent with isotropic elasticity, when the material is not elastic. Therefore, for the elastic analysis performed in this study, the Poisson's ratio of the subgrade was taken to be 0.3. This is consistent with the value found by Al-Tabbaa (1987) to best fit her two-surface model with a much larger elastic region. The stress distribution at the top of the

subgrade clay (i.e. at the top integration points) in a three-layer pavement due to an applied wheel load was computed, and is shown in Figure 3.31. This stress distribution was then applied to the surface of the clay subgrade for 51 cycles as shown in Figure 3.32. The stress change due to the applied wheel load is compared with the stress change due to the equivalent stress blocks in Figure 3.31.

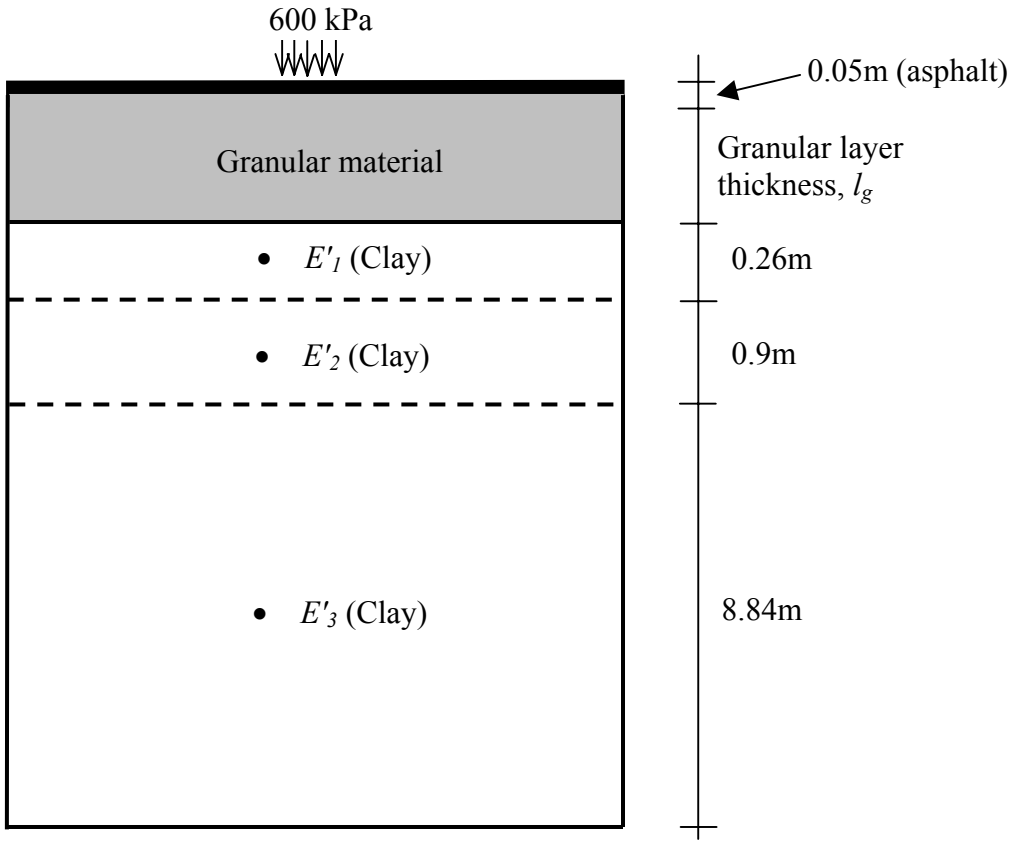

Figure 3.30. Schematic diagram showing the locations where the Young's moduli, E' are determined in the subgrade.

Granular layer thickness, l_g (mm)	**200**	**250**	**350**	**400**	**500**	**600**
E_1' (MPa)	39	45	55	59	64	68
E_2' (MPa)	82	97	98	100	100	100
E_3' (MPa)	101	101	101	101	101	101

Table 3.2. Stiffness of subgrade at centre of each layer for different granular layer thicknesses.

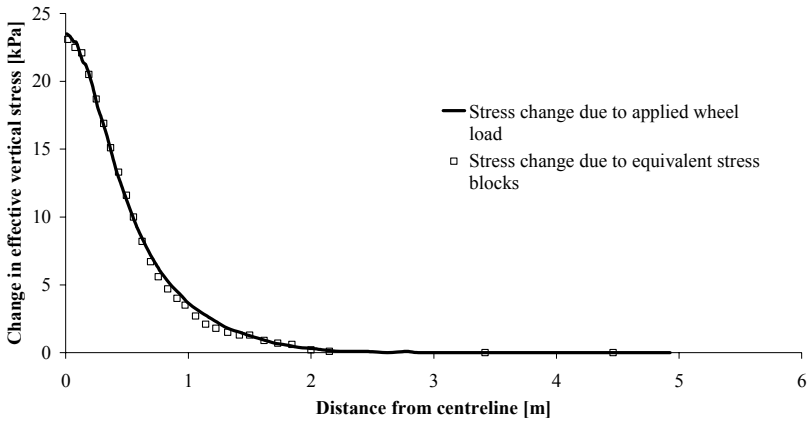

Figure 3.31. Stress distribution near the surface of the subgrade when a typical wheel load is applied at the surface of the bituminous layer.

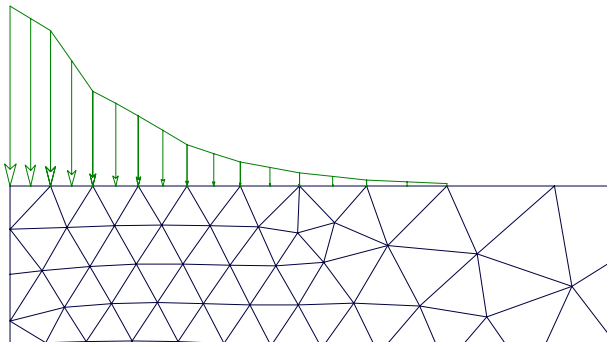

Figure 3.32. Equivalent stress blocks applied at the surface of the subgrade.

The quasi-elastic settlement caused by imposing the load on the 51st cycle was compared with the surface settlement calculated by BISAR using the elastic parameters determined from CRISP using the 3-SKH model. Figure 3.33 shows the typical surface profile for the 200mm granular material pavement with 50mm of asphalt material on top predicted by the 3-SKH model at 50th unloading followed by loading and unloading. It can be seen from this figure that the model is able to predict both the resilient (quasi-elastic) response over one application of wheel load, and accumulation of permanent deformation over many cycles. Figure 3.34 presents the quasi-elastic settlement predicted by the 3-SKH model at the 51st loading and the settlement predicted by BISAR (elastic analysis). The results show that the 3-SKH model predictions deformation on loading are slightly larger than the results of the BISAR elastic analysis; however they are in good agreement. The plastic strain predicted by the 3-SKH model is responsible for the larger quasi-elastic settlement

for the 51st loading predicted by CRISP compared to that predicted by the elastic analysis. Because of this, it can be seen from Figure 3.34 that the difference between the 3-SKH prediction and the prediction from the elastic analysis is becoming smaller as the thickness increased. The resilient deformation (i.e. recovered on unloading, 51st unloading) predicted by the 3-SKH is also shown in Figures 3.33 and 3.34. As can be seen from Figure 3.34, the predicted resilient deformation is closer to that predicted by the elastic analysis. This is because the stiffness calculated for BISAR was the resilient modulus (i.e. on unloading). From the results shown, it can be concluded that the 3-SKH model may be used to estimate the stiffness of the subgrade for input to a layered elastic program such as BISAR instead of estimating the stiffness from CBR values based on the empirical relationships.

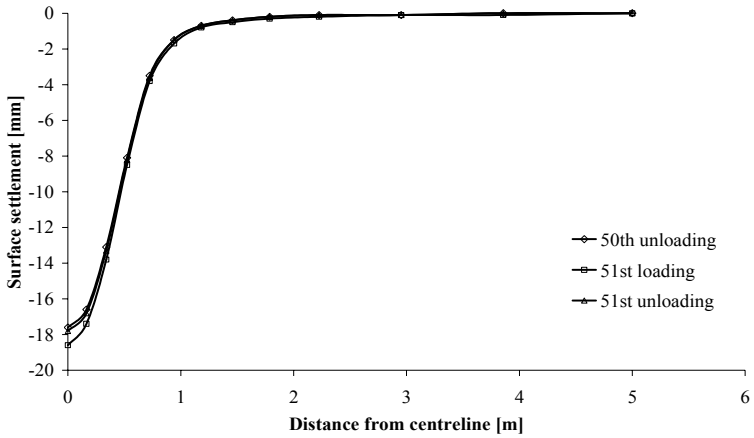

Figure 3.33. Surface profile predicted by the 3-SKH model showing the permanent and resilient response of a pavement with 200mm granular material.

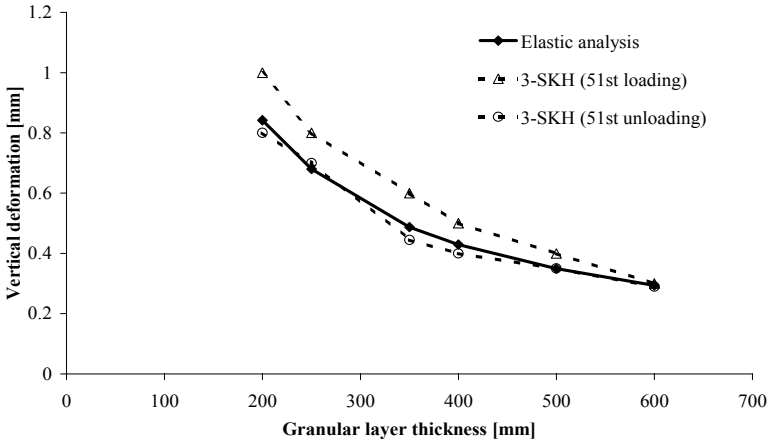

Figure 3.34. Comparison between the 3-SKH model prediction and BISAR for quasi-elastic settlement.

3.5.2 Permanent Deformation

One of the failure mechanisms in pavements is rutting, caused by the permanent deformation of the pavement layers. For lightly-trafficked pavements, the bituminous layer is relatively thin. Hence, the permanent deformation in the subgrade is assumed to contribute most to the formation of rut, as the vertical stresses in the subgrade layer are higher. The granular material and asphalt are assumed to settle with the subgrade in the long term. Some additional permanent deformation may also occur in the granular material, but the approximation has been made here that this does not occur. Brown (1996) reported that for thinly surfaced pavements, permanent deformations are likely to occur in the granular layer and subgrade. He also reported the pavement experiments by Little (1993), where up to a third of the surface rut was contributed by the granular layer, but there were cases where the subgrade was entirely responsible for the deformation.

The major advantage of the kinematic hardening models is the ability to predict the accumulation of strains under cyclic loading. In this section, the model predictions of a typical three-layer pavement problem are presented. The three-layer pavement consists of 100mm of bituminous material over a layer of granular material (sub-base) and clay (subgrade). The bituminous and granular layers were modelled as isotropic linear elastic, and the subgrade was modelled using the 3-SKH model. The parameters used for the 3-SKH model are given in Table 3.1. A typical constant wheel pressure of 600kPa was applied at the top of the bituminous layer and the problem is axi-symmetric. This analysis presents a fundamental modeling problem: if the material above the subgrade is assumed to be elastic, and the nodes are common at each material interface, the elastic layers will pull the subgrade into tension each time the pavement is unloaded. This can be overcome by calculating the stress distribution applied at the top of the subgrade during the first application of load, and then applying cycles of this stress distribution at the top of the clay alone for many cycles and calculating the permanent deformation. It must then be assumed that the granular and asphalt layers will follow the surface of the clay in the long term. Since it is the long-term behaviour that is of interest, the clay has been assumed to be fully drained.

The calculated stresses were used to apply equivalent stress blocks at the surface of the subgrade as shown in Figure 3.32, to approximate the stress distribution at the surface of the subgrade due to the application of wheel load. Figure 3.31 shows the stress distribution due to the first application of load at the integration points nearest to the top of the subgrade. This will mean that the stresses at the integration points due to the applied stress blocks at the top of the clay alone will be slightly less than those due to the first application of load as shown in Figure 3.31. In reality, the bituminous and granular layers will not pull the soil into tension, and hence the permanent settlement predicted by applying several rectangular stress blocks to the surface of clay ought to give a more realistic result.

Figures 3.35, 3.36 and 3.37 show the predicted permanent settlement, rate of settlement, and surface profile of the pavement subgrade respectively for different thicknesses of granular layer as a function of number of cycles. As expected, a thicker layer of granular material gives less settlement and a smaller rate of settlement. The rut depth predicted by the model is considered to be too large (60mm after 1,000 cycles for a 150mm granular layer). This is because the model over-predicts shear strain significantly, as has already been shown in Section 3.4.1.

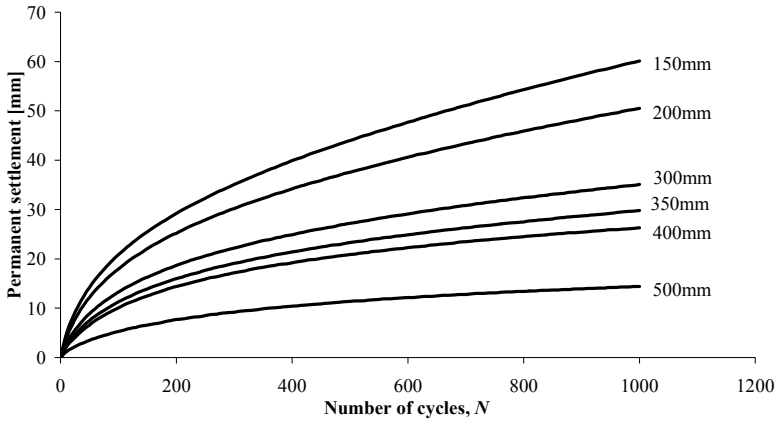

Figure 3.35. Model predictions for a one-layer pavement with equivalent stress distribution applied at the surface of the subgrade, showing the effect of granular layer thickness on the predicted permanent settlement as a function of number of cycles.

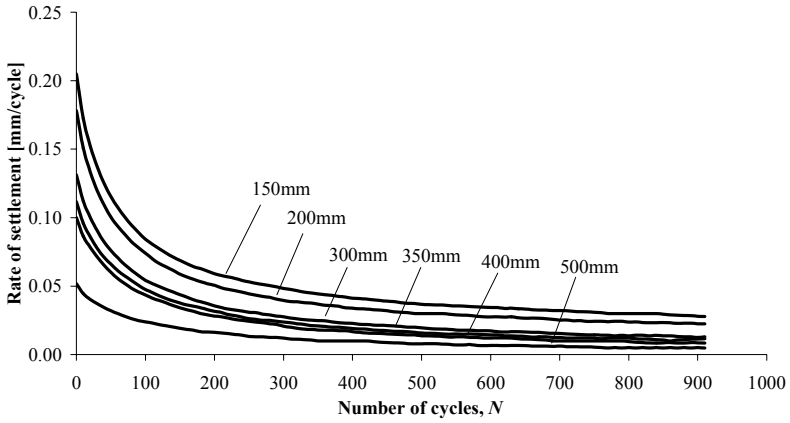

Figure 3.36. Model predictions for a one-layer pavement with equivalent stress distribution applied at the surface of the subgrade, showing the effect of granular layer thickness on the rate of settlement with number of cycles.

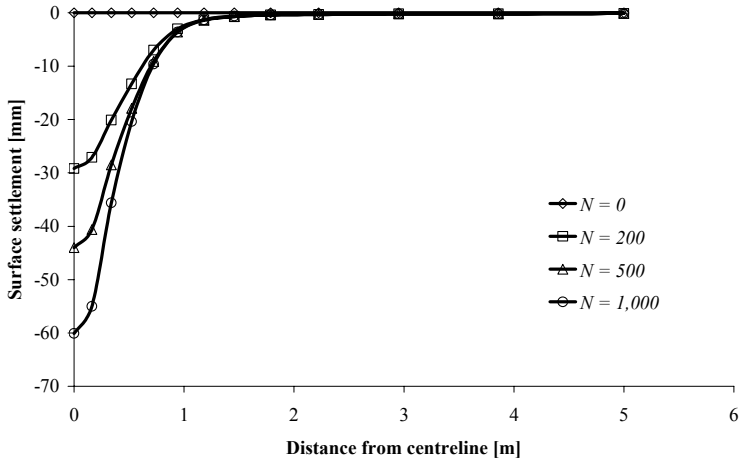

Figure 3.37. Model predictions for a one-layer pavement with equivalent stress distribution applied at the surface of the subgrade, showing the effect of granular layer thickness on the predicted surface profile for 150mm of granular material.

The two-surface model developed by Al-Tabbaa has also been used to model the same pavement problem. This model does not predict any accumulation of permanent settlement after the first loading due to the fact that the elastic region is too large and the stress in the subgrade is well inside the yield surface.

3.6 SUMMARY

The formulation of the 3-SKH model has been briefly described. The ability of the two-surface model and the 3-SKH model to predict the behaviour of soil under one-dimensional loading, unloading and reloading, and the behaviour of soil under drained cyclic loading has been described. It was found that these models could reproduce some of the essential features of soil behaviour under cyclic loading. However, by comparison with existing test data, these two models over-predict shear strain as well as the value of K_0 for normally consolidated soil. The 3-SKH model also suffers from a problem of generating negative shear strain under some stress conditions, which is due to the small stiffness during unloading which causes the shear strain decrement during unloading to be greater than the increment during loading. This negative shear strain problem only occurs under cycles of low stress where the stiffness during unloading is too small. Because the model over-predicts shear strain, this problem is magnified when the model is applied to cyclic loading behaviour where large numbers of cycles are involved. This will predict unrealistic deformation when analysing a pavement problem where large numbers of cycles are applied.

Pavement foundations are best described within the framework of critical state soil mechanics (Brown, 1996). The 3-SKH model has been applied in a pavement analysis to predict the resilient and permanent response of a pavement. The resilient response on unloading predicted by the 3-SKH model agrees well with the results from a multi-layered elastic analysis. However, the rut depth predicted by the 3-SKH model is too large. The two-surface model is not suitable for the prediction of the permanent response of a pavement as the elastic region for this model is too large and no accumulation of permanent strain is predicted by this model. Consequently, an alternative model is required which will reduce the amount of predicted shear strain. This is the subject of the next chapter.

4 FORMULATION OF A SIMPLE NON-ASSOCIATED THREE-SURFACE KINEMATIC HARDENING MODEL

4.1 INTRODUCTION

It has been shown in the previous chapter, that the 3-SKH model over-predicted the value of K_o for normally consolidated soil, and the model also over-estimated shear strain. This problem becomes significant when the model is used to model behaviour of clay subjected to cyclic loading, where too much shear strain accumulates over many cycles. Modification of the flow rule may give a better prediction of K_0 for normally consolidated soil and the shear strain induced by cyclic loading, and this will also affect the problem of generation of negative shear strain. The negative shear strain problem may be eliminated by modifying the hardening modulus.

This chapter describes the mathematical formulation of the new non-associated three-surface kinematic hardening model. The new model has been derived by modifying the flow rule of the 3-SKH model to allow more flexibility of the shape of the plastic potential. The critical state dissipation constant M was also made to be a function of Lode angle in stress space. The translation rules of the 3-SKH model have been retained. An extra parameter is required in the model to control the shape of the plastic potential, and by choosing an appropriate value for the new parameter, the amount of the shear strain predicted can be controlled. However, the problem of generation of negative shear strain still remains under certain stress conditions, and this causes the rut depth to decrease after a number of cycles when analysing the repeated loading of a pavement. The hardening modulus of the model was therefore modified in order to solve this problem and a new parameter was introduced; various expressions of the hardening modulus have been adopted and are presented in this chapter.

4.2 NON-SYMMETRICAL FLOW RULE

To improve the amount of shear strain predicted by the 3-SKH model, an attempt was made to change the flow rule. The flow rule proposed by McDowell (2000), described in Section 2.2.7 was adopted. This flow rule states that for points on the bounding surface, the ratio of the plastic strain increments is:

$$\frac{\mathrm{d}\varepsilon_p^p}{\mathrm{d}\varepsilon_q^p} = \frac{\mathrm{M}^{a+1} - \eta^{a+1}}{\eta^a} \tag{4.1}$$

and the plastic potential on the bounding surface is:

$$q = \mathrm{M}p'\left[\left(a+1\right)\ln\left(2p'_p/p'\right)\right]^{1/a+1} \tag{4.2}$$

where a is a constant controlling the shape of the potential, and p'_p is the hardening parameter for the potential.

From the flow rule the plastic potential for the yield surface was derived by translation of the origin in equation 4.2, giving the equation of the plastic potential in triaxial stress space:

$$\left(q - q_b\right) - \mathrm{M}(p' - p'_b + TSp'_o)\left[(a+1)\ln\left(\frac{2TSp'_p}{p' - p'_b + TSp'_o}\right)\right]^{\frac{1}{a+1}} = 0 \tag{4.3}$$

The hardening parameter p'_p can be obtained by substituting the current values of p' and q into equation 4.3 and solving for p'_p.

The hardening rule, which links $\delta p'_o$ with the plastic volumetric strain, is the same as that used by Modified Cam clay:

$$\delta p'_o = \frac{p'_o}{\lambda^* - \kappa^*}\delta\varepsilon_p^p \tag{4.4}$$

Since we know that the plastic strain increment vector is always normal to the plastic potential:

$$\delta\varepsilon_p^p = \chi \frac{\partial g}{\partial p'}$$
$$\delta\varepsilon_q^p = \chi \frac{\partial g}{\partial q} \tag{4.5}$$

where χ is a scalar multiplier.

The plastic strain increment on the yield surface can be found by combining the translation rule, consistency equation, hardening rule, and equation 4.5. The general expression for the plastic strain increment in triaxial stress space is:

$$\begin{bmatrix} \delta\varepsilon_p^p \\ \delta\varepsilon_q^p \end{bmatrix} = \frac{-1}{\left(\frac{\partial f}{\partial p'_o} + \frac{\partial f}{\partial p'_b}\frac{p'_b}{p'_o} + \frac{\partial f}{\partial q_b}\frac{q_b}{p'_o} \right) \cdot \frac{\partial p'_o}{\partial \varepsilon_p^p} \cdot \frac{\partial g}{\partial p'}} \times \begin{bmatrix} \frac{\partial f}{\partial p'} \cdot \frac{\partial g}{\partial p'} & \frac{\partial f}{\partial q} \cdot \frac{\partial g}{\partial p'} \\ \frac{\partial f}{\partial p'} \cdot \frac{\partial g}{\partial q} & \frac{\partial f}{\partial q} \cdot \frac{\partial g}{\partial q} \end{bmatrix} \begin{bmatrix} \delta p' \\ \delta q \end{bmatrix} \tag{4.6}$$

Substituting the derivatives of the yield surface and plastic potential for the model into equation 4.6 gives:

$$\begin{bmatrix} \delta\varepsilon_p^p \\ \delta\varepsilon_q^p \end{bmatrix} = \frac{1}{h_o} \times$$
$$\begin{bmatrix} (p'-p'_b)\left(B^{\frac{2}{a+1}-1} - B^{\frac{2}{a+1}} \right)(p'-p'_b+TSp'_o) & \frac{(q-q_b)}{M^2}\left(B^{\frac{2}{a+1}-1} - B^{\frac{2}{a+1}} \right)(p'-p'_b+TSp'_o) \\ \frac{(p'-p'_b)(q-q_b)}{M^2} & \left(\frac{(q-q_b)}{M^2} \right)^2 \end{bmatrix} \begin{bmatrix} \delta p' \\ \delta q \end{bmatrix} \tag{4.7}$$

where:

$$h_o = \frac{\left[p'(p'-p'_b) + \frac{q(q-q_b)}{M^2} \right] \cdot \left(B^{\frac{2}{a+1}-1} - B^{\frac{2}{a+1}} \right) \cdot (p'-p'_b+TSp'_o)}{\lambda^* - \kappa^*} \tag{4.8}$$

and:

$$B = (a+1)\ln\left(\frac{2TSp'_p}{p' - p'_b + TSp'_o}\right) \tag{4.9}$$

However, it was found to be very difficult to implement this flow rule into the 3-SKH model: the hardening modulus terms H_1 and H_2 in equations 3.26 and 3.27, need to be modified because the hardening modulus h_o is different from that in the 3-SKH model. In addition, there are six singularity points at which unlimited strains will be predicted. Two of these are the same as the two-surface model and the 3-SKH model; that is when the dot product of the vector joining the origin to the current stress state and the vector normal to the yield surface at that stress point is equal to zero – see Section 3.2.2. Two other singularity points are when $B = 1$, this happens when p'-$p'_b = 0$: i.e. at the top and bottom apexes. At these singularity points, infinite plastic strain is predicted. Another singularity point is when p'-$p'_b = -TSp'_o$ at which $h_o = 0$. This occurs when the stress point is at the left apex of the yield surface. However, the terms H_1 and H_2 may resolve this problem. The sixth singularity point occurs during isotropic normal compression. At this point, $B = 0$ and the plastic strain increment is undefined. Due to the complexity of this flow rule, it was abandoned and another simpler flow rule, which is symmetrical about the centreline of the yield surface and which will not introduce any extra singularity points, was proposed.

4.3 THE NON-ASSOCIATED THREE-SURFACE KINEMATIC HARDENING MODEL

In this section the derivation of the new non-associated model is described. The methods used to derive this model are largely similar to those used by Al-Tabbaa (1987) and Stallebrass (1990) to derive the two and three-surface models respectively, which are extensions of the Modified Cam clay model.

4.3.1 Model Description

This model has been derived within the framework of Critical State Soil Mechanics and it is an extension to the 3-SKH model developed by Stallebrass (1990). It has a Modified Cam clay yield surface in triaxial stress space as shown in Figure 3.1.

The outermost surface is now not a true yield surface, which encloses the truly elastic region, following the terminology used by Al-Tabbaa (1987) and Stallebrass (1990), this surface is called the 'bounding surface', with the inner two kinematic surfaces being the 'history surface' and 'yield surface' as described in Chapter 3. These two kinematic surfaces have the same shape as the bounding surface but are smaller in size, with this size expanding and contracting at a fixed ratio. The equations for the bounding, history and yield surface in the triaxial stress space are still as given in equations 3.1 - 3.3.

4.3.2 Stress-dilatancy Rule

The 3-SKH model is assumed to obey the normality rule i.e. the plastic potential is identical to the yield surface. Since the bounding surface is of the Modified Cam clay type, this will lead to an over prediction of shear strain and $K_{0,nc}$. The plastic strain increment ratio on the bounding surface is:

$$\frac{\mathrm{d}\varepsilon_p^p}{\mathrm{d}\varepsilon_q^p} = \frac{\mathrm{M}^2 - \eta^2}{2\eta} \tag{4.10}$$

In order to reduce the amount of shear strain predicted by the 3-SKH model, a new, simple and more flexible expression for the flow rule was proposed:

$$\frac{\mathrm{d}\varepsilon_p^p}{\mathrm{d}\varepsilon_q^p} = \frac{\mathrm{M}^2 - \eta^2}{k\eta} \tag{4.11}$$

which requires the specification of one additional new parameter k. This flow rule was also proposed by Ohmaki (1982) to predict correctly the value of $K_{0,nc}$ and used by Alonso et al. (1990) to model the behaviour of partially saturated clays.

This flow rule is associated at critical states and also for isotropic conditions, but non-associated between these points, where the plastic strain increment ratio at a given stress ratio depends on the value of k. This was implemented into the 3-SKH model to improve its prediction of $K_{0,nc}$ and hence shear strain. To illustrate the effect of using different values of k on the plastic strain increment vector, Figure 4.1 shows the directions of the plastic strain increment vectors for k = 0.5 and 1.0. The slope of the plastic strain increment vector has been reduced compared to that when the normality condition is applied (i.e. k = 2). This will reduce the plastic shear strain predicted by the model by a factor of 2/k. By choosing an appropriate value of k, the value of the coefficient of earth pressure at rest during one-dimensional compression $K_{o,nc}$ can be predicted more accurately than the 3-SKH model. The predicted results for the value of the coefficient of earth pressure at rest during one-dimensional loading, unloading and reloading are presented in section 4.3.7.

The plastic potential, g, can be obtained by integration of equation 4.11:

$$g = q^2 + \frac{\mathrm{M}^2}{1-k}\left(\frac{p'}{2p'_p}\right)^{\frac{2}{k}}\left(2p'_p\right)^2 - \frac{\mathrm{M}^2 p'^2}{1-k} = 0 \qquad (4.12)$$

except for k = 1 when

$$g = q - \mathrm{M}p'\sqrt{2\ln\left(2p'_p / p'\right)} = 0 \qquad (4.13)$$

where p'_p is the hardening parameter for the plastic potential.

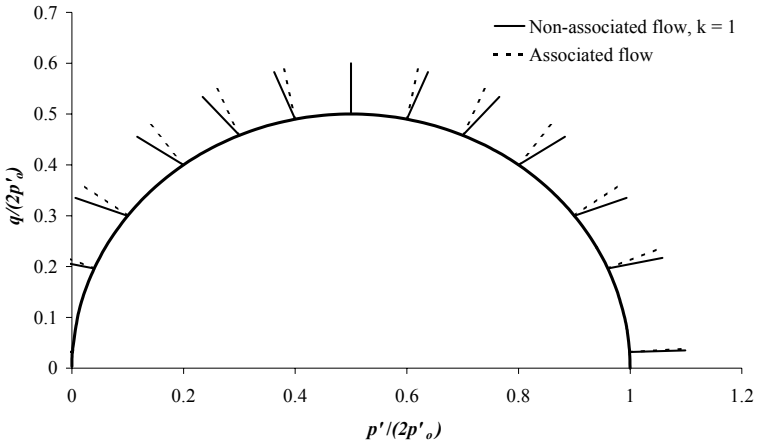

(a)

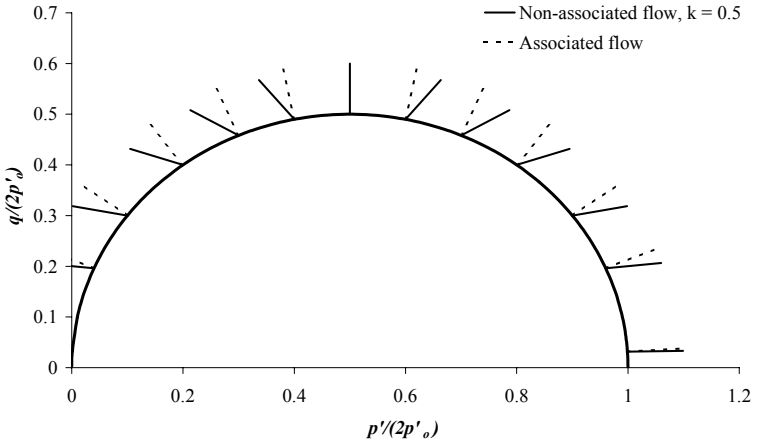

(b)

Figure 4.1. Comparison between associated and non-associated flow plastic strain increment vectors (a) k = 1, and (b) k = 0.5.

The shape of the plastic potential can be varied by using different values of k. The effect of parameter k on the shape of the plastic potential is shown in Figure 4.2.

By translation of the origin in equation 4.9, the plastic potential for the yield surface is therefore:

$$g = \frac{(q-q_b)^2}{\mathrm{M}^2} + \frac{1}{1-k}\left(\frac{p'-p'_b+TSp'_o}{2TSp'_p}\right)^{\frac{2}{k}}\left(2TSp'_p\right)^2 - \frac{\left(p'-p'_b+TSp'_o\right)^2}{1-k} = 0 \quad (4.14)$$

except for $k = 1$, when

$$(q-q_b)-\mathrm{M}(p'-p'_b+TSp'_o)\sqrt{2\ln\left(\frac{2TSp'_p}{p'-p'_b+TSp'_o}\right)}=0 \qquad (4.15)$$

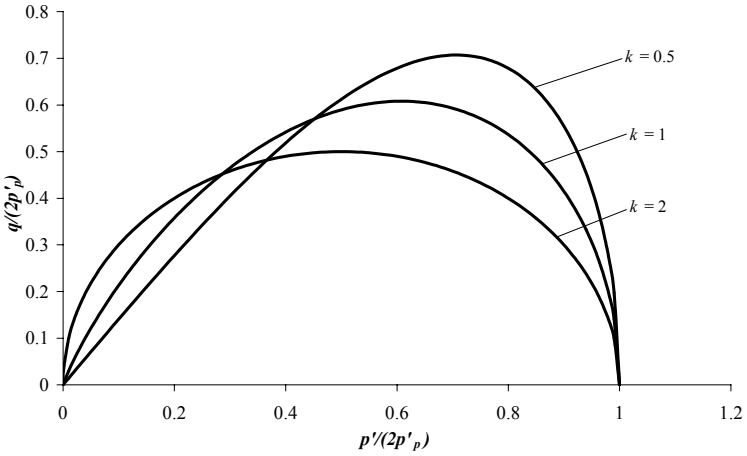

Figure 4.2. Plastic potentials for various values of k.

4.3.3 Hardening Rule

The way the hardening modulus is derived is the same as that used for the 3-SKH model; it is derived from the special case when all the surfaces are in contact, and is then generalised. However, there is a slight modification to the hardening moduli H_1 and H_2 of the new model. The hardening rule, which links $\delta p'_o$ with the plastic volumetric strain, is the same as that used by Modified Cam clay – see equation 4.4.

Substituting the derivatives of the yield surface and plastic potential for the model into equation 4.6 results in the following expression for the plastic strain increment on the yield surface:

$$\begin{bmatrix}\delta\varepsilon_p^p\\ \delta\varepsilon_q^p\end{bmatrix}=\frac{1}{h_o}\times\begin{bmatrix}\frac{2}{k}(p'-p'_b)^2 & \frac{2}{k}(p'-p'_b)\frac{(q-q_b)}{\mathrm{M}^2}\\ (p'-p'_b)\frac{(q-q_b)}{\mathrm{M}^2} & \frac{(q-q_b)^2}{\mathrm{M}^4}\end{bmatrix}\begin{bmatrix}\delta p'\\ \delta q\end{bmatrix} \qquad (4.16)$$

where the hardening modulus h_o is:

$$h_o = \frac{\left[p'\left(p' - p'_b\right) + \dfrac{q\left(q - q_b\right)}{M^2} \right] \cdot \dfrac{2}{k}\left(p' - p'_b\right)}{\lambda^* - \kappa^*} \tag{4.17}$$

Note that the hardening modulus h_o is reduced to that of the 3-SKH model when k = 2, and that only shear strains are affected for given values of p', q, $\delta p'$, $\delta q'$, p'_b and q_b (i.e. for a given stress path).

This hardening modulus, h_o, will predict infinite plastic strains at four singularity points, which are the same as those in the 3-SKH model. Hence the hardening moduli, H_1 and H_2, can be used without major modification. Detailed description of the singularity points can be found in Al-Tabbaa (1987) and has been briefly described in Chapter 3. Because of this instability region, described in Section 3.2.2, Stallebrass (1990) defined the hardening modulus h as a function $h = h_o + H_1 + H_2$. Hashiguchi (1985) expressed the hardening modulus as a function of the degree of approach of the surfaces such that the hardening modulus is zero when the surfaces are in touch. Following this, Stallebrass (1990) expressed H_1 as a function of b_1, the degree of approach of the history surface to the bounding surface and H_2 as a function of b_2, the degree of approach of the yield surface to the history surface. The H_1 and H_2 terms for the new model are slightly different from those used by the 3-SKH model; a factor of $2/k$ has been applied to these terms:

$$H_1 = \frac{1}{\lambda^* - \kappa^*} \frac{2}{k} \left(\frac{b_1}{b_{1\max}} \right)^{\psi} p'^{3}_{o} S^2 \tag{4.18}$$

$$H_2 = \frac{1}{\lambda^* - \kappa^*} \frac{2}{k} \left(\frac{T \cdot b_2}{b_{2\max}} \right)^{\psi} p'^{3}_{o} \tag{4.19}$$

the terms in these equations were explained in Section 3.2.2.

By using these expressions for H_1 and H_2, h_o, H_1 and H_2 are all scaled by $2/k$ so that the value of parameter k will affect only the plastic shear strain and not the plastic volumetric strain for given values of p', q, $\delta p'$, $\delta q'$, p'_b and q_b, so that the plastic

volumetric strain predicted by the new model will be the same as that predicted by the 3-SKH model. This is considered acceptable because Al-Tabbaa (1987) showed that volumetric strains were predicted well for kaolin by her two-surface model.

Thus, the constitutive relationship for the plastic strain increments is:

$$\begin{bmatrix} \delta\varepsilon_p^p \\ \delta\varepsilon_q^p \end{bmatrix} = \frac{1}{h} \times \begin{bmatrix} \frac{2}{k}(p'-p'_b)^2 & \frac{2}{k}(p'-p'_b)\frac{(q-q_b)}{\mathrm{M}^2} \\ (p'-p'_b)\frac{(q-q_b)}{\mathrm{M}^2} & \frac{(q-q_b)^2}{\mathrm{M}^4} \end{bmatrix} \begin{bmatrix} \delta p' \\ \delta q \end{bmatrix} \tag{4.20}$$

where:

$$h = \frac{1}{\lambda^* - \kappa^*} \times \left\{ \left[p'(p'-p'_b) + \frac{q(q-q_b)}{\mathrm{M}^2} \right] \cdot \frac{2}{k}(p'-p'_b) + \frac{2}{k}\left(\frac{b_1}{b_{1\max}}\right)^{\psi} p'^{\,3}_o S^2 + \frac{2}{k}\left(\frac{Tb_2}{b_{2\max}}\right)^{\psi} p'^{\,3}_o \right\} \tag{4.21}$$

The expressions for H_1 and H_2 are certainly not unique and can be modified to improve predictions. It will be shown that these expressions are not suitable for analysing a pavement problem where the stresses in the pavement foundation are relatively small. In Section 4.3.8, different expressions of the hardening modulus are proposed in order to improve the model predictions under cyclic loading.

4.3.4 Yield Surface and Plastic Potential in Deviatoric Plane

For the 'Bubble' model and the 3-SKH model, the critical state dissipation constant M is assumed to be constant. However, it is well known that the Mohr-Coulomb criterion is more appropriate to failure conditions in soils (Potts and Zdravković, 1999), so that the critical state constant M is a function of Lode angle in stress space. In the new model, the critical state dissipation constant M has been made to be a function of Lode angle, θ according to the expression proposed by Sheng et al. (2000):

$$M = M_c \left(\frac{2\alpha^4}{1+\alpha^4+(1-\alpha^4)\sin 3\theta} \right)^{1/4} \tag{4.22}$$

$$\alpha = \frac{M_e}{M_c} = \frac{3-\sin\phi'}{3+\sin\phi'} = \frac{3}{3+M_c} \tag{4.23}$$

$$\theta = \tan^{-1}\left[\frac{1}{\sqrt{3}} \left(2\frac{(\sigma'_2-\sigma'_3)}{(\sigma'_1-\sigma'_3)} - 1 \right) \right] \tag{4.24}$$

where M_c is the value of M in triaxial compression with θ = -30°, and M_e is the value of M in triaxial extension θ = 30°. The parameter ϕ' is the friction angle of the soil at a critical state, assumed to be independent of Lode angle. Figure 4.3 shows the failure surface in the deviatoric plane, having a similar shape to that proposed by Matsuoka and Nakai (1974). This surface coincides with the Mohr-Coulomb hexagon at all vertices in the deviatoric plane, and the failure surface remains convex if $\alpha \geq 0.6$ (i.e. $\phi' \leq 48.59°$ or $M_c \leq 2$) which is common for most clays (Sheng et al., 2000).

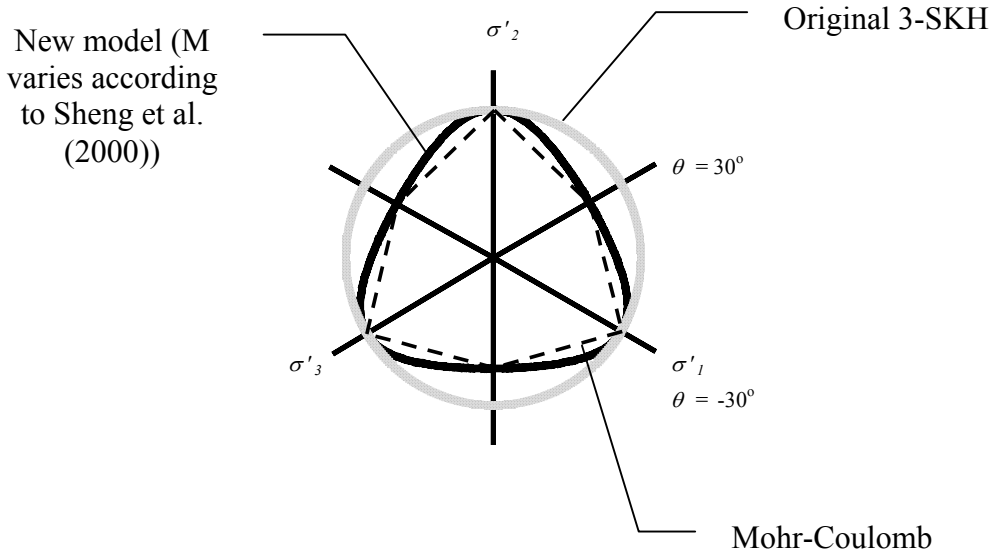

Figure 4.3. Failure surface in deviatoric plane given by equation 4.22.

In the new model, the shape of the yield surface, history surface, bounding surface and potential have all been assumed to have a shape in the deviatoric plane given by equation 4.22, and the Lode angle is calculated for the current point in stress space using a floating origin at the centre of the yield surface. For simplicity, the rate of change of the value M with respect to Lode angle, $\partial M/\partial \theta$, is assumed to be negligible. This implies that the yield surface and the plastic potential in the deviatoric plane remain circular in shape with the radius changing according to equation 4.22. This assumption will make the mathematical formulation much simpler and is justified in the next section by a typical boundary value problem using the model described by Yu and Khong (2002). The effect of $\partial M/\partial \theta$ will be important for the potential under plane strain conditions (Potts and Zdravković, 1999).

4.3.5 Justification of $\partial M/\partial \theta = 0$

In order to justify the assumption that the rate of change of M with respect to Lode angle is negligible, finite element analyses on footing problems using the model developed by Yu (1998) have been performed. This model was fully implemented in CRISP by Yu and Khong (2002), which also used the relationship between M and Lode angle (equation 4.22) proposed by Sheng et al. (2000). Three versions of this model have been implemented in CRISP: (1) M varies according to equation 4.22 with $\partial M/\partial \theta = 0$ for both the yield surface and the plastic potential in the deviatoric plane: i.e. circular shape, (2) M varies according to equation 4.22 for both the yield surface and plastic potential, and $\partial M/\partial \theta$ is allowed to vary according to equation 4.22 for both the yield surface and plastic potential (i.e. both the yield surface and plastic potential are of the Sheng et al. (2000) shape in Figure 4.3), and (3) M varies according to equation 4.22 for both the yield surface and the plastic potential, but $\partial M/\partial \theta$ is zero for the plastic potential only (i.e. circular potential and Sheng et al. (2000) type yield surface).

A rigid circular footing and a strip footing were analysed using these models to investigate the effect of the shape of the yield surface and plastic potential in the

deviatoric plane. The finite element mesh used to analyse the footing problems is shown in Figure 4.4. Cubic strain triangle elements were used in the analyses.

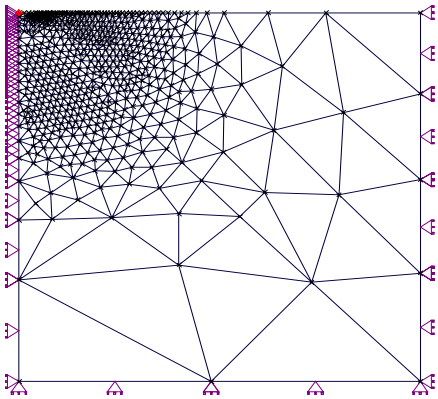

Figure 4.4 . Finite element mesh for footing problem.

The model parameters chosen are relevant to London clay (Yu and Khong, 2002). The first problem was a rigid circular footing under undrained loading conditions and the second problem was a rigid strip footing under the same loading conditions. Figures 4.5 and 4.6 show the plot of applied pressure against displacement for the circular footing and strip footing respectively. The first and second letters in the figure denote the shape of the yield surface and plastic potential in the deviatoric plane respectively, where 's' denotes Sheng et al. (2000) type surface and 'c' a circular shape. For a circular footing (axi-symmetry), the shapes of the yield surface and plastic potential in the deviatoric plane were found to be insignificant. However, the shape of the plastic potential in the deviatoric plane was found to be more significant for the plane strain problem. However, the shape of the yield surface in the deviatoric plane had no effect on the plane strain problem. These findings agree with the findings of Potts and Gens (1984) who showed that, in plane strain problems, the shape of the plastic potential in the deviatoric plane has a dominating influence on the predicted behaviour especially for drained conditions. According to Potts and Gens (1984), the plastic potential should predict the correct Lode angle at failure, θ_f, and the predicted value of θ_f affects the predictive capability for plane strain deformation. As for the effect of the yield surface, Potts and Gens (1984) also noticed that in their plane strain problem, this has little influence on the predictions, so long as the correct value of ϕ' at failure was produced. Hence, for simplicity, the

new model proposed in this research assumed that both the shape of the plastic potential and yield surface in the deviatoric plane were circular (i.e. $\partial M/\partial\theta = 0$), with the value of M varying with Lode angle according to equation 4.22. Further work is needed to justify this assumption for the new model.

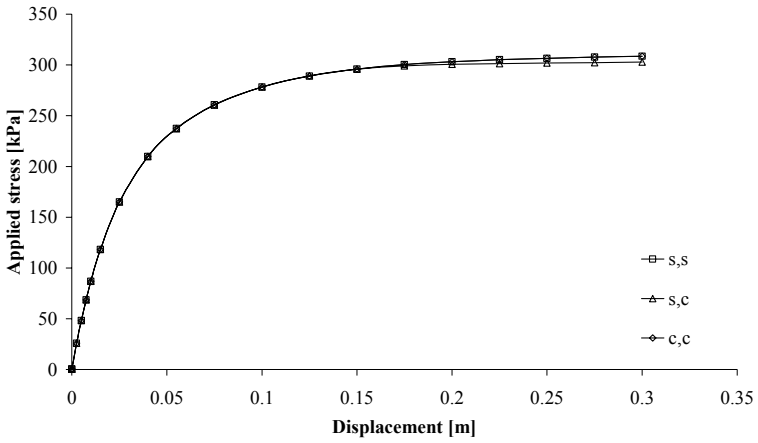

Figure 4.5. Results predicted by CASM (Yu, 1998; Yu & Khong, 2002) showing the effect of the shape of yield surface and plastic potential in the deviatoric plane for a circular footing (axi-symmetric problem).

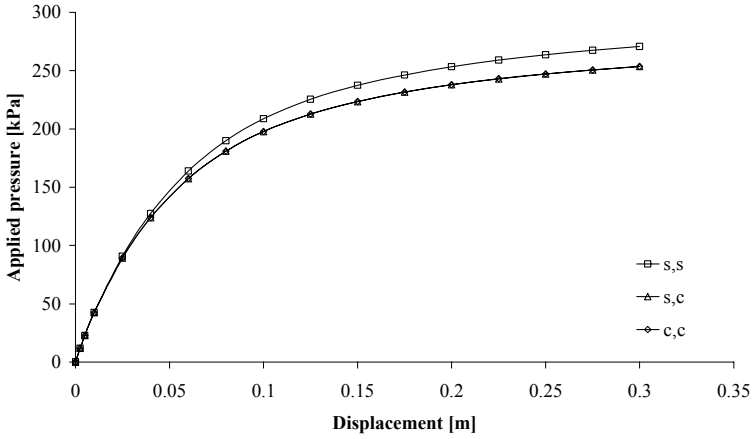

Figure 4.6. Results predicted by CASM (Yu, 1998; Yu & Khong, 2002) showing the effect of the shape of yield surface and plastic potential in the deviatoric plane for a strip footing (plane strain problem).

4.3.6 Generalisation of Model, Finite Element Implementation and Validation of the New Model in CRISP

To perform non-linear finite element analysis using elasto-plastic models, it is necessary to compute the elastic-plastic matrix, $[D^{ep}]$ relating an increment of strain to an increment of stress:

$$\{\Delta\sigma\} = [D^{ep}]\{\Delta\varepsilon\} \tag{4.25}$$

There is a standard method to obtain the expression for the elastic-plastic matrix, $[D^{ep}]$, which can be found in standard finite element textbooks such as Potts & Zdravković (1999):

$$[D^{ep}] = [D^{e}] - \frac{[D^{e}]\left\{\frac{\partial g}{\partial \sigma'}\right\}\left\{\frac{\partial f}{\partial \sigma'}\right\}^{T}[D^{e}]}{\left\{\frac{\partial f}{\partial \sigma'}\right\}^{T}[D^{e}]\left\{\frac{\partial g}{\partial \sigma'}\right\} + H} \tag{4.26}$$

where $[D^e]$ is the elastic matrix and H is the hardening/softening modulus. For the three-surface model:

$$H = h_o + H_1 + H_2 \tag{4.27}$$

where h_o is given by:

$$h_o = -\left(\frac{\partial f}{\partial p'_o} + \frac{\partial f}{\partial \sigma'_{bij}}\frac{\sigma'_{bij}}{p'_o}\right)\frac{\partial p'_o}{\partial \varepsilon_{ii}}\frac{\partial g}{\partial \sigma'_{ii}} \tag{4.28}$$

In order to implement the model into a finite element code, the model has to be formulated in general stress space. The equations of the yield surface and plastic potential are written in general stress space by substituting q with deviatoric stress tensor, the equations of the yield surface, f and plastic potential, g become:

$$f = \frac{3}{2}\frac{\left(s_{ij} - s_{ijb}\right):\left(s_{ij} - s_{ijb}\right)}{\mathrm{M}^2} + \left(p' - p'_b\right)^2 - T^2 S^2 p'^2_o = 0 \tag{4.29}$$

$$g = \frac{3}{2}\frac{\left(s_{ij} - s_{ijb}\right):\left(s_{ij} - s_{ijb}\right)}{\mathrm{M}^2} + \frac{1}{1-k}\left(\frac{p' - p'_b + TSp'_o}{2TSp'_p}\right)^{\frac{2}{k}}\left(2TSp'_p\right)^2 - \frac{\left(p' - p'_b + TSp'_o\right)^2}{1-k} = 0 \tag{4.30}$$

where s_{ij} is the deviatoric stress tensor. The relationship between q and s_{ij} is:

$$q = \sqrt{\frac{3}{2}}\left|s_{ij}\right| = \sqrt{\frac{3}{2}\left(s_x^2 + s_y^2 + s_z^2 + 2s_{xy}^2 + 2s_{yz}^2 + 2s_{xz}^2\right)} \tag{4.31}$$

where:

$$s_x = \sigma'_x - p', \quad s_y = \sigma'_y - p', \quad s_z = \sigma'_z - p', \; s_{xy} = \tau_{xy}, \; s_{yz} = \tau_{yz}, \; s_{xz} = \tau_{xz} \tag{4.32}$$

The symmetric tensor s_{ij} is expressed in matrix and vector forms as follows:

$$s_{ij} = \begin{bmatrix} s_{xx} & s_{xy} & s_{xz} \\ & s_{yy} & s_{yz} \\ sym. & & s_{zz} \end{bmatrix} = \left\{s_x, s_y, s_z, s_{xy}, s_{yz}, s_{xz}\right\} \tag{4.33}$$

The terms $\partial f/\partial\sigma'$ and $\partial g/\partial\sigma'$ needed for the formation of the elasto-plastic matrix in equation 4.26 can be obtained from the following equations:

$$\frac{\partial f}{\partial \sigma'_{ij}} = \frac{\partial f}{\partial p'}\frac{\partial p'}{\partial \sigma'_{ij}} + \frac{\partial f}{\partial s_{ij}}\frac{\partial s_{ij}}{\partial \sigma'_{ij}} + \frac{\partial f}{\partial \mathrm{M}}\frac{\partial \mathrm{M}}{\partial \theta}\frac{\partial \theta}{\partial \sigma'_{ij}} \tag{4.34a}$$

$$\frac{\partial g}{\partial \sigma'_{ij}} = \frac{\partial g}{\partial p'}\frac{\partial p'}{\partial \sigma'_{ij}} + \frac{\partial g}{\partial s_{ij}}\frac{\partial s_{ij}}{\partial \sigma'_{ij}} + \frac{\partial g}{\partial \mathrm{M}}\frac{\partial \mathrm{M}}{\partial \theta}\frac{\partial \theta}{\partial \sigma'_{ij}} \tag{4.34b}$$

Assuming the rate of change of M with respect to θ is negligible (i.e. circular shape in deviatoric plane), equations 4.34a and 4.34b become:

$$\frac{\partial f}{\partial \sigma'_{ij}} = \frac{\partial f}{\partial p'}\frac{\partial p'}{\partial \sigma'_{ij}} + \frac{\partial f}{\partial s_{ij}}\frac{\partial s_{ij}}{\partial \sigma'_{ij}} \tag{4.35a}$$

$$\frac{\partial g}{\partial \sigma'_{ij}} = \frac{\partial g}{\partial p'}\frac{\partial p'}{\partial \sigma'_{ij}} + \frac{\partial g}{\partial s_{ij}}\frac{\partial s_{ij}}{\partial \sigma'_{ij}} \tag{4.35b}$$

All the terms required for the elasto-plastic matrix can be found in the appendix.

From the definition of the Lode angle, equation 4.24, it should be noted that there is a discontinuity of Lode angle from $\sigma'_v > \sigma'_h$ to $\sigma'_h > \sigma'_v$ i.e. from compression to extension (i.e. at an isotropic stress state), the Lode angle is undefined. However, this should not create any difficulties in the implementation of the new model into a finite element code, because at this point, the flow rule is not affected by the Lode angle and hence any value of Lode angle can be assumed at this point. At isotropic stress states, only volumetric strains occur (the plastic strain increment ratio $d\varepsilon_p^p / d\varepsilon_q^p$, is equal to infinity), so any value of the Lode angle can be assumed at this point.

The original 3-SKH model was implemented in CRISP and the new model was implemented by amending the source code for the original 3-SKH model. The new flow rule with constant M was first implemented followed by the implementation of M as a function of Lode angle. After the implementation, the program was tested by the following methods to ensure that the implementation was correct:

1. Constant M

- For the new model with constant M, it was ensured that the results predicted were the same as the original model for $k = 2$.

- For other values of k, it was ensured that the shear strain predicted by the new model was approximately $k/2$ times the shear strain predicted by the original

model (the relationship is approximate because the factor 2/k applies to plastic strains only).

- The volumetric strain predicted by the new model should be exactly the same as that predicted by the original model for any value of k for a given stress path.

2. Varying M

- After the new model with varying M was implemented, a triaxial extension simulation was performed to ensure that the soil reached a critical state at a stress ratio equal to M_e. This critical state stress ratio could be calculated from M_c using equation 4.23.

- In addition, an undrained triaxial simulation was performed with all the surfaces initially centralised. The model should predict a straight line for the undrained stress path in the $q - p'$ space.

The model predicted the correct response for all these loading paths.

4.3.7 Evaluation of the New Model

It has been shown in Chapter 3 that the 3-SKH model is able to capture most of the essential features of cyclic loading of soil behaviour. However, this model over predicts $K_{0,nc}$ and shear strain on loading. Figure 3.18 shows that the 3-SKH model greatly over-predicts shear strain for a shear test at constant p', and it has also been shown that in Figure 3.9 the earth pressure coefficient at rest during normal compression and unloading is over-estimated. By changing the flow rule of the 3-SKH model, the predicted shear strain can be scaled down and hence the earth pressure coefficient at rest can be correctly predicted – at least for normally consolidated conditions. It was considered that if the value of k could be found such that the model correctly predicted $K_{0,nc}$, then this would result in better predictions of shear strain for a given cyclic stress path. According to McDowell and Hau (2003)

the value of k required to correctly predict $K_{0,nc}$ may be estimated from equation 4.11, neglecting elastic strains, so that for one-dimensional conditions:

$$\frac{\mathrm{d}\varepsilon_p}{\mathrm{d}\varepsilon_q} = \frac{\mathrm{d}\varepsilon_1}{2\mathrm{d}\varepsilon_1/3} = 1.5 = \frac{\mathrm{M}^2 - \eta^2}{k\eta} \tag{4.36}$$

where the critical state parameter M in triaxial compression is related to the critical state angle of friction ϕ', according to the equation:

$$\mathrm{M} = \frac{6\sin\phi'}{3 - \sin\phi'} \tag{4.37}$$

The effect of k on values of K_0 during normal compression for different values of ϕ' is also shown in Figure 4.7.

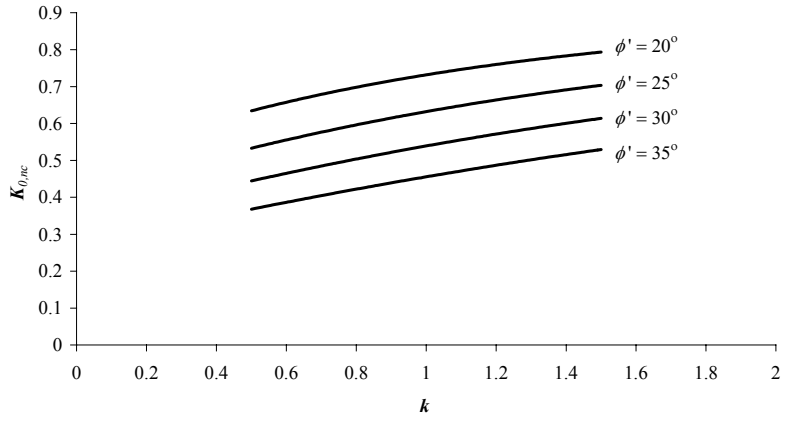

Figure 4.7. Effect of parameter k on the prediction of K_0 at normally consolidated state.

For kaolin, Al-Tabbaa (1987) obtained a value of $K_{0,nc}$ = 0.69 ($\eta_{0,nc}$ = 0.39) and M = 0.89. Substituting these values into equation 4.36 gives k = 1.1. For soils that satisfy the Jâky (1944) equation 2.37, the stress ratio $\eta_{0,nc}$ during one-dimensional compression is given approximately by the equation:

$$\eta_{0,nc} \approx 0.6\mathrm{M} \tag{4.38}$$

Equation 4.38 can be verified by substituting different values of ϕ' into equations 2.37 and 4.37. Substituting equation 4.38 into equation 4.11 for one-dimensional; conditions with $d\varepsilon_p^p / d\varepsilon_q^p = 1.5$ (i.e. neglecting elastic strains) gives:

$$k \approx 0.7\mathrm{M} \tag{4.39}$$

for such soils.

Figure 4.8 shows the prediction of $K_{0,nc}$ of the new model with $k = 0.7$M for different angles of friction compared with the values predicted by the 3-SKH model and various relationships proposed by other researchers (Jâky, 1944; Brooker & Ireland, 1965; Bolton, 1991b; Simpson, 1992) which have been described in Section 2.2.9. The result shows that the new model has greatly improved the prediction of $K_{0,nc}$ compared to the original model which over-estimates $K_{0,nc}$.

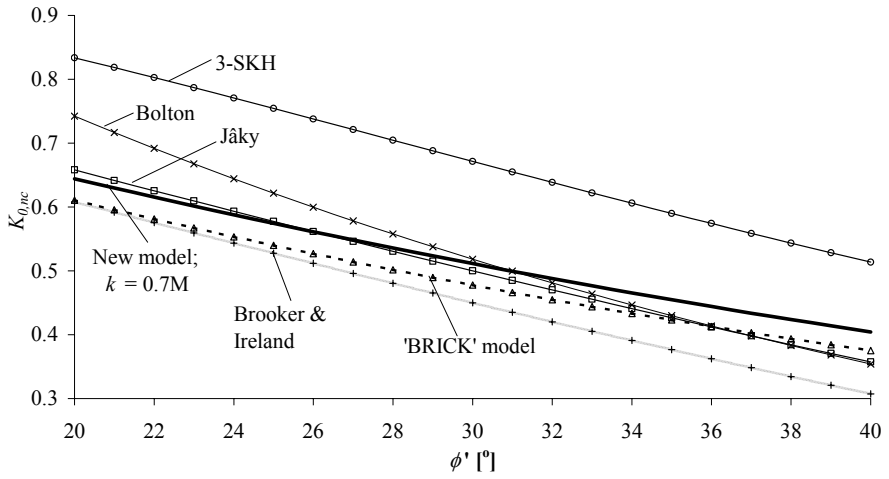

Figure 4.8. Comparison of the values of $K_{0,nc}$ predicted by the new model and by other models.

Figure 4.9 shows the prediction of the K_0 for kaolin during loading, unloading and reloading by the new model with a constant value of M, and with M varying according to equation 4.22, using a value of $k = 1.1$. This value of k would give $K_{0,nc} = 0.684$ ($\eta_{0,nc} = 0.40$) which agrees well with the value of $K_{0,nc} = 0.69$ obtained by Al-Tabbaa (1987). According to equation 4.11 with $\eta_{0,nc} = 0.40$, the value for $d\varepsilon_p^p/d\varepsilon_q^p$ is 1.44. This illustrates that the elastic strains can be neglected in the

determination of the value of k. It can be seen that the prediction of the value of K_0 during normal compression is better than the original 3-SKH model. Figure 4.9, curve A, shows the values of K_0 predicted by equation 2.48. The values predicted by the new model with constant M are given by curve B. It can be seen that the prediction of K_0 on unloading is worse than that given by the 3-SKH model (curve C). It was considered that this was because the stress ratio at failure, M, had been assumed to be independent of the Lode angle in stress space. The effect of allowing M to be a function of Lode angle, on the predicted value of K_0 for primary unloading, is given in Figure 4.9, curve D. It can be seen that the prediction is much better than that given by using a constant value of M (curve B), and is better than the 3-SKH model (curve C). If required, k could be permitted to be different under compression and extension conditions. This is equivalent to applying a different flow rule in compression and extension. A suitable formulation in generalised stress space, following equations 4.22 – 4.24, would be:

$$k(\theta) = k_c \left(\frac{2\alpha^4}{1+\alpha^4+(1-\alpha^4)\sin 3\theta} \right)^{1/4} \tag{4.40}$$

$$\alpha = \frac{k_e}{k_c} \tag{4.41}$$

where k_e relates to triaxial extension (θ = +30°) and k_c to compressive (θ = -30°) conditions. The value of α could be determined by trial error. A constant value of k may be insufficient to fit both the values of $K_{0,nc}$ and K_0 on unloading. Equations 4.40 and 4.41 are useful for this purpose.

For reloading, curve A in Figure 4.9 shows the empirical relation proposed by Schmidt (1983) given by equation 2.48 with OCR_{max} = 10. The prediction of the 3-SKH model is also shown (curve C), together with the new model using k = 1.1 (curve D). It appears that the 3-SKH model is better than the new model, but this is mainly because of the higher value of of $K_{0,nc}$. The prediction of K_0 on reloading cannot be expected to be correct, as the model exhibits strong ratcheting under

drained cyclic loading: this is a function of the H_1 and H_2 terms in the hardening modulus.

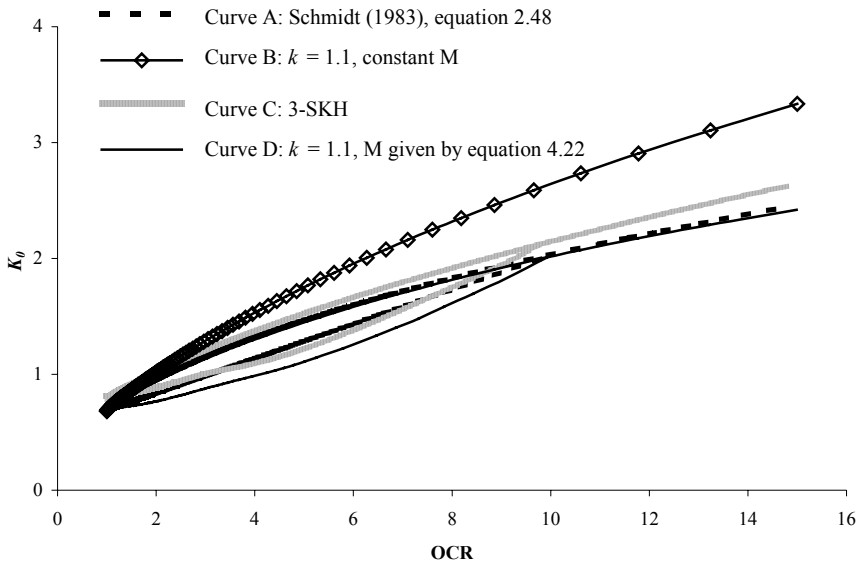

Figure 4.9. Comparison between model predictions of K_0 and empirical result.

It was considered that if the value of k could be found such that the model correctly predicted $K_{0,nc}$, then this would result in a better prediction of shear strain. Figure 4.10 shows the predictions of the original model and the new model (with M given by equation 4.22) for the constant p' drained cyclic loading test performed by (Stallebrass, 1990) – see Figure 3.18. It can be seen that the shear strain predicted has been greatly improved by the new model. However, the shear strain on reloading is still over-predicted. As pointed out by Stallebrass (1990), this is because the stiffness drops rapidly when the stress state reaches the history surface, and a more appropriate expression for H_1 may improve this. In addition, the ratcheting phenomenon is still exhibited by the new model as seen in Figure 4.10, but the increase in shear strain caused by the unload – reload cycle is reduced by about 40%.

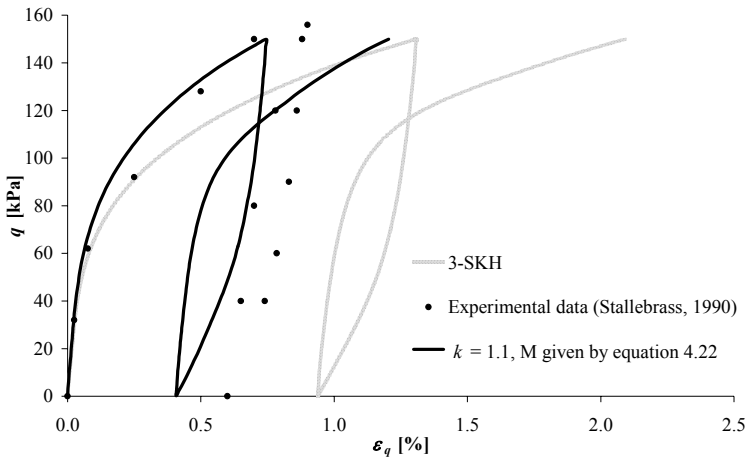

Figure 4.10. Comparison between model predictions and experimental data from Stallebrass (1990).

Now, the pavement problem presented in Chapter 3 is analysed using the new model with k = 1.1. The rest of the parameters are the same as those used in Chapter 3. The finite element mesh used for the pavement analysis is shown in Figure 4.11. Figures 4.12 and 4.13 show the model prediction of the permanent settlement at the centreline of the surface of the subgrade in a one-layer pavement with an equivalent stress distribution (to that caused at the surface of the subgrade by a wheel load in a three-layer pavement) applied at the surface of the subgrade and the surface profile of the subgrade. The model predicts an initially increasing settlement followed by a decreasing settlement. The shear strain of the element located at the top of the subgrade and near the centreline, is plotted against number of cycles, and the results are presented in Figure 4.14. The results show that the shear strain increment becomes negative as the number of cycle increases. This is due to the negative shear strain problem described in Section 3.4.2. The negative shear strain problem that already existed in the 3-SKH model becomes significant when the new proposed flow rule is used because the shear strain on loading is reduced by a factor of 2/k and by adopting a value M, which is a function of Lode angle, the shear strain on unloading does not change much. This causes the negative shear strain problem under some stress conditions.

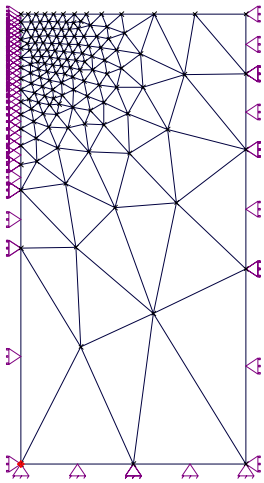

Figure 4.11. Finite element mesh of the one-layer pavement.

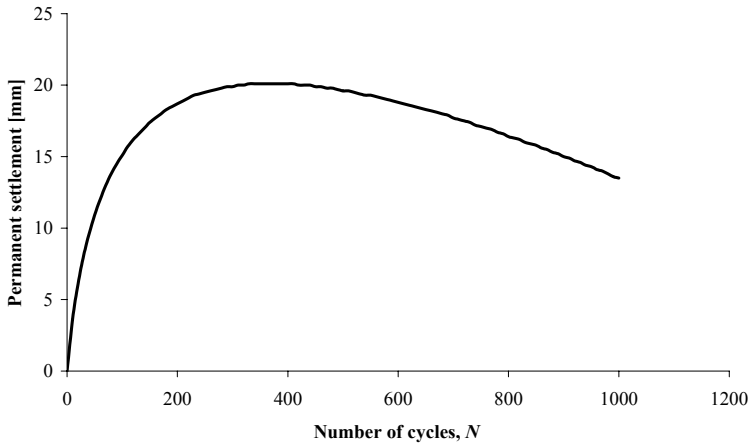

Figure 4.12. Predicted permanent settlement versus number of cycles.

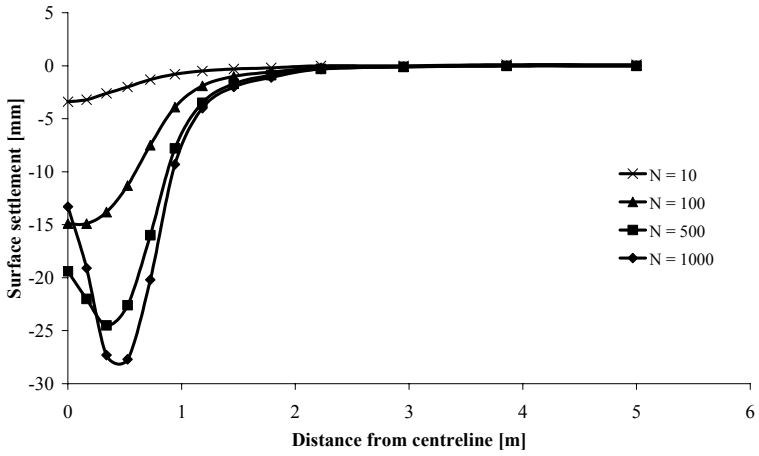

Figure 4.13. Surface profile predicted by the new model.

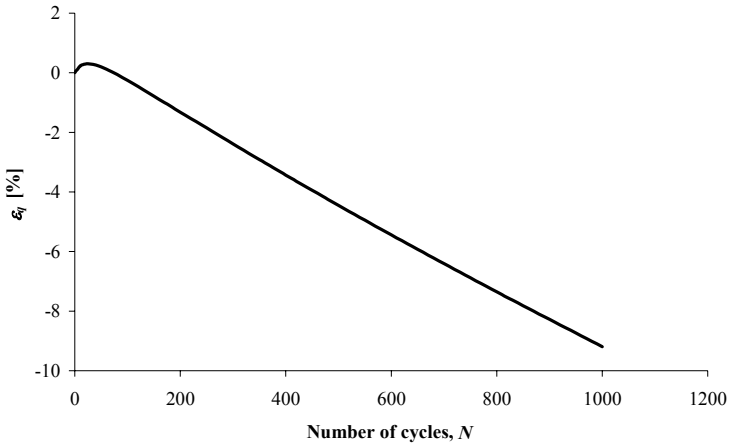

Figure 4.14. Accumulation of negative shear strain with number of cycles in pavement element.

4.3.8 Modification of the Hardening Modulus

It has been shown in the previous section that the problem of accumulation of negative shear strain occurs in the pavement analysis. This is due to the fact that the shear strain decrement on unloading is greater than the increment during loading under some stress conditions. As already discussed in Section 3.4.2, the negative shear strain problem can be eliminated by modifying the hardening modulus such that the stiffness on unloading is greater. In this section, the hardening modulus is modified slightly in order to give a realistic prediction for the analysis of a pavement.

Several modifications to the hardening moduli H_1 and H_2 were made in order to try to eliminate the negative shear strain problem, such as using different values of ψ in these terms (i.e. ψ_1 in H_1 term and ψ_2 in H_2 term), using $2p'_o$ instead of p'_o as the scaling parameter in these terms, introducing the term p'_c/p' into these terms, and using different values of k in extension and compression according to equation 4.40. None of these modifications eliminate the accumulation of negative shear strain problem in the pavement analysis. Therefore a better modification is proposed below.

For the two-surface model, Al-Tabbaa (1987) assumed that the hardening modulus, h is expressed in the following form:

$$h = Fh_o + H \tag{4.42}$$

where F and H are scalar quantities which may be functions of stress state. For both the two-surface model and the 3-SKH model the function $F = 1$. The negative shear strain problem is due to the low stiffness on unloading; therefore the simplest way to solve this problem is to increase the stiffness on unloading. The hardening modulus, h, is expressed in the following form:

$$h = F\left(h_o + H_1 + H_2\right) \tag{4.43}$$

$$F = \left(\frac{2\alpha^4}{1+\alpha^4+\left(1-\alpha^4\right)\sin 3\theta}\right)^{1/4} \tag{4.44}$$

$$\alpha = F_e \tag{4.45}$$

where F_e is the value of F in triaxial extension (θ = +30°). With this additional function, F, the modulus on unloading can be adjusted whereas the modulus on loading will remain unchanged.

A pavement problem was analysed using the new model with the value of k varying according to equation 4.40, and using the function F according to equation 4.44. Figure 4.15 shows the shear strain of the element located at the top of the subgrade near the centreline (see Figure 4.15) as a function of number of cycles predicted by these two models. Note that the equivalent stress blocks at the top of the subgrade had to be calculated for each model. It can be seen that the negative shear strain problem still exists when k is made to be a function of Lode angle according to equation 4.40, with k_c = 1.1 and k_e = 0.5. Comparing Figure 4.14 with Figure 4.15, the negative shear strain problem was slightly improved by using equation 4.40. However, a more realistic prediction was obtained by using the function F for the

hardening modulus in equation 4.44. Therefore, it was considered that the introduction of the function F in the hardening modulus was more appropriate.

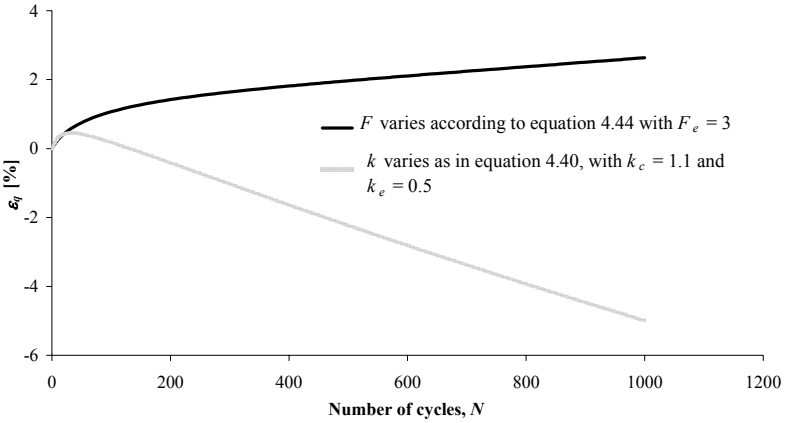

Figure 4.15. Predicted shear strain as a function of number of cycles.

4.3.9 Determination of Parameters

Ten parameters are now required to fully describe the new model:

e_{cs} – The voids ratio at p' = 1kPa on the critical state line.

M – The slope of the critical state line in $q - p'$ space.

-λ^* – The slope of the isotropic normal compression line and critical state line in ln v – ln p' space.

-κ^* – The initial slope of the swelling lines in ln v – ln p' space.

G_e – The elastic shear modulus.

T – The ratio of the size of the history surface to that of the bounding surface.

S – The ratio of the size of the yield surface to that of the history surface.

ψ – The exponent in the hardening moduli H_1 and H_2.

k – The parameter which controls the shape of the plastic potential.

F_e – The value of the multiplier in the hardening modulus in triaxial extension.

If the shear modulus is assumed to be dependent on the mean normal effective stress p' and R_o according to equation 3.7, three extra parameters, A, n and m are needed.

However, these can be determined approximately if the plasticity index of the soil is known (Viggiani and Atkinson, 1995).

The determination of the parameters for the 3-SKH model was described in Chapter 3. The additional parameter k for the new model is chosen such that the value of K_0 during normally compression is correctly predicted. This can be determined by neglecting elastic strains in the stress-dilatancy rule for one-dimensional conditions as discussed in Section 4.3.7. For soils that satisfy the Jâky (1944) equation 2.37, the parameter k can be determined from equation 4.39.

This serves as a guide to choosing the value of the new parameter k, and if equation 4.39 is being used, this means that only one extra parameter, F_e, is needed for the new model.

The parameter F_e is determined by trial and error. It is shown in Chapter 5 that the parameter F_e is suitable for modelling cyclic loading data, and in Chapter 6, it is shown that the introduction of the parameter F_e leads to more realistic modelling of pavement response.

4.4 SUMMARY

A new flow rule has been proposed in this chapter. With one additional parameter, k, a family of plastic potentials can be obtained. The formulation of a three-surface kinematic hardening model based on this flow rule has been presented. This new non-associated three-surface kinematic hardening model is an extension of the 3-SKH model (Stallebrass, 1990), which itself is an extension of the 'Bubble' model (Al-Tabbaa, 1987). By choosing a suitable value of k, more realistic predictions of shear strain and $K_{0,nc}$ can be obtained. These are over-predicted by the 3-SKH model (Stallebrass, 1990). The simple non-associated flow rule is able to scale down the plastic shear strain by a factor of $k/2$, and still gives associated flow under isotropic conditions and at a critical state. The value of K_0 on unloading can also be correctly predicted if the value of the critical state parameter M is made to be a function of

Lode angle. If required, the value of parameter k could be permitted to be different under compression and extension conditions. The value of the parameter k required to correctly predict the value of K_0 during normal compression may be determined by trial and error, or it can be obtained by ignoring elastic strains in the stress-dilatancy rule for one-dimensional normal compression. The new model was implemented into a finite element code and triaxial simulations were performed and it was shown that the prediction of shear strain and K_0 during normal compression and unloading were improved, although there is still some error on reloading: this is a function of H_1 and H_2 and is due to the strong ratcheting phenomenon exhibited by the model. The prediction of the value of K_0 on reloading by the 3-SKH model is better than the new model, but this is mainly because of the higher value of $K_{0,nc}$. As for the 3-SKH model, the new model also suffers from the problem of accumulation of negative shear strain under some stress conditions where the hardening modulus on unloading is not large enough. However, this can be eliminated by modifying the hardening modulus, h. The hardening modulus was modified such that it would become larger on unloading by introducing a scaling factor F_e. This is examined in detail in Chapter 5.

5 EXPERIMENTAL VALIDATION OF THE NON-ASSOCIATED THREE-SURFACE KINEMATIC HARDENING MODEL

5.1 INTRODUCTION

A new non-associated three-surface kinematic hardening model was proposed in the previous chapter. In this chapter, the model parameters for kaolin clay are determined by triaxial testing using the methods proposed by Stallebrass (1997) – see Section 3.2.3. Drained cyclic loading tests were performed to validate the model and to determine the parameters ψ, and F_e, that best fit the data. Due to time constraints caused by the difficulties in the commissioning of the equipment, only two drained cyclic loading tests were performed. Each test took approximately five weeks to complete.

5.2 TRIAXIAL TEST

This section briefly describes the triaxial apparatus used, the sample preparation, and the procedure followed in performing the tests. The GDS advanced triaxial testing system was used in this research. A detailed description of the triaxial apparatus can be found in Menzies (1988) and the GDS Laboratory manual (GDS Instruments Ltd, 2002). All of the tests reported here were performed on samples of Speswhite kaolin prepared by mixing Speswhite kaolin powder with distilled water at a water content of 130% and then consolidating in an oedometer. The test results are reported and discussed in this chapter.

5.2.1 Description of the Triaxial Apparatus

The GDS triaxial testing system was used for this research to carry out the necessary triaxial testing. A brief description of this system is given in this section.

The system consists of a triaxial cell, two standard and one advanced computer controlled pressure sources, an eight-channel data acquisition pad, a computer and a multiplexer which allows up to four devices to be connected to a communication port on the computer. The system layout is shown in Figure 5.1.

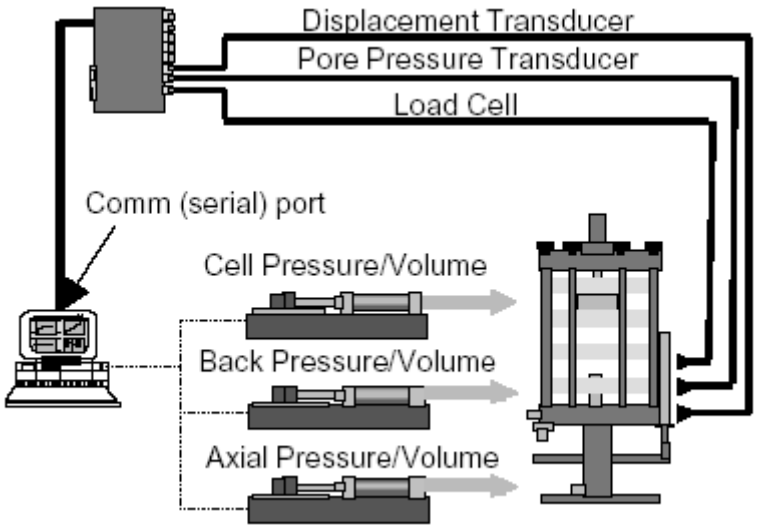

Figure 5.1. Schematic diagram showing the layout of the triaxial system (GDS Instruments Ltd, 2002).

Triaxial cell

The triaxial cell is a Bishop and Wesley (1975) cell which has a maximum safe working pressure of 1700kPa. Both 38mm and 50mm diameter specimens can be tested using this cell. Axial force is exerted on the test specimen by a piston fixed to the base pedestal. This piston moves vertically upwards and downwards actuated hydraulically from the lower chamber in the base of the cell, which contains water. Known displacements may be applied by pumping a known volume of water from a GDS pressure controller into the lower chamber. GDS standard pressure/volume controllers are used to control both the lower chamber pressure and the cell pressure. A 2kN internal submersible load cell which has an accuracy of 2N, one external

axial displacement transducer with a range of 40mm and an accuracy of 0.1mm, and one 2000kPa range pore pressure transducer with an accuracy of 2kPa are used. The back pressure is applied to the top of the sample by a GDS advanced pressure/volume controller and the volume change of the sample is also measured by this controller. The pore pressure is measured at the base of the sample. The measurement of local strain is discussed later.

Pressure/volume controller

The triaxial system consists of three 2MPa pressure/volume controllers: two standard pressure/volume controllers to control the cell pressure and lower chamber pressure and one advanced pressure/volume controller for the back pressure source. The volumetric capacity of these controllers is $2\times10^{-4}m^3$. The resolution of the pressure control is 2kPa and the resolution of pressure measurement is 1kPa.

Hall effect transducers

If current is flowing through a semiconductor plate that is placed in a magnetic field where flux lines are directed perpendicular to both the material and the current flow, voltage is produced across the plate in a direction normal to the current flow. This is known as the Hall effect. The application of Hall effect transducers to measure local axial and radial deformation in the triaxial test has been successfully performed at the University of Surrey (Clayton et al., 1989). The radial strain-measuring device consists of a calliper, which is mounted on the test specimen by pins or bonded to the membrane by adhesive. The Hall effect transducer is positioned across the opening at the calliper where it measures the opening and closing of the jaws. Figure 5.2 shows the radial strain-measuring device mounted on the test specimen. For axial strain measurement, the device consists of a spring-mounted pendulum that holds a magnet assembly, which is suspended from a mounting block. This mounting block is fixed to the test specimen by pins or bonded to the membrane by adhesive. The lower part of the transducer, which is mounted on the specimen by pins or adhesive, consists of a metallic container holding the linear output Hall effect semiconductor. The range of the Hall effect transducer is ±3mm with an accuracy of 0.05mm; at this

range the output of the transducer is almost linear. The Hall effect transducers were used in all the triaxial tests performed.

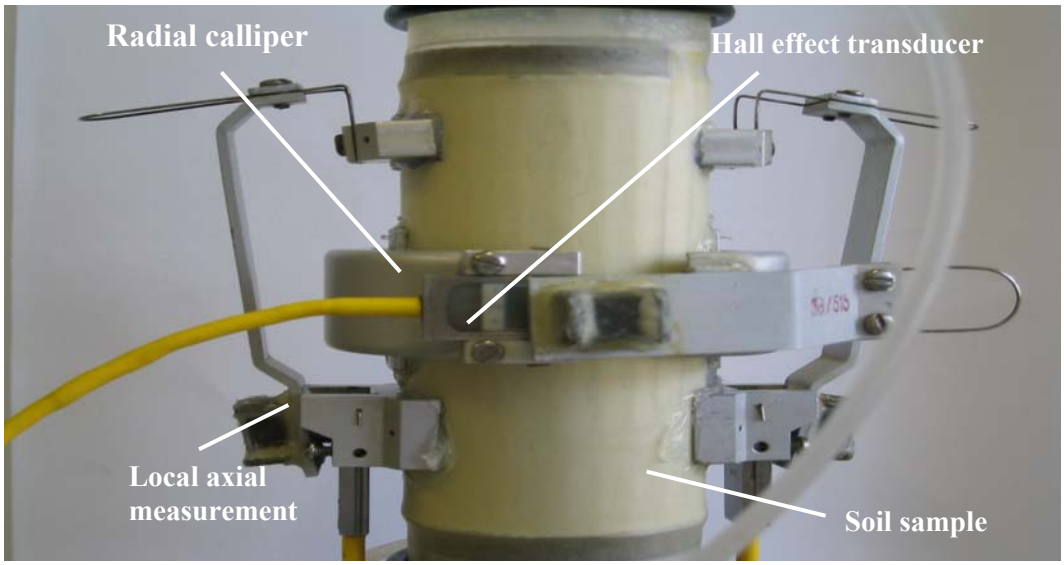

Figure 5.2. Picture showing the on-sample instrumentation.

5.2.2 Soil Used in the Experimental Test

The soil used in this research is Speswhite kaolin provided in dry powder form. The soil sample was prepared by mixing the kaolin powder with distilled water of twice the liquid limit and consolidating in an oedometer. Index tests were performed to determine the liquid limit and plastic limit. The liquid limit and plastic limit were found to be 63% and 31% respectively. Other researchers have obtained similar value for Speswhite kaolin. The liquid limit and plastic limit obtained by Atkinson (1987) were 65% and 35% respectively, by Al-Tabbaa (1987) 69% and 38% respectively, and by Martin & Houlsby (2000) 65% and 34% respectively.

5.2.3 Sample Preparation

A 100mm diameter oedometer was used to prepare samples for triaxial testing. Figure 5.3a shows the base, top cap and porous stones for the oedometer. Sufficient amount of dry Speswhite kaolin powder was mixed with distilled water at a moisture

content of 130% (twice the liquid limit) to form the slurry. The slurry was then poured into the oedometer with care to ensure that no air was trapped. Filter paper was soaked in water and placed on the top and bottom porous stones so that clay would not clog them. Drainage was allowed at the top and bottom. The vertical pressure was applied using a pressure regulator which had been calibrated against a load cell. A photograph of the oedometer in use is shown in Figure 5.3b. The kaolin slurry was one-dimensionally consolidated to a vertical pressure of 200kPa. This pressure was applied in increments of 10, 20, 50, 100, and 200kPa. Each increment of pressure was held for a period of at least 48 hours to allow the excess pore pressure to dissipate. The sample was then unloaded to 100kPa and the sample was left under this pressure until extrusion. This would leave the sample in an approximately isotropic state of $p' \approx 100$kPa (Al-Tabbaa, 1987) which could then be easily recreated in the triaxial cell. The whole process took approximately three weeks. During extrusion, a thin wire was run along the circumference of the sample to reduce the friction between the soil specimen and the oedometer when it was being pushed out. The sample was then trimmed to the required size using a wire saw and a trimming apparatus. During the process of extrusion and trimming, great care was taken in order to keep the sample disturbance to a minimum. Initial dimensions, weight and moisture content of the specimen were measured before setting up the specimen in the triaxial apparatus.

(a) *(b)*

Figure 5.3. (a) Oedometer, porous stones, top and base caps, and (b) sample under one-dimensional consolidation.

5.2.4 Specimen Set Up and Test Procedure

After the sample was trimmed to the required dimensions, in this case a diameter of 38mm and height 76mm, the specimen was ready to be set up in the triaxial apparatus. Before the specimen was set up in the triaxial apparatus, the pore pressure line was de-aired by flushing it with water and the reading of the pore pressure was set to zero. A porous stone which had been soaked overnight was slid over a layer of water on the base pedestal without trapping any air. Filter paper and the specimen were then placed on the porous stone. The second filter paper and porous stone were then placed on top of the specimen. After that, three filter strips of ¾ of the length of the sample were placed on the side of the specimen for side drainage. For the extension test, fishnet spiral filter strips were used in order to minimise the stiffness of the filter paper. After that, a rubber membrane was put onto the sample using a membrane stretcher. A vacuum was applied to the membrane stretcher to help put the membrane on. A de-aired top cap was then placed on top of the sample. Two O-rings were used for each end to seal the membrane to the base pedestal and the top cap. The Hall effect transducers were installed at this stage. For triaxial extension, a vylastic sleeve and an extension top cap were used. The vylastic sleeve was smeared with a layer of silicone grease to prevent leakage. The triaxial cell was then assembled, and the load cell reading set to zero. The cell was filled with water with the air bleed open. When the water level reached the mid height of the sample, the cell and lower chamber pressure readings were set to zero. The load cell was lowered slowly until it just made contact with the top cap. When the extension top cap was used, a very small vacuum was applied to ensure contact between the top cap and the extension cap. When the cell was completely filled with water the air outlet valve was closed and the specimen was ready for testing. Initially, a cell pressure of 50kPa was applied with the drainage valve closed. This was to measure the initial effective stress of the sample. The pressure was held for a period of time until pore pressure stabilized, and the effective stress was noted. After that, the drainage valve was opened and back pressure saturation was performed by applying back pressure and cell pressure simultaneously and incrementally to keep the effective stress unchanged. The back pressure used was about 430kPa for all the tests and the B-

value obtained was about 0.97 for both the tests. These procedures were the same for both the tests performed for this research.

The testing rates used in the tests were $\delta\sigma'_a = \delta\sigma'_r$ = 5kPa/hr for isotropic tests, $\delta\sigma_r'$ = 3kPa/hr for a one-dimensional compression test, and an axial strain rate of 0.1%/hr was used for drained shearing test. Similar testing rates were used by a number of researchers performing triaxial tests on kaolin (Al-Tabbaa, 1989; Atkinson, 1987; Stallebrass, 1990). These testing rates were checked to see that excess pore pressures were negligible, using the method proposed by Menzies (1988). In this method, the pore pressure difference between the top and bottom ends of the test specimen i.e. the excess pore pressure is restricted to a fixed value. According to Menzies (1988), an excess pore pressure of 5% of the total axial stress may be permissible. Figure 5.4 shows a schematic diagram of the triaxial test system applying a constant back pressure u_b to the top end, and measuring the pore pressure u at the base of the specimen. Drainage is allowed only at the top of the specimen. During all the tests, the excess pore pressure measured using this method was about 5kPa.

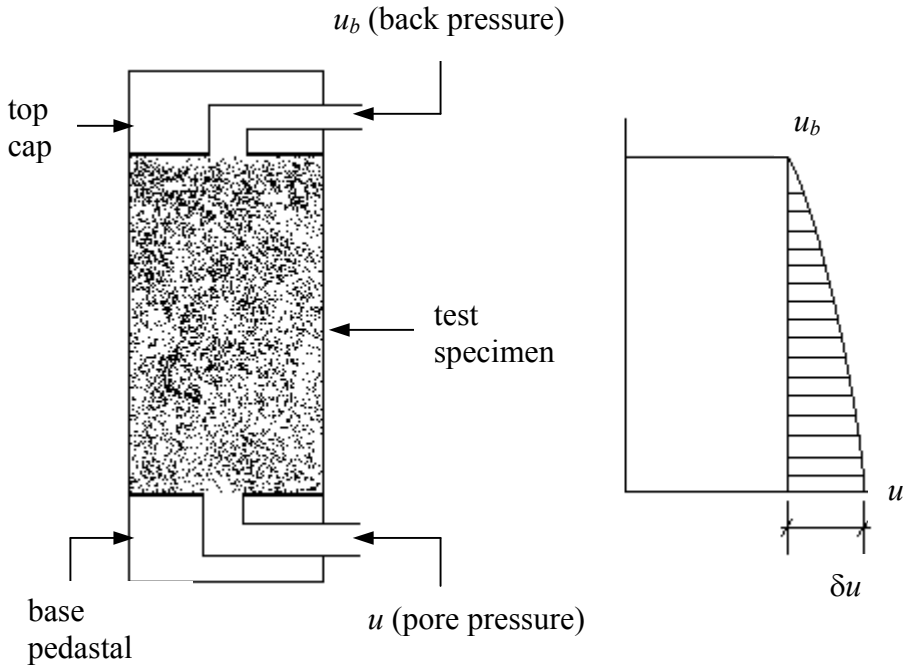

Figure 5.4. Schematic diagram showing the excess pore water pressure measured during a drained test (Menzies, 1988).

5.2.5 Analysis of Data

The test results were interpreted in terms of the deviatoric stress $q = (\sigma'_a - \sigma'_r)$ and the effective mean normal stress $p' = (\sigma'_a + 2\sigma'_r)/3$, where σ'_a and σ'_r are the axial and radial effective stresses respectively. The corresponding strains were shear strain $\varepsilon_q = 2(\varepsilon_a - \varepsilon_r)/3$ and volumetric strain $\varepsilon_p = \varepsilon_a + 2\varepsilon_r$, where ε_a and ε_r are the axial and radial strains respectively. Following Stallebrass (1990), all the strains used were true strains calculated from the engineering strains as these strains eliminate errors when strains become large and are more appropriate for comparison with incremental constitutive soil models. The axial strain is defined as:

$$\varepsilon_a = \int_l^{l_o} \frac{\mathrm{d}l}{l} = -\ln\left(1 - \varepsilon_o\right) \tag{5.1}$$

where compressive strain is positive, l_o is the initial height l is the current height, and ε_o is the engineering strain:

$$\varepsilon_o = \frac{\delta l}{l_o} \tag{5.2}$$

5.3 DETERMINATION OF MODEL PARAMETERS

In this section, the results which were used for determination of parameters are presented. There are ten parameters required to define the new model; five of which are Modified Cam clay parameters, plus the parameters to define the size of the kinematic surfaces, T and S, the parameter ψ, and the new parameters k, and F_e. The method described by Stallebrass (1997) was used to obtain the required parameters and this has been described briefly in Section 3.2.3. For this purpose, the bulk stiffness $K' = \delta p'/\delta\varepsilon_p$ was calculated by fitting a straight line to data points on the graph of p' versus ε_p over a stress change of approximately 15kPa (Stallebrass, 1990). The new parameter k was obtained from a one-dimensional normal compression test and the parameters ψ and F_e were determined by fitting the cyclic loading test results.

5.3.1 Model Parameters

(i) Modified Cam clay model parameters

Figures 5.5 and 5.6 shows the isotropic normal compression and swelling lines in v – ln p' space and ln v – ln p' space respectively for a test performed on a specimen of Speswhite kaolin. The slopes of the normal compression line in v – ln p' space and ln v – ln p' space are denoted by $-\lambda$ and $-\lambda^*$ respectively. The values for λ and λ^* were found to be 0.19 and 0.073 respectively, and the isotropic line is fixed at the point p' = 400kPa and v = 2.071.

Following Stallebrass (1990), by plotting K'/p' against p'/p'_m (p'_m is the maximum mean effective pressure to which the soil has been loaded) for isotropic swelling from a normally consolidated state, the value of κ^* can be estimated as the initial value of p'/K'. The value of κ^* is not very reliable because measuring stiffness at very small strains is difficult. Figure 5.7 shows the result for K'/p' versus p'/p'_m. The parameter κ^* was determined from the initial part of the curve with p'/p'_m = 1, and was found to be 0.003. For a linear isotropic normal compression line in v – ln p' space, the value of v at 1kPa, denoted by N, would be 3.209. This gives the critical state void ratio e_{cs}, at p' = 1kPa a value of e_{cs} = 2.056 (e_{cs} can be calculated from $\ln(1+e_{cs}) = \ln N - (\lambda^* - \kappa^*) \ln 2$).

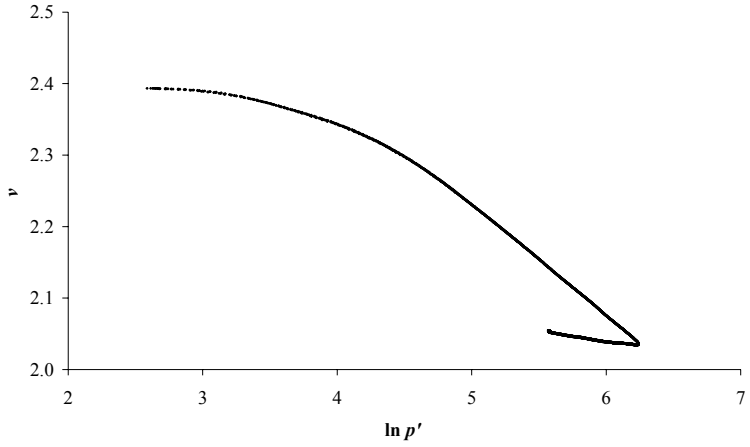

Figure 5.5. Isotropic normal compression line and swelling line in v – ln p' space.

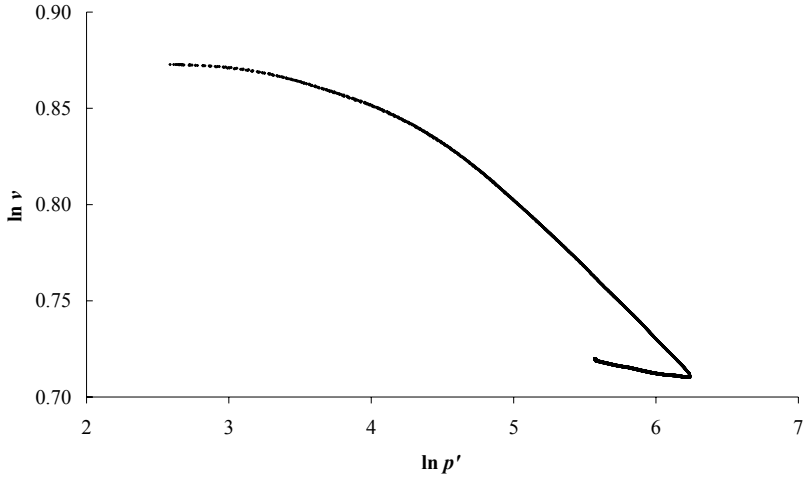

Figure 5.6. Isotropic normal compression line and swelling line in ln v – ln p′ space.

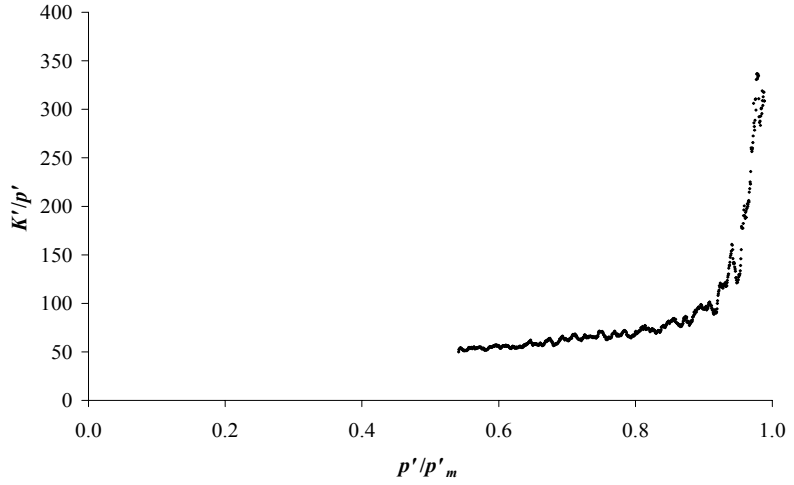

Figure 5.7. Result showing K′/p′ versus p′/p′$_m$ during isotropic unloading.

The critical state dissipation constant, M, was obtained from a strain-controlled drained shearing test at 0.1%/hr with constant cell pressure. A critical state is said to have been reached when the soil undergoes large deviatoric strains at constant stress ratio, and at constant volume. The results for stress ratio versus shear strain, and volumetric strain versus shear strain are presented in Figures 5.8 and 5.9 respectively. A clearly defined critical state has been reached at a stress ratio M = 0.86 after a deviatoric strain $\varepsilon_q \approx 18\%$. This value of M corresponds to a friction angle $\phi' = 22°$.

The elastic shear modulus was estimated from the relationship proposed by Viggiani and Atkinson (1995) – see Equation 3.7. The coefficients A, m, and n can be obtained from Figure 5.10 produced by Viggiani and Atkinson (1995) if the plasticity index is known. These charts were derived from test data for different soil types with different plasticity indices. The coefficients A, m, and n obtained by Viggiani and Atkinson (1995) for Speswhite kaolin clay were 1964, 0.2, and 0.65. However, the plasticity index of their soil was 24%, which is smaller than the value obtained in this present study (PI = 32%). From Figure 5.10, for soil with PI = 32% the coefficients A, m, and n are approximately 1,000, 0.8, and 0.24 respectively. Figure 5.11 shows the effect of these parameters on the prediction of permanent settlement in a pavement problem. The resilient deformations predicted using the coefficients obtained by Viaggiani & Atkinson (1995) and from Figure 5.10 with PI = 32% were 0.26mm and 0.25mm respectively. In addition, the results in Figure 5.11 show that the values of these parameters have no significant influence on the predicted permanent deformations. Hence, the coefficients used by Stallebrass (1997) will be used since they have been well established by bender element tests.

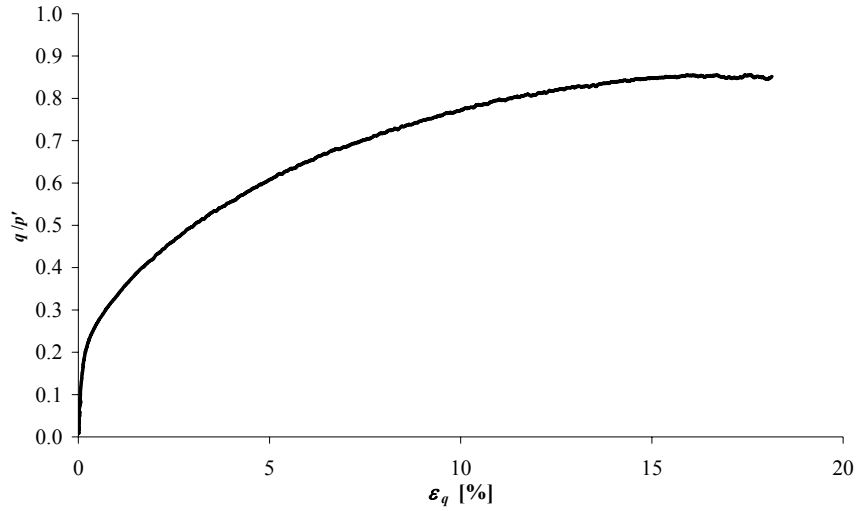

Figure 5.8. Deviatoric stress-strain curve for a conventional drained triaxial test.

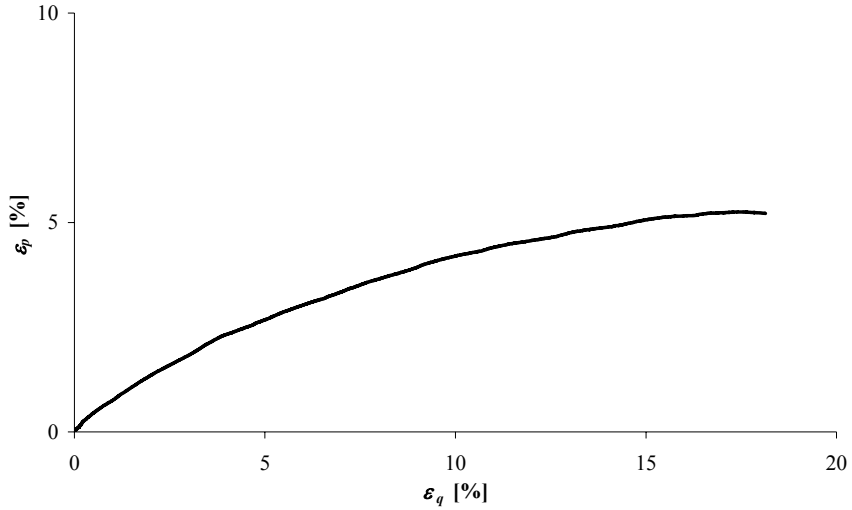

Figure 5.9. Volumetric strain during conventional drained shearing.

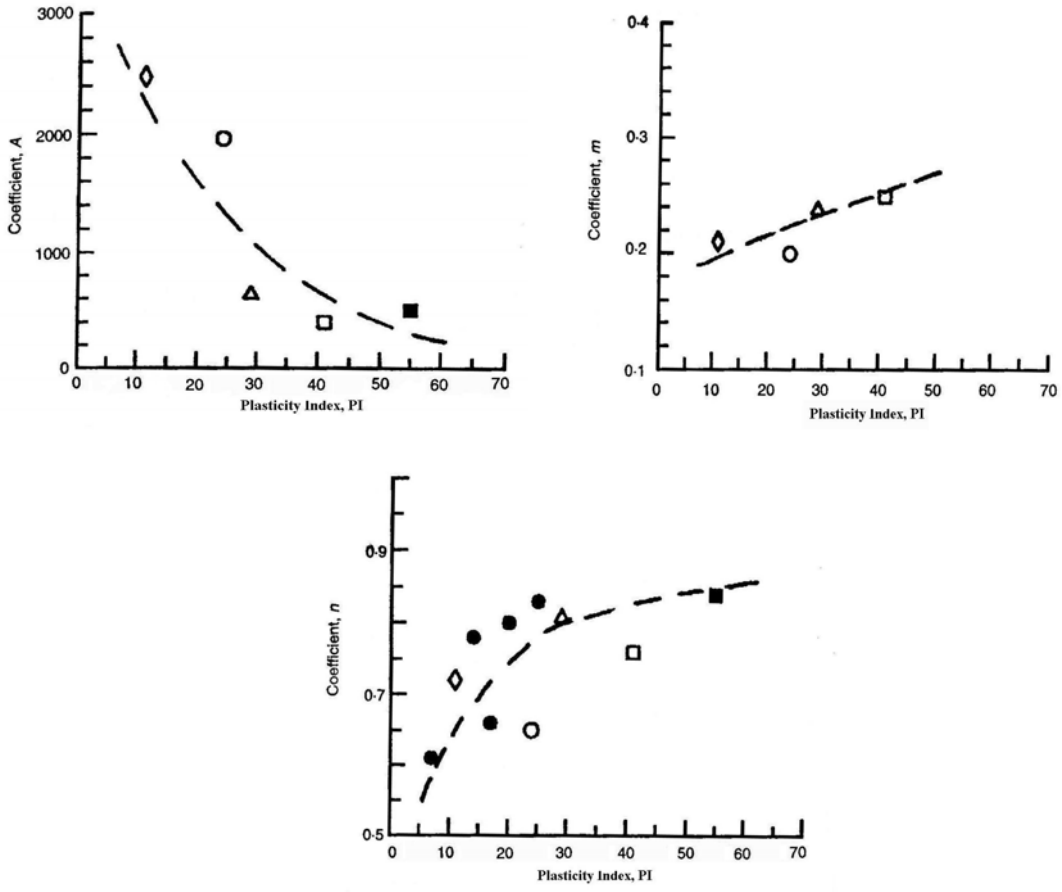

Figure 5.10. Variation of coefficients for G_e with plasticity index (Viggiani and Atkinson, 1995).

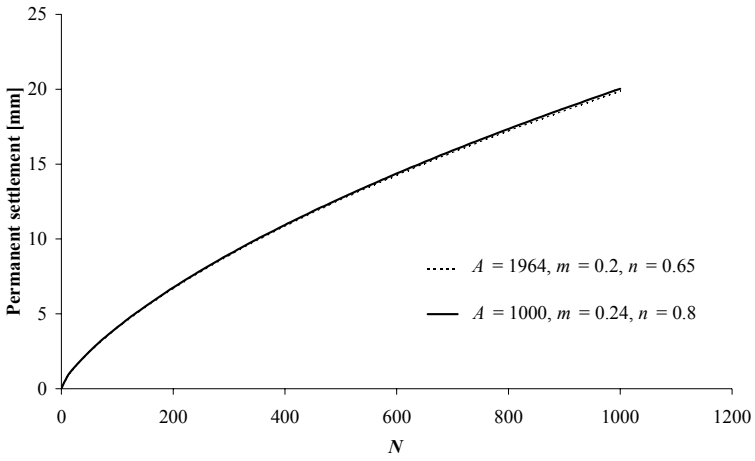

Figure 5.11. Effect of parameters A, m, and n on the predicted permanent settlement of a three-layer pavement.

(ii) T and S

The parameters T and S that determine the size of the history and the yield surfaces were determined by isotropic unloading and reloading as described by Stallebrass (1997), see Section 3.2.3. The stress path followed in this test is shown in Figure 3.6 with $p' = p'_m$ = 510kPa (point O), followed by swelling back to p' = 250kPa (point B). Figures 5.12 presents the results of the bulk stiffness versus change in stress for stress paths with angles of stress rotation, $\varphi = 0°$ and $\varphi = 180°$. To determine the parameter T, the stress change, $\Delta p' = 2Tp'_o$ at which the two stiffness curves meet, is obtained from Figure 5.12. From the data presented in this figure, there is not a well-defined point where the two stiffness curves meet. Inspection of Figure 5.12 shows that the stiffness curves merge at approximately $\Delta p'$ = 140kPa, which gives T a value of approximately 0.27. The very small strain stiffness, which is needed to determine the size of the elastic region, cannot easily be measured using a triaxial apparatus, as the very small strain stiffness usually occurs at strain levels below 0.001% (Atkinson, 2000). The stiffness at this strain level is usually measured using bender elements or a resonant column; unfortunately these devices were not available for this research. So based on this study and that of Stallebrass (1990), values of T = 0.25 and S = 0.08 might be appropriate. It will be shown that these values are appropriate for modelling behaviour under cyclic loading.

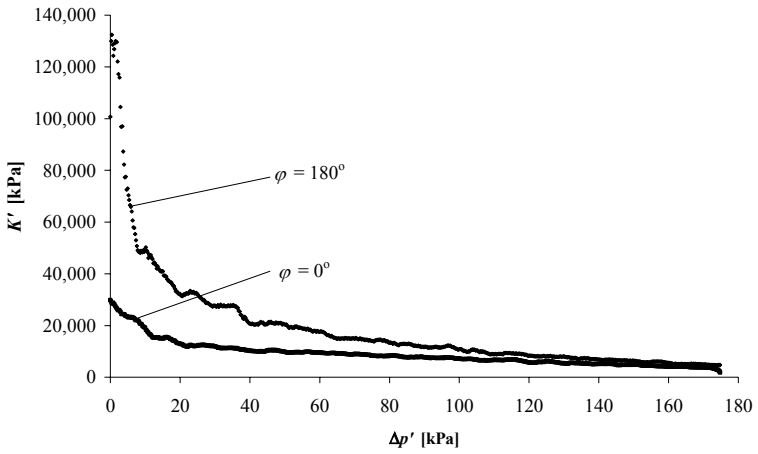

Figure 5.12. Curves showing the variation in bulk stiffness with $\Delta p'$ for stress rotations $\varphi = 0°$ and $\varphi = 180°$.

(iii) *k*

The new parameter, *k*, which determines the shape of the plastic potential and hence the value of $K_{0,nc}$, can be obtained from a one-dimensional normal compression test. Figure 5.13 shows the results of $K_{0,nc}$ versus ε_a during a one-dimensional loading test. The value of $K_{0,nc}$ reached a constant value of 0.72 ($\eta_{0,nc} = 0.344$) at axial strain of approximately 14%. Al-Tabbaa (1987) obtained a $K_{0,nc}$ value of 0.69 for her test on kaolin. By neglecting elastic strains, the parameter *k* can be estimated, given the friction angle ϕ' and the value of $K_{0,nc}$. The value of *k* corresponding to $\phi' = 22°$ (M = 0.86) and $K_{0,nc} = 0.72$ ($\eta_{0,nc} = 0.344$) is 1.2, according to equation 4.38 (i.e. ignoring elastic strains) or Figure 4.7.

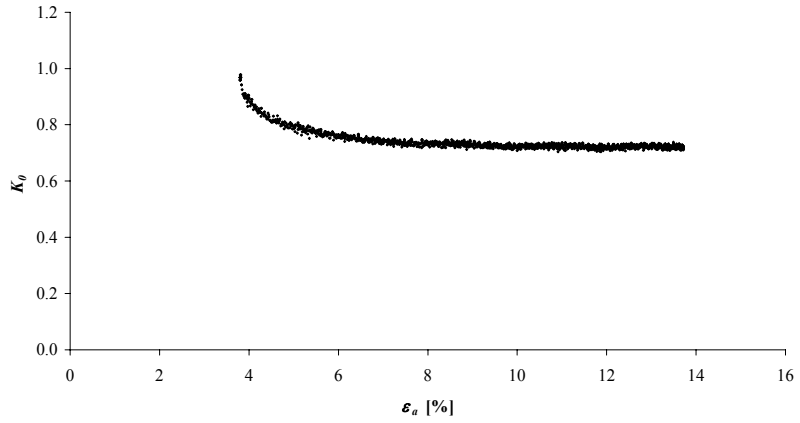

Figure 5.13. Experimental data showing K_0 values versus axial strain, ε_a.

All the model parameters can be determined directly, except ψ and F_e which can only be determined by trial and error (i.e. parametric studies). However, the values of T, S, and κ^*, cannot be measured very accurately, as discussed. Consequently, parametric studies have been performed using cyclic loading data to determine the parameters ψ, and F_e, and better estimates of the parameters T, S, and κ^*, suitable for modelling cyclic loading. This is described in the next section.

5.3.2 Parametric Study

The purpose of this study was to determine the parameters ψ and F_e that best fit experimental data and to make better estimates of the parameters T, S, and κ^* for the purpose of modelling behaviour under cyclic loading. The effect of the parameters ψ and F_e will first be investigated (these can only be determined by trial and error): before continuing to investigate the effects of other parameters, sensible values of these parameters are required. This is followed by an investigation of the influence of parameters T, S, and κ^*. The rest of the parameters were unchanged during these simulations. The values were M = 0.86, $\lambda^* = 0.073$, $k = 1.2$, and G_e varied according to equation 3.7 with $A = 1964$, $m = 0.2$, and $n = 0.65$.

For this parametric study, the stress-strain behaviour of a conventional drained cyclic test on Speswhite kaolin was simulated and compared with the experimental data. The recent stress histories of the sample were simulated in the finite element modelling. The drained cyclic test was performed using the same sample that had been used for the determination of the model parameters T and S. After the isotropic stress reversal ($\varphi = 180°$) for the determination of the stiffness curve, the sample was isotropically compressed to $p' = 545$kPa and a cyclic stress ratio was applied at a constant cell pressure between $\eta = 0$ and $\eta = 0.2$. Figure 5.14 presents the stress-strain curves for the test.

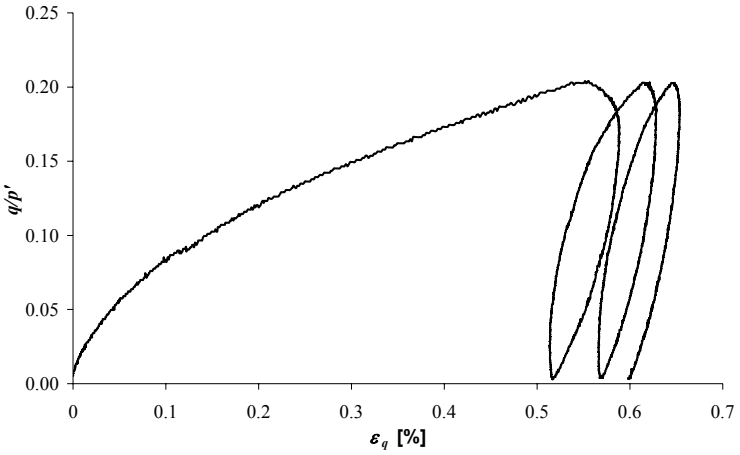

(a)

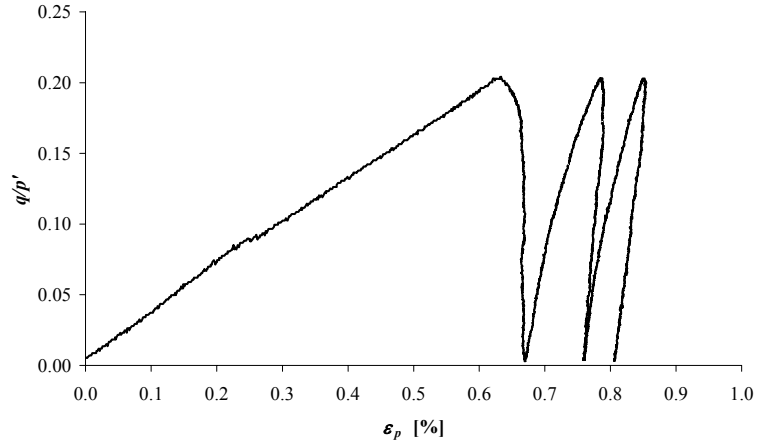

(b)

Figure 5.14. Experimental data from drained cyclic triaxial test on Speswhite kaolin (a) q/p' versus ε_q, and (b) q/p' versus ε_p.

(i) ψ

For these simulations, the parameters were set to $\kappa^* = 0.003$, $F_e = 1$, $T = 0.25$, $S = 0.08$. The value of ψ was varied from 1.0 to 2.5. The model predictions are shown in Figure 5.15. The rate of decay of stiffness is influenced by parameter ψ, increasing the value of ψ would increase the rate of decay of stiffness and hence give larger plastic strains. The experimental data shows that volumetric strain increases on unloading, and this feature is captured by the model. Larger volumetric strains are predicted with increasing values of ψ.

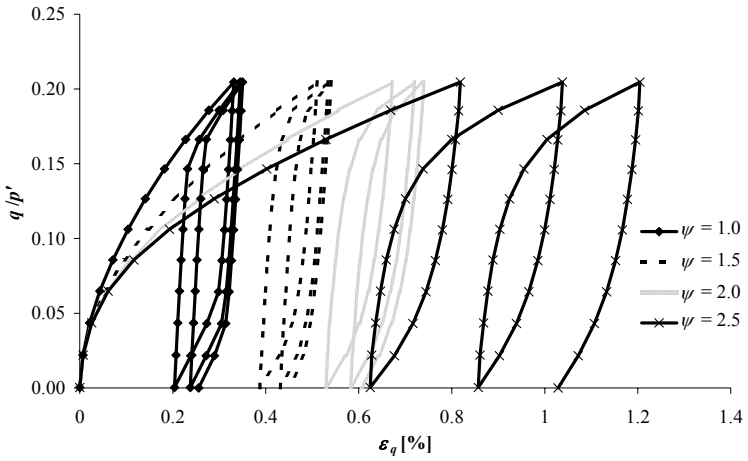

(a)

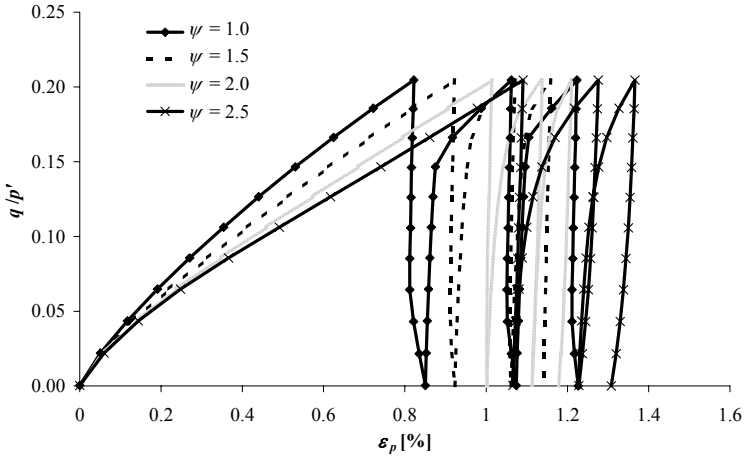

(b)

Figure 5.15. Effect of ψ on the stress-strain behaviour (a) q/p' versus ε_q, and (b) q/p' versus ε_p.

(ii) F_e

By comparing the results presented in Figures 5.14 and 5.15, the value ψ=1.5 was chosen to investigate the effect of the parameter F_e (ψ = 2 could have been chosen, but this gives too much shear strain on first loading). The rest of the parameters are the same as in the above parametric study of parameter ψ. The parameter F_e was varied from 1 to 4 and the effect of this parameter on the stress-strain curves is illustrated in Figure 5.16. As can be seen from this figure, the volumetric strain is

relatively insensitive to the variation of the parameter F_e. Increasing the value of F_e increases the stiffness on unloading and hence smaller strains are recovered on unloading. The predicted total shear strains are larger with a larger value of F_e.

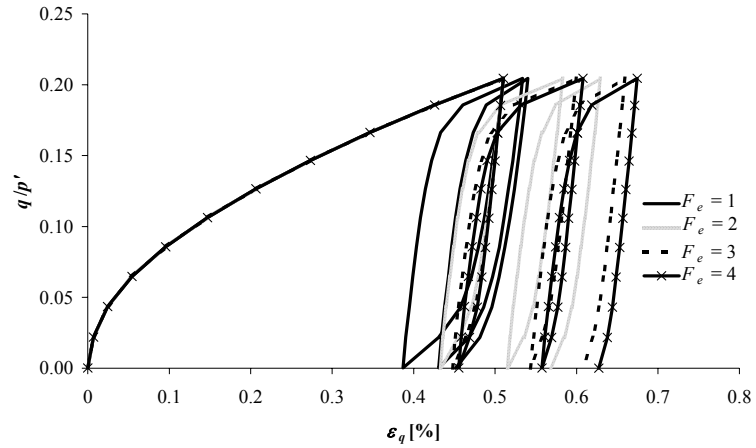

(a)

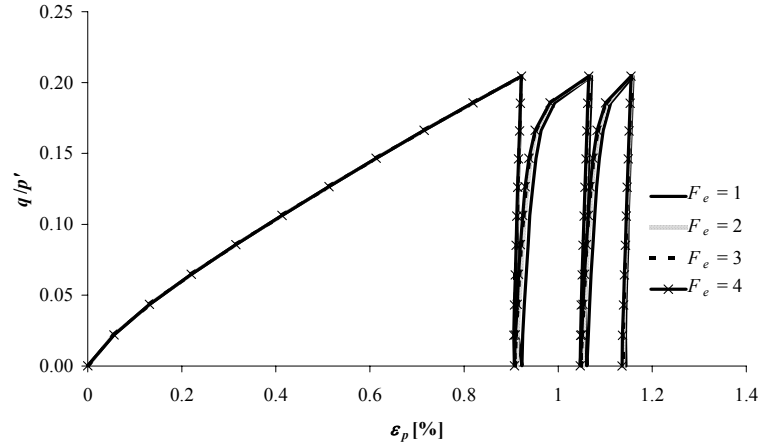

(b)

Figure 5.16. Effect of F_e on the stress-strain behaviour (a) q/p' versus ε_q, and (b) q/p' versus ε_p.

(iii) κ^*

The influence of κ^* on the stress-strain curves is shown in Figure 5.17. The value of κ^* was varied from 0.003 to 0.007 and by comparing Figures 5.14 and 5.16, the value $F_e = 3$ was chosen in this parametric study. Increasing the value of κ^* leads to

the accumulation of smaller plastic strains. A value of $\kappa^* = 0.003$ was found to fit the data quite well.

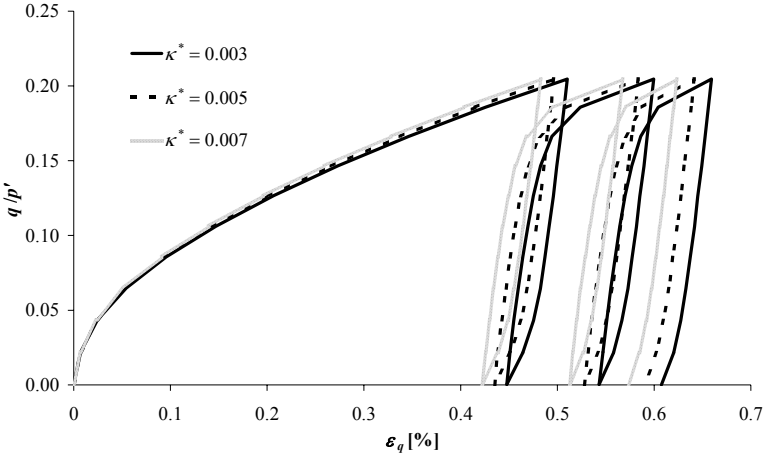

(a)

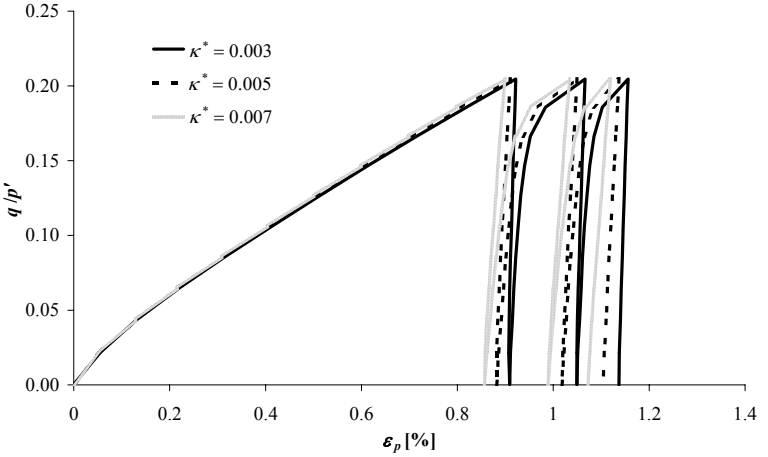

(b)

Figure 5.17. Effect of κ^* on the stress-strain behaviour (a) q/p' versus ε_q, and (b) q/p' versus ε_p.

(iv) *TS*

This section investigates the effect of the size of the elastic region on the stress-strain behaviour. The size of the elastic region was varied from $TS = 0.01$ to $TS = 0.03$ with the size of the history surface (i.e. T) unchanged. The parameters were set to $\kappa^* = 0.003$, $F_e = 3$, $\psi = 1.5$, and $T = 0.25$. The results are shown in Figure 5.18. It can be

seen from the results that the larger the elastic region the greater the total plastic strain predicted. Stallebrass (1990) found that in her parametric study, the rate of decay of stiffness would be faster for a larger elastic region.

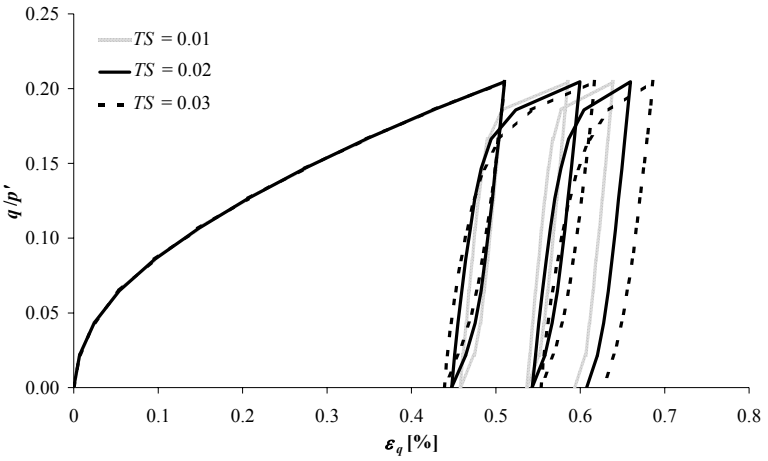

(a)

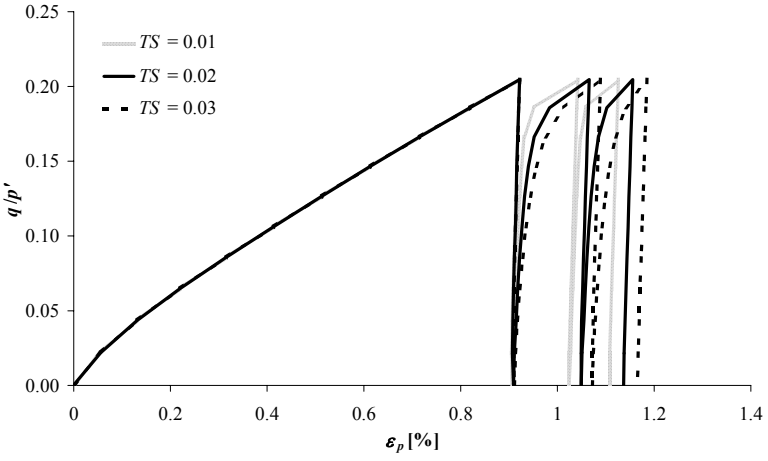

(b)

Figure 5.18. Effect of TS on the stress-strain behaviour.

(v) *T*

The effect of parameter *T* was investigated by keeping the size of the elastic region constant, *TS* = 0.02, and *T* was varied between 0.2 and 0.3. The results are shown in Figure 5.19. It can be seen from the figure that initially, when the stress state is inside the history surface, the predicted strain decrement on unloading is larger for a

smaller history surface as stiffness decays more quickly. The total strain accumulated increases with decreasing size of the history surface.

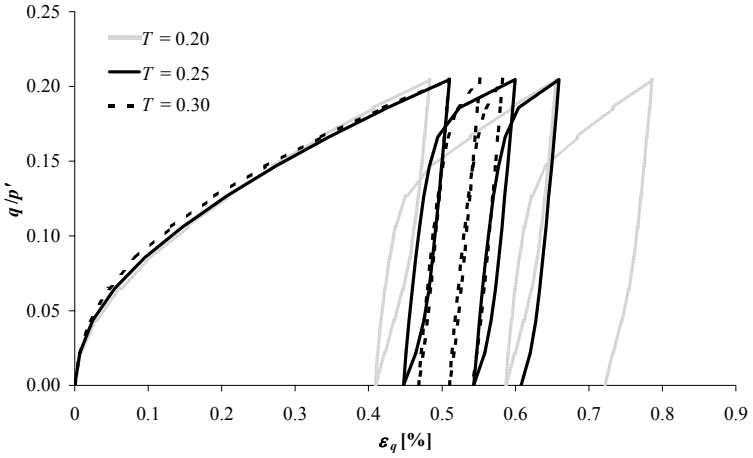

(a)

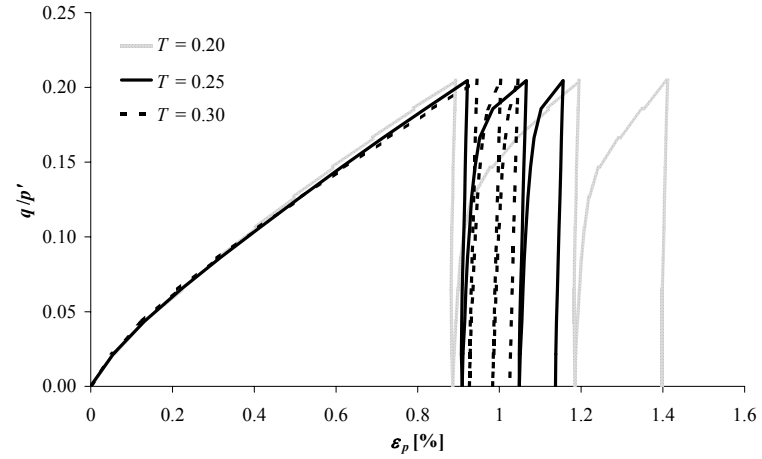

(b)

Figure 5.19. Effect of T on the stress-strain behaviour (a) q/p' versus ε_q, and (b) q/p' versus ε_p.

For the range of values used in this parametric study for parameters κ^*, *T*, *and S*, it was found that κ^* and the size of the yield surface (for a given *T*) have relatively little influence on the stress-strain behaviour. For a given size of the yield surface *TS*, the size of the history surface *T* has a much greater effect, and the parameter ψ also has a considerable effect on the stress-strain behaviour. Generally the model is able to fit the experimental data well, but the model slightly over-predicts volumetric

strain. The model can reproduce some of the features of soil under repeated loading as observed in the experiments, such as the increase in volumetric strain during unloading, and the gradual decrease of the strain increments with increasing number of cycles.

From the comparison between the experimental data and the model predictions shown in Figures 5.14 – 5.19, the model parameters that best represent Speswhite kaolin were obtained. These were: M = 0.86, $\lambda^* = 0.073$, $\kappa^* = 0.003$, $e_{cs} = 2.056$, $A = 1964$, $m = 0.2$, $n = 0.65$, $T = 0.25$, $S = 0.08$, $k = 1.2$, $\psi = 1.5$, and $F_e = 3$. These parameters are used in all subsequent analyses presented in Chapters 5 and 6. The comparison between the model predictions using these parameters and the experimental data are presented in Figure 5.20.

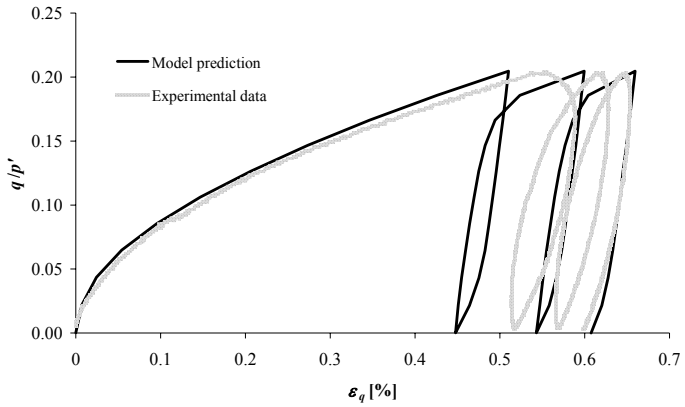

(a)

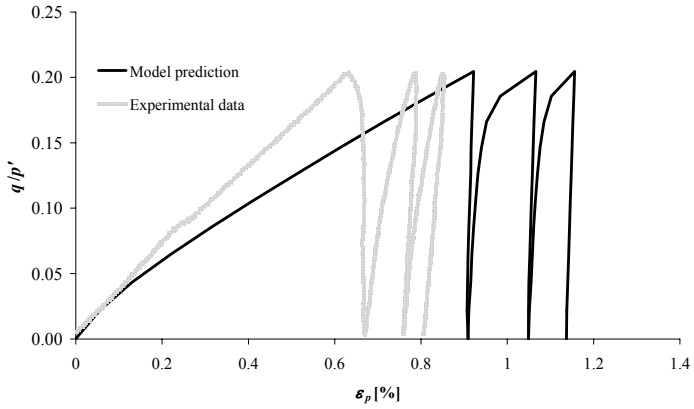

(b)

Figure 5.20. Comparison of model predictions and experimental data (a) q/p' versus ε_q, and (b) q/p' versus ε_p.

5.4 REPEATED LOADING RESULTS AND MODEL PREDICTIONS

A cyclic triaxial test was performed on a sample with a one-dimensional history, similar to that experienced by pavement subgrades in a 'cut' condition (Brown, 1996). The sample was initially one-dimensionally compressed to $\sigma'_{v,\max}$ = 460kPa then unloaded to σ'_v = 40kPa and recompressed to σ'_v = 117kPa. It was then cyclically loaded between stress ratios of η = 0.24 and η = 0.61. The stress path for the one-dimensional loading, unloading and reloading is shown in Figure 5.21, and the variation of the values of K_0 with OCR is shown in Figure 5.22. In Figure 5.23, Al-Tabbaa (1987) compared the variation of the values of K_0 with OCR as obtained by various researchers, and her data for kaolin showed that the values of K_0 vary drastically. The K_0 values measured in this research are slightly lower than those shown in Figure 5.23.

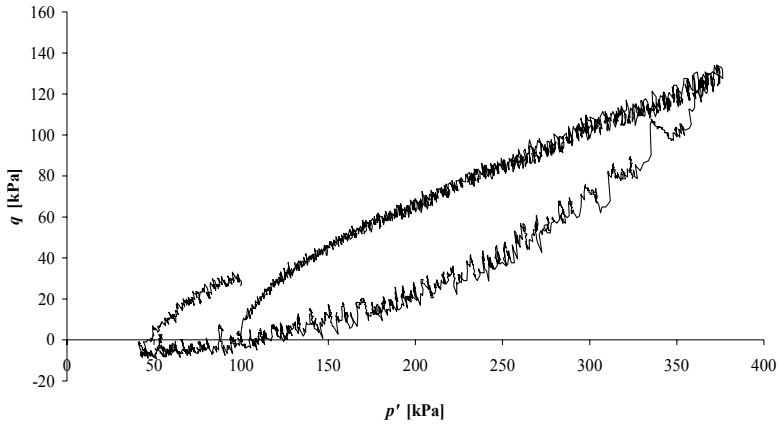

Figure 5.21. Stress path for one-dimensional loading, unloading and reloading.

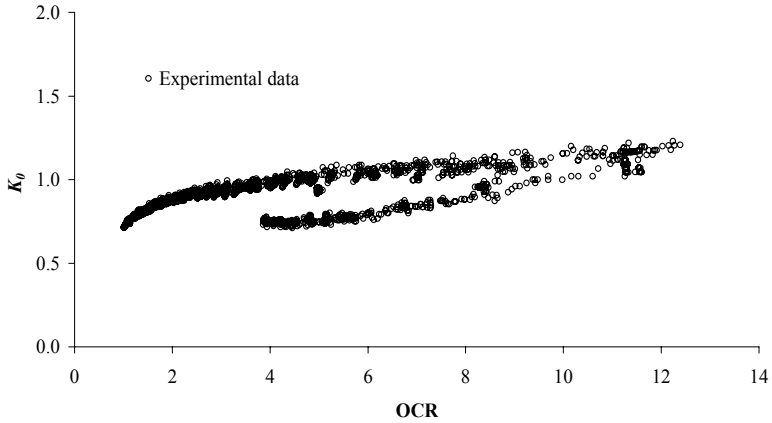

Figure 5.22. Variation of K_0 with OCR.

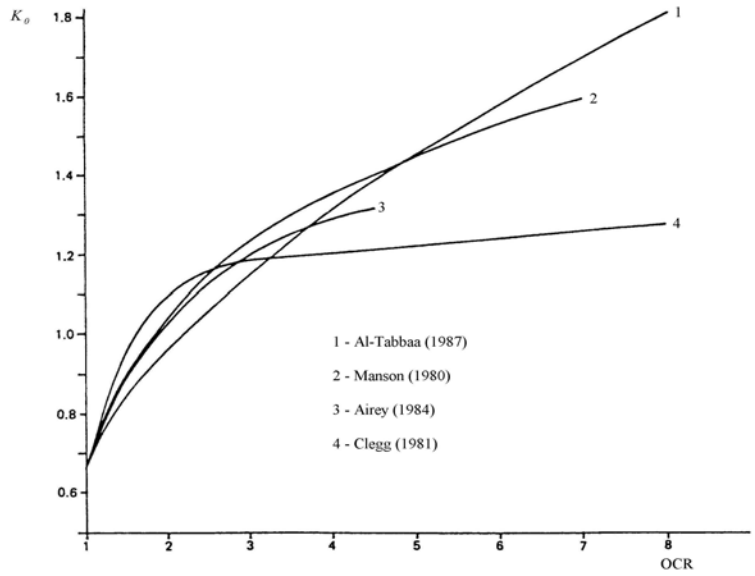

Figure 5.23. Comparisons of K_0 measured by various researchers (Al-Tabbaa, 1987)

Various relations for the variation of K_0 with OCR have already been described in Section 2.2.9. Figure 5.24 shows the comparison of the values of K_0 predicted by these relations and the measured values. It was found that the data are best fitted by the expression proposed by Průska (1973) with a value of $\phi' = 22°$; the other relations over-predicted the measured values of K_0 considerably.

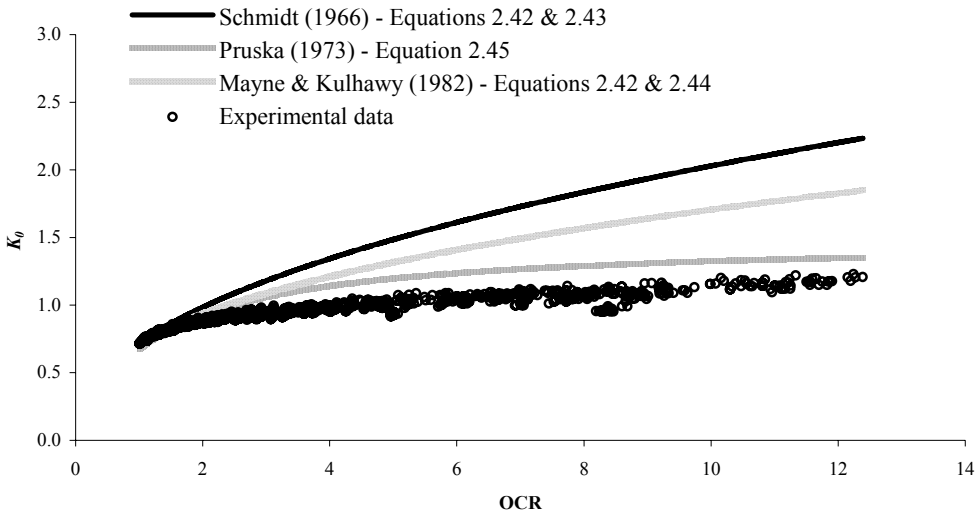

Figure 5.24. Variation of K_0 with OCR on unloading predicted by various researchers compared with measured values.

The new model prediction of the variation the values of K_0 with OCR on unloading and reloading, is shown in Figure 5.25. Using a value of k = 1.2, the model predicts a value of $K_{0,nc}$ of 0.714 ($\eta_{0,nc}$ = 0.353) compared to 0.72 measured from the triaxial test and $d\varepsilon_p^p/d\varepsilon_q^p$ = 1.45. It can be seen that the model over-predicts K_0 on both unloading and reloading. This is because of the value of F_e and ψ chosen, which make the stiffness on unloading higher, giving a higher value of K_0. However, it should be noted that the values of K_0 measured are relatively lower compared to the values of K_0 obtained by other researchers. For pavement problems, it is more important to be able to predict the behaviour of a clay subgrade under cyclic loading than to predict the correct value of K_0; therefore the model parameters have been determined by fitting a set of cyclic loading data. If K_0 is of interest, alternative model parameters can be chosen.

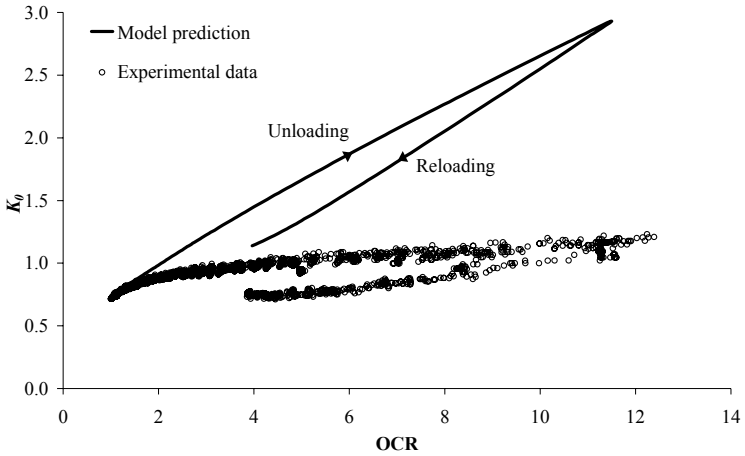

Figure 5.25. Comparison of model prediction and experimental data.

Figures 5.26 and 5.27 show the cyclic test results and model predictions respectively. It should be noted that for the triaxial simulation, the stress history is approximately the same as that for the sample in the triaxial test, so that the yield surface and history surface start off at the correct positions before cyclic loading. The predicted shear strain after ten cycles is close to the measured value. However the model predicts a strong ratcheting behaviour which is not observed experimentally. This ratcheting problem will cause the rut depth to be over-estimated under large numbers of cycles in a pavement analysis; this is shown later in Chapter 6. The shear strain increments measured in the apparatus are decreasing with increasing number of

cycles whilst the shear strain increment after the first cycle predicted by the model remains constant. It can be seen that from Figure 5.26, the volumetric strain was compressive for the first cycle and became dilative. The model predicted the same trend of behaviour but the actual predicted values of volumetric strain were more dilative.

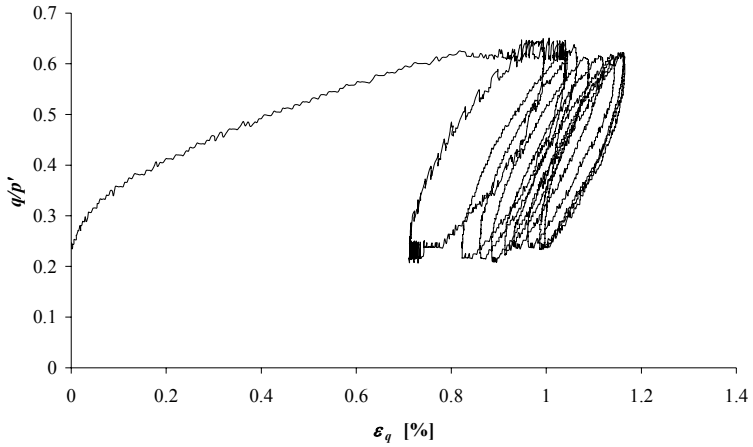

(a)

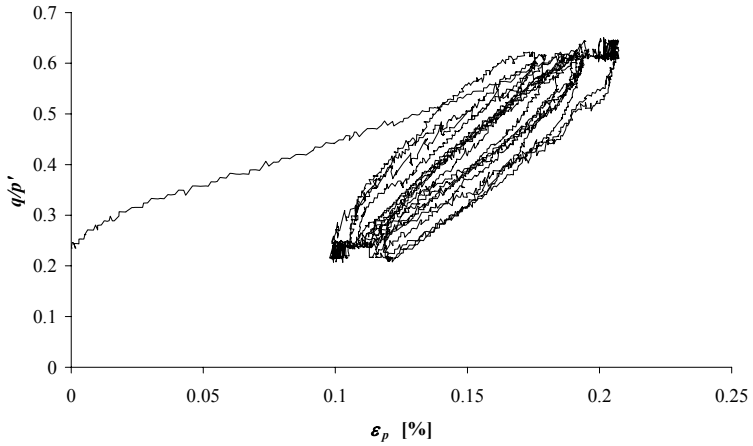

(b)

Figure 5.26. Cyclic triaxial test results (a) q/p' versus ε_q and (b) q/p' versus ε_p.

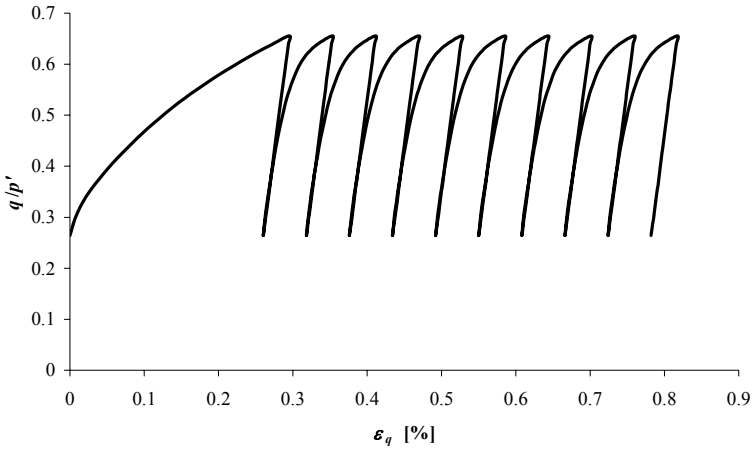

(a)

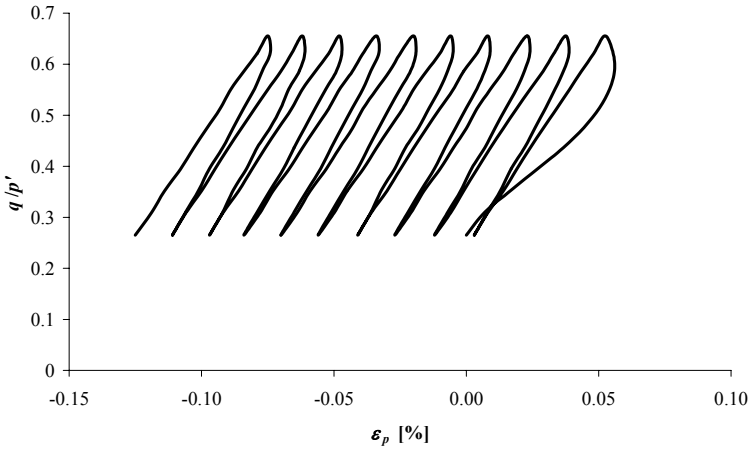

(b)

Figure 5.27. Model predictions (a) q/p' versus ε_q and (b) q/p' versus ε_p.

5.5 SUMMARY

Triaxial tests have been performed to determine the model parameters and provide data for validation of the model to predict the behaviour of soil under cyclic loading. Cyclic triaxial tests have been conducted on soil elements with a stress history similar to that experienced by the subgrade in a typical pavement. A parametric study was performed to determine the best set of parameters for kaolin, suitable for modelling cyclic loading of an isotropically normally consolidated soil. It was found

that the values of K_0 were over-predicted by the model; however, if the values of K_0 are of interest a different set of parameters can be established.

The new model was used to predict the behaviour under cyclic loading for a sample with a one-dimensional stress history, similar to the stress history experienced by pavement subgrades in a 'cut' condition. It can be seen that the real clay stress-strain behaviour tends to stabilise after a few cycles giving a closed hysteresis loop. However, in the model, shear strain continues to accumulate with increasing numbers of cycles. The strong ratcheting feature of the model may over-predict the shear strain after a large number of cycles. Therefore the rut depth of a completed pavement may be overestimated by the model for a large number of cycles. The strong ratcheting feature of the model is a function of the hardening modulus and is also present because the new model is a volumetric hardening model. This means that the volumetric strain will stabilise if p'_o stabilises, and the shear strain increment will be ultimately the same for each cycle. Furthermore, the assumptions of constant T and S in the model are unnecessary. The size of the elastic region could be made to be a function of number of cycles so that the soil will behave elastically after a large number of cycles. However, this will require further modification if the soil is then subjected to a different stress path.

Cyclic loading soil behaviour is very different from that of monotonic loading. The aim of this chapter has been to try to develop a model with parameters suitable for cyclic loading. Although the ratcheting problem still exists, it is hoped that the new model, with values of parameters as presented in this chapter, will be able to eliminate the problems of negative shear strain and decreasing rut depth with increasing number of cycles, experienced in Chapter 4. This is examined in the next chapter. It must be emphasised, however, that the model may still not be suitable for very large numbers of cycles because of the ratcheting phenomenon: this may require a completely new formulation of the model. In addition, it must be recognised that for monotonic tests, alternative parameters will need to be established.

6 FULL-SCALE PAVEMENT ANALYSIS

6.1 INTRODUCTION

All the required parameters for the new model on Speswhite kaolin have been determined in the previous chapter. In this chapter, the model is applied to the repeated loading of a thinly surfaced pavement to determine the resilient and permanent strains response of a pavement.

Multi-layered elastic analysis is commonly used in pavement engineering. This analysis requires the determination of the stiffness of each layer. In conventional pavement engineering the stiffness of the subgrade is normally estimated from an empirical relationship: usually one which relates the stiffness to CBR. However, it is widely known that the stiffness is not a simple function of CBR. Stiffness is a function of stress level and stress history. One of the design criteria in thinly-surfaced pavements is to limit the resilient vertical compressive strain at the surface of the subgrade during the construction stage. The new model and the original 3-SKH model are used to estimate the stiffness of the subgrade for input to a multi-layered elastic analysis, and the required thickness of granular layer is then determined which gives an acceptable vertical strain at the top of the subgrade during the construction stage. The required thickness of granular material predicted by each model is then examined to see whether the values are realistic.

Another criterion used to design a pavement during the construction stage is to limit the rut depth of the unsurfaced pavement to a maximum of 40mm after a maximum of 1,000 passes of construction traffic, depending on the length of road under construction. In this chapter, the rut depth of a two-layer pavement (granular material and subgrade) is analysed for both the 3-SKH model and the new model and the required thickness of granular material is determined.

Following these studies, the effect of the granular layer thickness on the formation of the rut depth is investigated. The assumptions made in the pavement analyses are:

1. Permanent deformation in thinly-surfaced pavements is mainly due to the deformation of the subgrade.

2. In the long-term, the asphalt and granular layers will deform follow the settlement trough of the subgrade.

3. In the long-term, the drained condition is appropriate. At the surface of the subgrade where a permeable granular material is placed on top, the drainage path is very small such that the subgrade condition under traffic loading may be assumed to be a drained condition.

6.2 PAVEMENT FOUNDATION DESIGN

In the U.K., the design of a pavement occurs in two stages. The first stage involves the design of the pavement foundation which includes the determination of an appropriate thickness of granular material to be placed above the subgrade. This is the most critical design case as the partially completed pavement has to be able to carry heavy vehicles for as many as 1,000 wheel passes depending on the length of road under construction (Hardman et al. 1976). There are two design criteria during this stage (Dawson & Gomes Correia, 1996):

1. The resilient deformation should be limited to ensure that the asphalt layer can be adequately compacted. Excess resilient deformation results from inadequate stiffness of the pavement foundation.

2. No excessive surface rutting should develop for a given traffic level. The permissible rut depth is commonly set at 40mm if the sub-base is compacted efficiently (Powell et al., 1984).

The second design stage is for the completed pavement subjected to a larger number of load passes. The design requirements are prevention of fatigue cracking and

rutting. The latter is a key requirement for design, particularly for unsurfaced and thinly surfaced pavements where the stress levels are usually higher than in thicker pavements (Brown, 1996; Dawson, 1997).

6.2.1 Resilient Deformation During Construction Stage

As already described above, a pavement foundation is required to resist excessive resilient deformation to ensure satisfactory compaction of the asphalt layer. The resilient strain is normally calculated from a multi-layered analysis, such as BISAR, provided that the stiffness and Poisson's ratio of each layer are known. Due to the non-linearity and inelasticity of pavement foundation materials, it is difficult to estimate the stiffness of the pavement foundation. It has been shown in Chapter 3 that the 3-SKH model can be used to estimate the stiffness of the subgrade which is required for the input to an elastic analysis program such as BISAR. In this section, the resilient modulus of the subgrade is estimated from a finite element analysis of a two-layer pavement (i.e. during the construction stage) with the new model and the original 3-SKH model for input into the multi-layered elastic analysis program BISAR, to determine the required thickness of the granular layer. In the current analytical pavement foundation design method, the required granular layer thickness is determined such that the maximum compressive strain in the subgrade is within a certain limit depending on the cumulative traffic (Powell et al., 1984), and/or so that excessive rutting does not develop during the construction process. The resilient modulus, M_r, which is required for input to a linear-elastic calculation is normally estimated from empirical relationships such as equations 2.56 and 2.57, and the latter is currently being adopted in the Design Manual for Roads and Bridges: Volume 7 (Highway Agency, 1994) for the design of pavement foundations. However, Brown et al. (1987) showed that for three materials, the relationship between resilient modulus and CBR was not consistent with either equation 2.56 or 2.57 – see Figure 2.19. Hence, alternative methods of estimating stiffness are clearly required. Figure 6.1 shows the permissible compressive strain versus number of cycles during the construction stage derived from the performance of experimental roads (Powell et al., 1984).

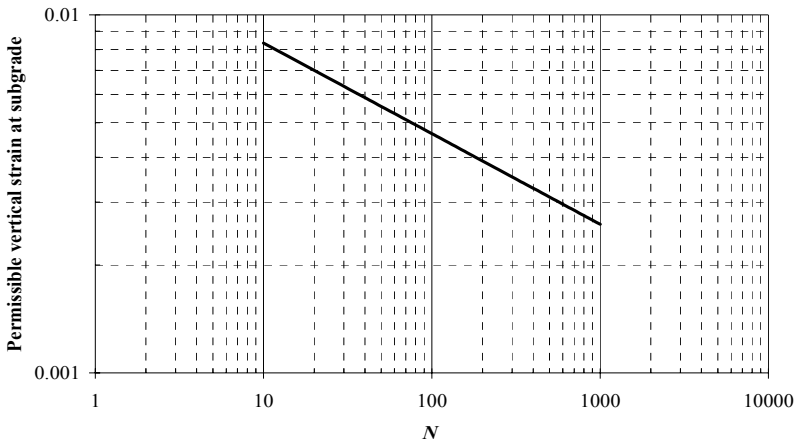

Figure 6.1. Permissible compressive strain at subgrade (Powell et al., 1984)

The method used to estimate the stiffness of the subgrade is exactly the same as that used in Section 3.5.1. Figure 6.2 shows the two-layer pavement and the locations where the stiffness have been estimated. A pressure of 500kPa with radius of 0.2m, equivalent to a 62kN wheel load (due to construction traffic), was applied to the surface of the granular material (following Cheung, 1994). The granular layer was assumed to be isotropic and linear-elastic, and the subgrade was first modelled with the new model proposed in Chapter 4. Values of E' = 100MPa and μ' = 0.3 were assumed for the granular material. The same stress history of the subgrade as described in Section 3.5.1 was modelled. The change in effective vertical stress at different depths due to the applied pressure was computed and this increase in effective vertical stress due to the first application of wheel load was then applied as a stress increment, to a triaxial sample at constant cell pressure in CRISP with a similar initial stress history, for 50 cycles. The resilient (i.e. unloading) Young's modulus E' for the 50^{th} cycle were then computed for the input to the elastic analysis. This was repeated for different granular layer thicknesses. The vertical strain at the top of the subgrade was then calculated using BISAR. The Poisson's ratio used was 0.3 as in Chapter 3. The stiffnesses estimated by the new model, for each sub-layer for different thicknesses of granular layer, are summarized in Table 6.1. The predicted stiffness for each layer is seen to increase with depth, and with thickness of granular layer indicating the ability of the model to take into account of the effect of stress level on stiffness. The stiffness of the lowest layer remained constant, since the stress change is very small at this depth. The estimated stiffness is slightly on the high side due to the introduction of the F_e term in the hardening modulus. For a CBR

of 10% (i.e. stiff subgrade) the expected value of modulus would be roughly 100MPa and the predicted stiffnesses are at least of the same order as those quoted by Dawson & Plaistow (1993) for stiff to firm subgrade. Therefore, the stiffnesses predicted by the new model are not unrealistic.

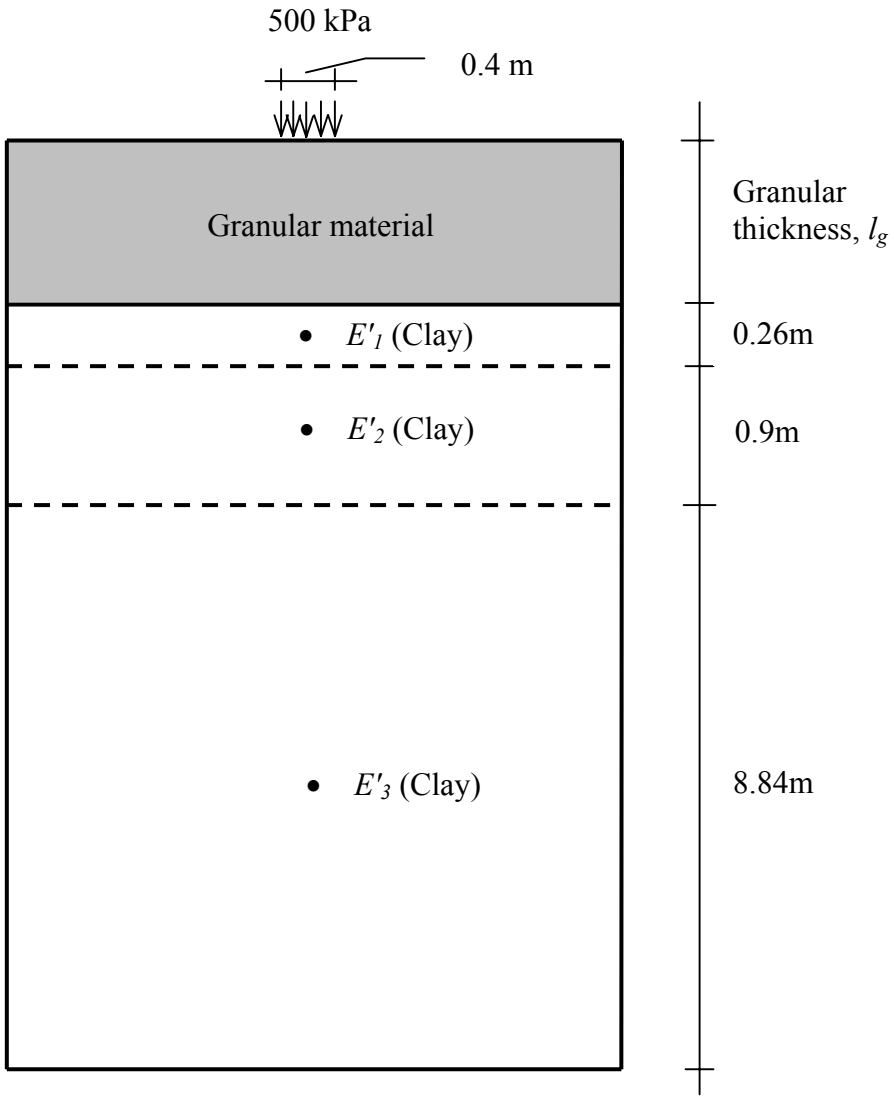

Figure 6.2. Cross-section of a two-layer pavement.

The vertical strain at the top of the subgrade was computed from the elastic analysis using the stiffness estimated by the new model for each thickness of granular material. The results are shown in Figure 6.3. This was then used in Figure 6.1 to establish the required amount of granular material to ensure that the subgrade strain criterion is met. The cumulative traffic during construction was assumed to be 1,000 cycles, in which case Figure 6.1 gives the permissible vertical strain for this traffic

level as 0.0026. Hence the results presented in Figure 6.3 predict that a granular layer 280mm thick is required to protect the subgrade.

Granular layer thickness, l_g (mm)	150	200	300	350	400	500	600
E_1 (MPa)	51	54	110	111	118	120	122
E_2 (MPa)	117	124	125	125	126	126	126
E_3 (MPa)	157	157	157	157	157	157	157

Table 6.1. Stiffness of subgrade predicted by the new model.

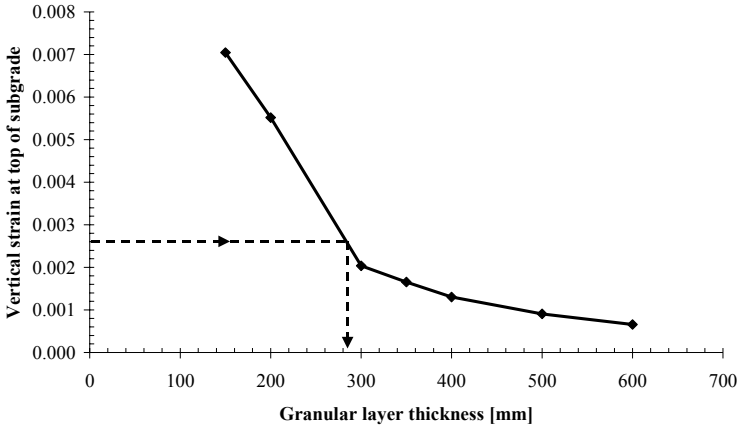

Figure 6.3. Computed vertical strain at subgrade using elastic analysis versus granular layer thickness.

Exactly the same analyses were repeated using the 3-SKH model with model parameters shown in Table 3.1 to predict the stiffness of the subgrade. The predicted stiffnesses are summarized in Table 6.2. As can be seen from the results, the stiffnesses predicted by the 3-SKH model are much lower than those predicted by the new model. Figure 6.4 presents the vertical strain at the top of the subgrade computed using these stiffnesses, compared with the results derived from the new model shown in Figure 6.3. The thickness of granular material required to give an acceptable vertical strain predicted by the 3-SKH model is higher (≈ 450mm) than that predicted by the new model. According to the design chart proposed by Powell et al. (1984), even for a soft subgrade of CBR = 2 %, the required granular layer

thickness is only 400mm (see equation 6.1 in the next section). Therefore it is considered that the new model will give a more realistic thickness of granular layer even though the stiffness of the subgrade may be an overestimate.

Granular layer thickness, l_g (mm)	**150**	**200**	**300**	**350**	**400**		**600**
E_1 (MPa)	15	16	19	25	34	45	52
E_2 (MPa)	58	62	66	68	69	72	83
E_3 (MPa)	126	126	126	126	126	126	126

Table 6.2. Stiffness of subgrade predicted by the 3-SKH model.

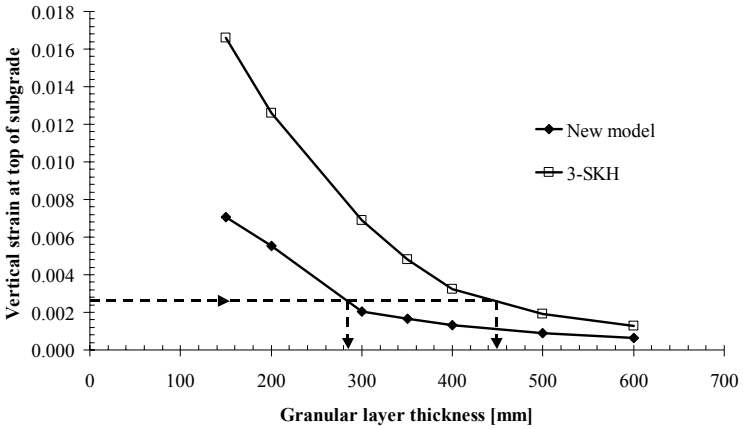

Figure 6.4. Computed vertical strain at subgrade using elastic analysis versus granular layer thickness.

6.2.2 Rut Depth of Unpaved Roads Under Construction Traffic

The design of the pavement foundation during the construction stage when the granular layer has been placed and is carrying construction traffic is the most critical design case for the foundation. The essential requirement for the pavement during the construction stage is not to develop excessive rutting. Therefore, it is essential to determine the amount of granular material required in order to protect the subgrade from rutting under construction traffic. The maximum rut depth that can be tolerated

is commonly set at 40mm (Powell et al., 1984). The number of load applications during the construction stage can be estimated from the length of road under construction (Hardman et al., 1976). For a 1km road, the expected construction traffic is 1,000 passes. Based on extensive pilot-scale trials in the U.K., Powell et al. (1984) proposed an empirical relationship for the determination of the amount of granular material required to limit the rut depth to 40mm for a given traffic level and subgrade CBR:

$$\log N = \frac{l_g \left(\mathrm{CBR}\right)^{0.63}}{190} - 0.24 \tag{6.1}$$

where N is the number of load passes during the construction stage, and l_g is the thickness of granular material in mm.

In this section, a two-layer pavement is analysed using CRISP to determine the thickness of granular material required to provide an acceptable rut depth. The granular material was modelled as an isotropic linear elastic material with E' = 100MPa and μ' = 0.3 and the subgrade was modelled with the new model under drained conditions. The applied pressure at the surface of the granular material was 500kPa with a radius of 0.2m. The stress distribution at the surface of the subgrade due to the first load application at the surface of the granular layer was first computed and the equivalent stress blocks were then applied to the surface of the subgrade (one-layer pavement) for 1,000 cycles. The reason for this has already been explained in Section 3.5.2. The finite element mesh of the one-layer pavement is shown in Figure 4.11. Figure 6.5 shows the predicted rut depth after 1,000 cycles for different granular layer thicknesses. It was found that a granular layer of thickness 350mm would satisfy the required rut depth criterion set by Powell et al. (1984).

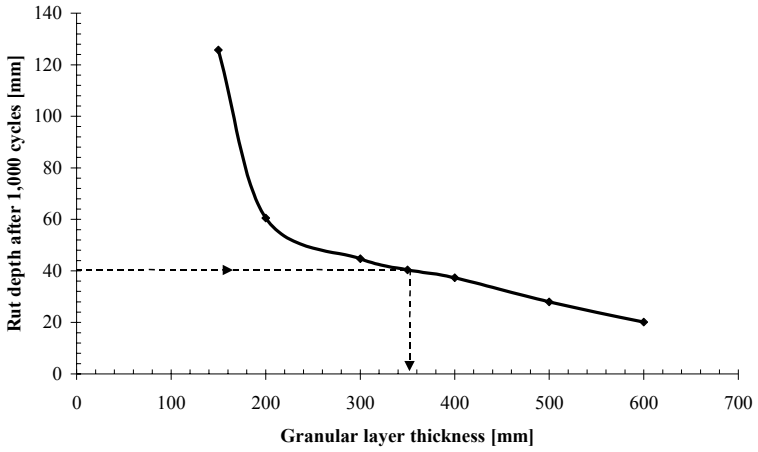

Figure 6.5. Predicted rut depth after 1,000 cycles of load application versus granular layer thickness.

An attempt was made to analyse these two-layer pavement problems with the 3-SKH model but the negative shear strain problem as already described in Section 3.4.2 made the results unrealistic.

From the above results in Figures 6.3 and 6.5, the new model predicts that a granular layer of 350mm is required to satisfy the resilient deformation and rut depth criteria specified by Powell et al. (1984) during the construction stage for a construction road length of 1km. This lends credibility to the kinematic hardening method and its applicability to pavement problems.

6.3 THREE-LAYER PAVEMENT ANALYSIS – EFFECT OF GRANULAR LAYER THICKNESS AND ASPHALT LAYER THICKNESS

Having determined the minimum amount of granular material required to protect the subgrade during the construction stage, the effect of the granular layer thickness and the asphalt layer thickness on the development of permanent settlement in a completed pavement (three-layer pavement), is investigated.

A three-layer pavement with 50mm of asphalt on top of a layer of granular material was analysed. The top two layers were modelled as isotropic linear elastic materials with Young's moduli and Poisson's ratios specified in Section 3.5.2 The stress history of the subgrade was modelled as in a 'cut' condition as discussed in Section 3.5.2. A wheel load of 600kPa and radius 0.15m was applied at the surface of the asphalt layer and the stress distribution due to this wheel load was calculated at the integration points near the top of the subgrade. This stress distribution was applied at the surface of the subgrade by equivalent stress blocks for 1,000 cycles and the permanent settlement at the surface of the subgrade plotted against the number of cycles in Figure 6.6 for different granular layer thicknesses. As can be seen from Figure 6.6, a thicker granular layer helps to reduce the permanent settlement. An increase of 100mm of granular material would reduce the permanent settlement by approximately 40% after 1,000 cycles.

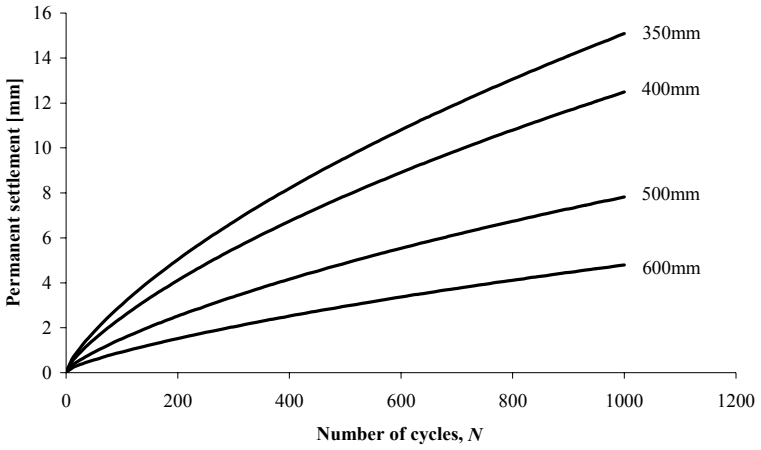

Figure 6.6. Predicted settlement of a three-layer pavement for different granular layer thicknesses.

Figure 6.7 shows effect of granular layer thickness on the predicted rate of settlement for a three-layer pavement. As the granular layer thickness increases, the rate of settlement reduces.

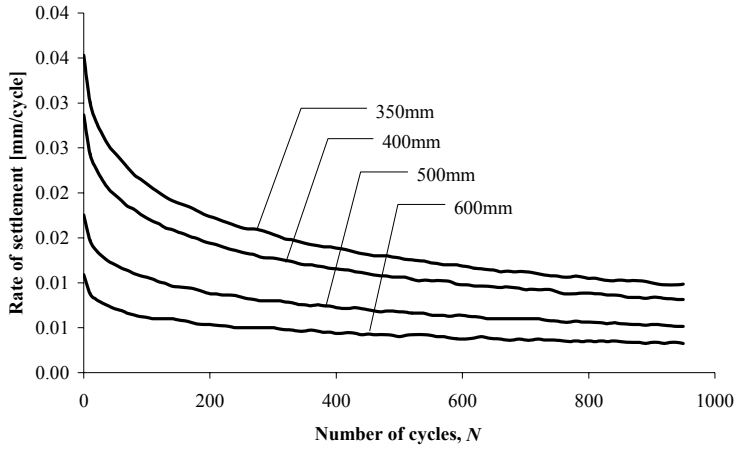

Figure 6.7. Predicted rate of settlement of a three-layer pavement for different granular layer thicknesses.

The effect of the asphalt thickness on permanent settlement was investigated by varying the asphalt thickness from 30mm to 100mm and a fixed amount of granular material of 350mm. Figure 6.8 shows the effect of asphalt thickness on the development of permanent settlement. Increasing the thickness of the asphalt layer has a similar effect as increasing the amount of granular material used. An increase in asphalt thickness of 50mm, which has a stiffness of 5GPa, has approximately the same effect as an increase of 150mm of granular material, which has a stiffness of 100MPa, in terms of reducing the settlement after 1,000 cycles.

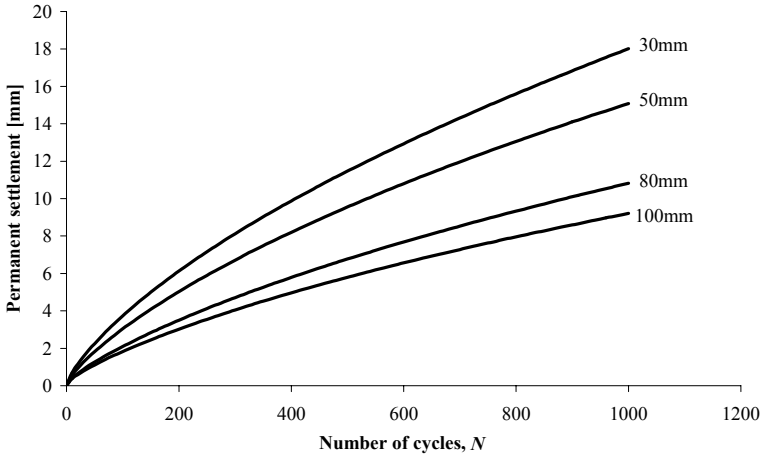

Figure 6.8. Predicted settlement of a three-layer pavement for different asphalt thicknesses.

The predicted rate of settlement versus number of cycles for different asphalt thicknesses is shown in Figure 6.9. An increase of asphalt thickness reduces the rate of settlement. This has a similar effect to increasing the granular layer thickness.

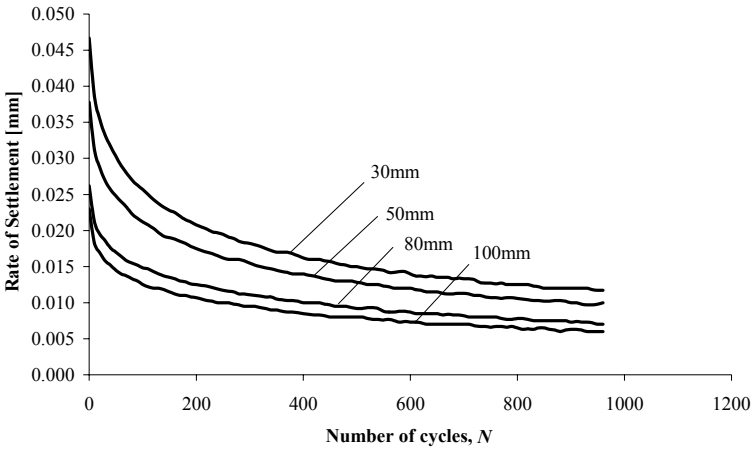

Figure 6.9. Predicted rate of settlement of a three-layer pavement for different asphalt thicknesses.

A three-layer pavement problem with 100mm of asphalt on top of 350mm of granular material was analysed for 10,000 cycles. The permanent settlement versus number of cycles is presented in Figure 6.10. A 33mm rut after 10,000 cycles was predicted by the model, about 30% of which had developed during the first 1,000 cycles. Figure 6.11 shows the predicted rate of settlement versus number of cycles. It can be seen that the rate is decreasing with increasing number of cycles. The predicted rut depth after 10,000 is still considered to be too large, due to the strong ratcheting feature of the model. However, the approach shows much promise in modelling the behaviour of pavements subjected to repeated loading: the model is clearly capable of applying many cycles of load and the rate of deformation decreases with increasing number of cycles. The rut depths predicted by the new model after 10,000 cycles are not unrealistic.

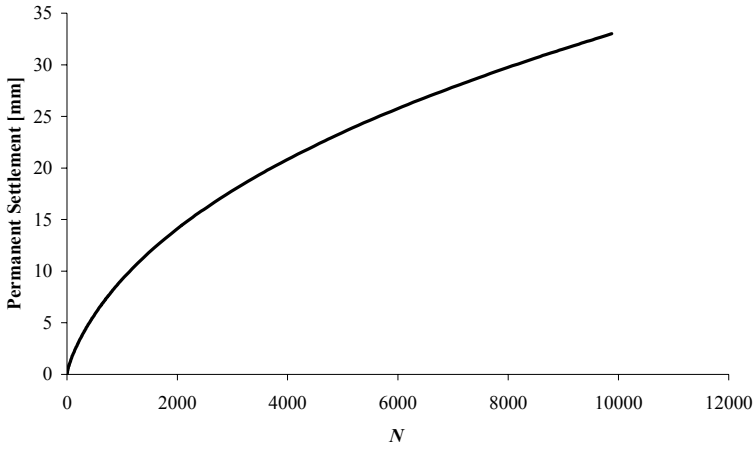

Figure 6.10. Predicted settlement of a three-layer pavement as a function of the number of cycles N.

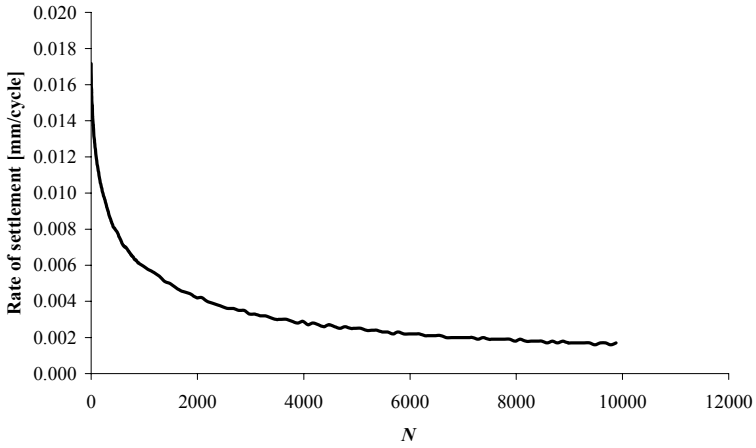

Figure 6.11. Predicted rate of permanent settlement of a three-layer pavement as a function of the number of cycles N.

6.4 SUMMARY

The new model has been applied to the prediction of the resilient and permanent response of a pavement problem. A partially completed pavement (during the construction stage) and a completed pavement have been analysed. The required granular layer thickness in order to protect the subgrade has been determined by satisfying the permissible resilient subgrade strain and pavement rut depth criteria. The required amount of granular material predicted by the new model is more

realistic, compared to the 3-SKH model. In addition, the granular layer thickness predicted by the new model is considered to be conservative and hence the new model may serve as a design guide for pavement foundations.

The effect of granular layer thickness and asphalt thickness on the development of the permanent settlement have been investigated using the new model. Increasing the granular layer thickness has a similar effect as increasing the asphalt thickness. An increase in the thickness of asphalt of 50mm has roughly the same effect as an increase of 150mm of granular material in terms of reducing the settlement after 1,000 cycles. A three-layer pavement subjected to a large number of cycles (10,000 cycles) was also analysed. The permanent settlement predicted by the new model is still considered to be too large, and is due to the ratcheting feature of the model. A more appropriate hardening modulus is needed in order to predict realistic settlements after a large number of cycles. However, the new model shows much promise in being able to capture many essential features of pavements subjected to repeated loading.

7 CONCLUSIONS AND SUGGESTIONS FOR FUTURE RESEARCH

7.1 SUMMARY AND CONCLUSIONS

The design of lightly trafficked roads has adopted design standards developed specifically for the design of heavily trafficked roads. This has resulted in inappropriate and uneconomical design specifications for this sector. The application of fundamental soil mechanics principles to the design of pavement foundations is needed and is particularly important if economies are to be introduced for lightly trafficked road design and maintenance.

In the literature review, it has been shown that the current approaches of pavement analysis are based largely on empirical relations, whereas, various cyclic loading models for soil have been developed based on the Critical State Soil Mechanics concept. Little effort has previously been made to apply these models to the prediction of pavement response.

The main aims of the research reported in this thesis were as follows:

1. To evaluate the 3-SKH model in the prediction of the behaviour of clay under repeated loading.
2. To study the behaviour of pavement subgrades under repeated loading using the kinematic hardening model.
3. To modify the 3-SKH model to better predict the behaviour of soil under repeated loading.
4. To apply the new constitutive model to the prediction of resilient and permanent deformation of pavement subgrades under repeated loading using the finite element method.

The ability of the 3-SKH model to predict the behaviour of soil subjected to cyclic loading, has been studied. Comparison between the predictions of the model and

experimental results obtained by other researchers, has shown that the model is capable of predicting most of the aspects of soil behaviour under cyclic loading, such as accumulation of permanent strains and hysteresis. A procedure used to provide an estimate of the subgrade stiffness has been proposed using the 3-SKH model, and comparison of the resilient deformation predicted by a layered-elastic analysis using the estimated stiffness and the resilient deformation predicted by the 3-SKH model, shows good agreement. This implies that the proposed method can be used to estimate subgrade stiffness using the 3-SKH model for the input into a linear elastic analysis program such as BISAR. However, the 3-SKH model has some deficiencies in that it over-predicts shear strain, and predicts an accumulation of negative shear strain with increasing number of cycles under some stress conditions. This will give unrealistic predictions when applied to pavement analysis. A new model, which is a modified version of the 3-SKH model, has therefore been proposed.

A new non-associated three-surface kinematic hardening model, which requires two extra parameters, has been developed by:

1. Modifying the flow rule
2. Making the critical state constant, M, a function of Lode angle in stress space
3. Modifying the hardening modulus

The new model has been implemented into the finite element code CRISP.

Triaxial tests have been performed to determine the model parameters and to provide data for validation of the model. The parameters were determined by fitting cyclic loading data. The model predicts well the triaxial cyclic loading results but it shows a strong ratcheting feature. It was found that the new model correctly predicted the value of K_0 for normally consolidated clay, but the prediction of the value of K_0 on unloading and reloading was too high. It was considered that if the values of K_0 are of interest, the model parameters can be determined by fitting a set of one-dimensional loading, unloading and reloading data. In pavement analysis the value of K_0 is relatively less important than the behaviour of the subgrade under cyclic

loading. Therefore, the parameters determined from cyclic loading data were used to analyse a pavement problem.

The new model was applied to the prediction of both the resilient and permanent response of a pavement. Two loading conditions were considered: that due to the construction traffic (two-layer pavement) and that resulting from traffic once the pavement is complete and open to traffic (three-layer pavement). The stiffness of a pavement subgrade during the construction stage was estimated using the new model for input into the multi-layered elastic analysis program (BISAR). The resilient vertical strain at the top of the subgrade was then computed and related to the maximum allowable strain proposed by Powell et al. (1984) to determine the required granular layer thickness. A realistic thickness (280mm) was obtained using the new model, whereas the thickness obtained using the 3-SKH model was too high (450mm). The rut depth criterion suggested by Powell et al. (1984) was also used to determine the required granular layer thickness. The rut depth of a partially completed pavement during the construction stage was predicted by the new model as a function of granular layer thickness, and the required granular layer thickness to give a permissible rut depth of 40mm after 1,000 cycles, was determined. A realistic value of 350mm was obtained using the new model. An attempt was made to predict the rut depth for the two-layer pavement using the 3-SKH model prediction, but the 3-SKH model predicted an accumulation of negative shear strain for this stress condition, so it was inappropriate. The effect of the thickness of asphalt and granular material on the development of the rut depth was also studied using the new model. It was found that an increase in asphalt thickness of 50mm has approximately the same effect as an increase of 150mm of granular material in terms of reducing the settlement after 1,000 cycles. A three-layer pavement subjected to 10,000 cycles was analysed using the new model. The results showed that the rut depth is still increasing after 10,000 cycles; this is due to the strong ratcheting feature of the model. However, the rate of increase of rut depth decreases with increasing number of cycles, and the model shows much promise in being able to model the behaviour of pavements subjected to many cycles of load.

The new model is therefore able to predict realistic deformation in a pavement analysis, which the 3-SKH model is incapable of predicting. The proposed model

may therefore be considered to be an improvement on the 3-SKH model, in terms of the prediction of pavement response to repeated loading.

To summarise, the conclusions that can be drawn from this research are:

- Critical State Soil Mechanics has not been applied in the past to the prediction of pavement response.

- Current approaches to pavement foundations design are mainly based on empirical models.

- It is necessary to apply the Critical Soil Mechanics concept to the design of pavement foundations, especially thinly surfaced pavement foundations where stresses are higher in the foundation layers and the non-linear and inelastic properties of these layers become crucial.

- A more theoretically based constitutive model for pavement subgrades is needed if more appropriate designs for thinly surfaced pavements are required.

- It was found that the 3-SKH model is suitable for predicting the soil behaviour under cyclic loading. However, this model over-predicts the value of $K_{0,nc}$ and shear strain on loading. In addition, the model also predicts an accumulation of negative shear strain with increasing number of cycles under some stress conditions.

- Due to the over-prediction of shear strain by the 3-SKH model, the predicted rut depth of a pavement is too large.

- The 3-SKH model can be used to estimate the stiffness of the subgrade for use in a layered elastic analysis.

- A new non-associated three-surface kinematic hardening model, which requires two extra parameters, has been developed by modifying the flow

rule, making the critical state constant, M, a function of Lode angle in stress space, and modifying the hardening modulus. The new model has been implemented into a finite element code – CRISP.

- The new non-associated 3-SKH model is able to predict the value of $K_{0,nc}$ correctly and is able to reduce the amount of shear strain predicted.

- Parameters for the new model have been determined by fitting cyclic loading data.

- The new model over-predicts the values of K_0 on unloading and reloading if these parameters are used.

- The new model exhibits a strong ratcheting feature (as does the original 3-SKH model).

- Despite the strong ratcheting feature of the model, the new model gives realistic predictions of pavement response.

- Based on the maximum allowable strain criterion at the top of the subgrade during the construction stage, the new model predicts that a thickness of 280mm of granular material is required. This is realistic. However, the 3-SKH model gives a thickness of 450mm, which is unrealistically high.

- Based on the maximum permissible rut depth criterion during the construction stage, the new model predicts that a thickness of 350mm of granular material is required. The original 3-SKH model could not be used as it gave a rut depth which decreased with increasing numbers of cycles.

- From the study of the effect of granular layer thickness on the development of rut depth, it was found that an increase in the thickness of granular of 100mm material would reduce the rut depth by approximately 40% after 1,000 cycles.

- It was found that an increase in the asphalt thickness of 50mm, which has a stiffness of 5GPa has, approximately the same effect as an increase in the thickness of granular material of 150mm, which has a stiffness of 100MPa.

- Although only pavements with one-dimensional stress history have been considered, based on these analyses, the new model is considered to be an improvement on the 3-SKH model in terms of the prediction of pavement response under repeated loading.

7.2 RECOMMENDATIONS FOR FUTURE WORK

One of the assumptions of the model is the fixed ratio of the size of the yield surface to that of the history surface i.e. constant T and S. This is certainly not necessary; in order to improve the model prediction, the parameters T or S, or both, can be made to be functions of shear strain or number of cycles. This may eliminate the problem of the constant increment of shear strain predicted by the model as opposed to that observed experimentally in Chapter 5. However, some thought must be given to how T and S would then be modified if the stress path changes after a large number of cycles.

For the pavement analysis performed in this research, the additional permanent deformation in the granular layer was neglected; Brown (1996) discussed pavement experiments conducted by Little (1993) in which there were cases where all the permanent deformation developed in the subgrade. However, in other cases there was also evidence that the granular layer contributed to the surface rut. Therefore the pavement model could be modified further to allow the granular material to exhibit plasticity. A kinematic hardening model based on the model presented here may be a useful starting point.

The rate of change of M with Lode angle θ has been assumed to be unimportant: i.e. $\partial M/\partial\theta = 0$. This requires further investigation for problems involving cyclic loading.

However, it is anticipated that it will only be important for the plastic potential under plane strain conditions.

The model has so far been validated with experimental data on kaolin. More laboratory tests on a variety of soils are required in order to provide further data for validation of the model.

Before the new model can be incorporated into any pavement foundation design guide, extensive full-scale pavement tests have to be performed to validate the model predictions. In addition, the model exhibits too much ratcheting, so the predicted rut depth after a large number of cycles is too large. Further modification of the hardening modulus will be required to eliminate this problem. This will require an extensive review of bounding surface plasticity and kinematic hardening, in order to attempt to formulate a suitable model.

APPENDIX

Derivations of the terms required to form the elasto-plastic matrix, $[D^{ep}]$ for the new model.

$$\frac{\partial f}{\partial p'} = 2\left(p' - p'_b\right) \tag{A1}$$

$$\frac{\partial f}{\partial s_{ij}} = \frac{3}{\mathrm{M}^2}\left\{s_{ij} - s_{bij}\right\} \tag{A2}$$

$$\frac{\partial p'}{\partial \sigma'} = \left\{\frac{1}{3}, \frac{1}{3}, \frac{1}{3}, 0, 0, 0\right\} \tag{A3}$$

$$\frac{\partial s_{ij}}{\partial \sigma'_x} = \left\{\frac{2}{3}, -\frac{1}{3}, -\frac{1}{3}, 0, 0, 0\right\} \tag{A4}$$

$$\frac{\partial s_{ij}}{\partial \sigma'_y} = \left\{-\frac{1}{3}, \frac{2}{3}, -\frac{1}{3}, 0, 0, 0\right\} \tag{A5}$$

$$\frac{\partial s_{ij}}{\partial \sigma'_z} = \left\{-\frac{1}{3}, -\frac{1}{3}, \frac{2}{3}, 0, 0, 0\right\} \tag{A6}$$

$$\frac{\partial s_{ij}}{\partial \tau_{xy}} = \{0,0,0,1,0,0\} \tag{A7}$$

$$\frac{\partial s_{ij}}{\partial \tau_{yz}} = \{0,0,0,0,1,0\} \tag{A8}$$

$$\frac{\partial s_{ij}}{\partial \tau_{xz}} = \{0,0,0,0,0,1\} \tag{A9}$$

$$\frac{\partial f}{\partial \sigma'_x} = \frac{2}{3}\left(p' - p'_b\right) + \frac{3}{\mathrm{M}^2}\left(s_x - s_{xb}\right) \tag{A10}$$

$$\frac{\partial f}{\partial \sigma'_y} = \frac{2}{3}\left(p' - p'_b\right) + \frac{3}{\mathrm{M}^2}\left(s_y - s_{yb}\right) \tag{A11}$$

$$\frac{\partial f}{\partial \sigma'_z} = \frac{2}{3}\left(p' - p'_b\right) + \frac{3}{\mathrm{M}^2}\left(s_z - s_{zb}\right) \tag{A12}$$

$$\frac{\partial f}{\partial \tau_{xy}} = \frac{6}{\mathrm{M}^2}\left(s_{xy} - s_{xyb}\right) \tag{A13}$$

$$\frac{\partial f}{\partial \sigma'_{bij}} = -\frac{\partial f}{\partial \sigma'_{ij}} \tag{A14}$$

$$\frac{\partial f}{\partial p'_o} = 2T^2 S^2 p'_o \tag{A15}$$

$$\frac{\partial g}{\partial p'} = \frac{4}{k} \cdot \left(p' - p_b'\right) \tag{A16}$$

$$\frac{\partial g}{\partial s_{ij}} = \frac{3}{\mathrm{M}^2}\left\{s_{ij} - s_{bij}\right\} \tag{A17}$$

$$\frac{\partial g}{\partial \sigma'_x} = \frac{2}{3} \cdot \frac{2}{k}\left(p' - p'_b\right) + \frac{3}{\mathrm{M}^2}\left(s_x - s_{xb}\right) \tag{A18}$$

$$\frac{\partial g}{\partial \sigma'_y} = \frac{2}{3} \cdot \frac{2}{k}\left(p' - p'_b\right) + \frac{3}{\mathrm{M}^2}\left(s_y - s_{yb}\right) \tag{A19}$$

$$\frac{\partial g}{\partial \sigma'_z} = \frac{2}{3} \cdot \frac{2}{k}\left(p' - p'_b\right) + \frac{3}{\mathrm{M}^2}\left(s_z - s_{zb}\right) \tag{A20}$$

$$\frac{\partial g}{\partial \tau_{xy}} = \frac{3}{\mathrm{M}^2}\left\{s_{ij} - s_{bij}\right\} : \left\{0,0,0,1,0,0\right\} = \frac{6}{\mathrm{M}^2}\left(s_{xy} - s_{xyb}\right) \tag{A21}$$

$$\frac{\partial g}{\partial \sigma_{ii}} = \frac{4}{k}\left(p' - p'_b\right) \tag{A22}$$

$$\frac{\partial p'_o}{\partial \varepsilon_{ii}} = \frac{3p'_o}{\lambda^* - \kappa^*} \tag{A23}$$

All the terms required for the elasto-plastic matrix have been specified.

REFERENCES

Airey, D. W. (1984). *Clays in circular simple shear apparatus*. PhD dissertation, University of Cambridge.

Almeida, J. C. G. R. (1993). *Analytical techniques for the structural evaluation of pavements*. PhD dissertation, University of Nottingham.

Alonso, E. E., Gens, A. & Josa, A. (19900. A constitutive model for partially saturated soils. *Géotechnique* **40**, No. 3, 405–430.

Al-Tabbaa, A. (1987). *Permeability and stress-strain response of Speswhite kaolin*. PhD dissertation. University of Cambridge.

Ashby, M. F. & Jones, D. R. H. (1980). *Engineering materials 1: an introduction to their properties and application*. Oxford: Butterworth-Heinemann.

Atkinson, J. H., Richardson, D. & Robinson, P. J. (1987). Compression and extension of K_0 normally consolidated kaolin clay. *Journal of Geotechnical Engineering*, *ASCE* **113**, No. 12, 1468–1482.

Atkinson, J. H., Richardson, D. & Stallebrass, S. E. (1990). Effect of recent stress history on the stiffness of overconsolidated soil. *Géotechnique* **40**, No. 4, 531–540.

Barksdale, R. D. (1972) Laboratory of rutting in base course materials. *Third International Conference on Structural Design of Asphalt Pavements*, London, pp. 161–174.

Behrens, I. L. C. (1999). Overview of low volume roads: keynote address. *Transportation Research Record* **1652**, Transportation Research Board, Washington, DC, 1–4.

Bishop, A. W. & Henkel, D. J. (1957). *The measurement of soil properties in the triaxial test*. Edward Arnold Ltd.

Bishop, A. W. & Wesley, L. D. (1975). A hydraulic triaxial apparatus for controlled stress path testing. *Géotechnique* **25**, No. 4, 657–670.

Bolton, M. D. (1991a). *A guide to soil mechanics*. MD & K Bolton.

Bolton, M. D. (1991b). Geotechnical stress analysis for bridge abutment design. *Transport and Road Research Laboratory Contractor Report* **270**, London.

Boyce, J. R. (1980). A non-linear model for the elastic behaviour of granular materials under repeated loading. *Proc. Int. Symp. Soils under Cyclic Transient Loading*, Swansea, pp. 285–294.

British Standards Institution (1990). BS 1377: *British Standard Methods of test for soils for civil engineering purposes*. B.S.I., London.

Britto, A. M. & Gunn, M. J. (1987). *Critical state soil mechanics via finite elements*. Chichester: Ellis Horwood.

Brooker, E. W. & Ireland, H. O. (1965). Earth pressures at rest related to stress history. *Canadian Geotechnical Journal* **2**, No. 1, 1–15.

Brown, S. F. & Brunton, J. M. (1986). *An introduction to the analytical design of bituminous pavements*, 3rd edition, University of Nottingham.

Brown, S. F. & Dawson, A. R. (1992). Two-stage mechanistic approach to asphalt pavement design. *Proceedings of the 7th International Conference on Asphalt Pavements* 1, Nottingham, 16–34.

Brown, S. F. & Pappin, J. W. (1981). Analysis of pavements with granular bases. *Transportation Research Record* **810**, Transportation Research Board, Washington, DC, pp. 17–22.

Brown, S. F. (1996). Soil mechanics in pavement engineering. *Géotechnique* **46**, No. 3, 383–426.

Brown, S. F., Lashine, A. K. F. & Hyde, A. F. L. (1975). Repeated load triaxial testing of a silty clay. *Géotechnique* **25**, No. 1, 95–114.

Brown, S. F., Loach, S. C. & O'Reilly, M. P. (1987). Repeated loading of fined grain soils. *Contractor Report* **72**, Transportation Research Laboratory.

Brown, S. F., Tam, W. S. & Brunton, J. M. (1987). Structural evaluation and overlay design: analysis and implementation. *Proc. 6th Int. Conf. Structural Design of Asphalt Pavements*, Ann Arbor, Michigan, **1**, 1013–1028.

Butterfield, R. (1979). A natural compression law for soils. *Géotechnique* **29**, No. 4, 469–480.

Carter, J. R., Booker, J. R. & Wroth, C. P. (1982). A critical state soil model for cyclic loading. *Soil Mechanics – Transient and Cyclic Loads*, eds. G. N. Pande, & O. C. Zienkiewicz, pp. 219–252, John Wiley & Sons Ltd.

Cheung, L. W. (1994). *Laboratory assessment of pavement foundation materials*. PhD dissertation, University of Nottingham.

Clayton, C. R. I, Khatrust, S. A., Bica, A. V. D. & Siddique, A. (1989). The use of hall effect semiconductors in geotechnical instrumentation. *Geotechnical Testing Journal*, ASTM **12**, No. 1, 69–76.

Clayton, C. R. I., Matthews, M. C. & Simons, N. E. (1995). *Site investigation*. Blackwell Sciences Ltd.

Clegg, D. P. (1981). *Model piles in stiff clay*. PhD dissertation, University of Cambridge.

Coop, M. R. (1990). The mechanics of uncemented carbonate sands. *Géotechnique* **40**, No. 4, 607–626.

Dafalias, Y. F. & Herrmann, L. R. (1982). Bounding surface formulation of soil plasticity. *Soil Mechanics – Transient and Cyclic Loads*, eds. G. N. Pande, & O. C. Zienkiewicz, pp. 253–282, John Wiley & Sons Ltd.

Dawson, A. R. & Correia, A. G. (1996). The effects of subgrade clay condition on the structural behaviour of road pavements. *Flexible Pavements*, eds. A. Gomes Correia, Balkema, Rotterdam, pp. 113–120.

Dawson, A. R. & Plaistow, L. C. (1993). Parametric study – flexible pavements. *Proc. European Symposium on Flexible Pavements*. Lisbon, Session 4: Flexible Pavement Design, pp.1–12.

Dawson, A. R. (1997). Rutting in unsurfaced roads - materials and structure interaction effects. *Proc. Symposium on Thinly Surfaced Pavements*, Univ. New Brunswick, Fredericton, Canada, pp. 101–108.

Desai, C. S. (1979). *Elementary finite element method*. Prentice Hall.

GDS Instruments Limited (2002). *GDS Laboratory manual*.

Ghaboussi, J. & Momen, H. (1982). Modelling and analysis of cyclic behaviour of sands. *Soil Mechanics – Transient and Cyclic Loads*, eds. G. N. Pande & O. C. Zienkiewicz, John Wiley & Sons Ltd, pp. 313–342.

Graham, J., Noonan, M. L., & Lew, K. V. (1983). Yield states and stress-strain relationships in a natural plastic clay. *Canadian Geotechnical Journa*l **20**, No. 3, 502–516.

Hardman R., Heaton, B. S., Jordan, P. G. & Abell, R. (1976). The economics of construction traffic on the sub-base of a road pavement. *Laboratory Report* **606**, Transport and road Research Laboratory, Crowthorne.

Hashiguchi, K. (1985). Two- and three-surface models of plasticity. *Proceedings of 5th International Conference on Numerical Methods in Geomechanics, Nagoya*, pp. 285–292.

Hashiguchi, K. (1993). Mechanical requirements and structures of cyclic plasticity models. *International Journal of Plasticity* **9**, 721–748.

Heukelom, W. & Klomp, A. J. G. (1962). Dynamic testing as a means of controlling pavements during and after construction. *Proc. of 1st Int. Conf. On Structural Design of Asphalt Pavements*, Ann Abor, Michigan.

Hicks, R. G. & Monismith, C. L. (1971). Factors influencing the resilient response of granular materials. *Highway Research Record* **345**, Highway Research Board, Washington, DC, pp.15–31.

Highways Agency (1994) *Design manual for roads and bridges: volume 7*. Pavement design and maintenance, HMSO.

Hveem, F. N. & Carmany, R. M. (1948). The factors underlying the rational design of pavements, *Proc. Highway Research Board* **28**, Washington, DC, pp. 101–136.

Hveem, F. N. (1955). Pavement deflections and fatigue failures, *Highway Research Board Bulletin*, No. 114, Washington, DC, pp. 43–87.

Iwan, W. D. (1967). On a class of models for the yield behaviour of continuous and composite systems. *Journal of Applied Mechanics*, ASME **34**, 612–617.

Jâky, J. (1944). A nyugalmi nyomâs tényezöje (The coefficient of earth pressure at rest). *Magyar Mérnök és Epitész-Egylet Közlönye (J. of the Union of Hungarian Engineers and Architects)*, 355–358.

Lagioia, R., Puzrin, A. M. & Potts, D. M. (1996). A new versatile expression for yield and plastic potential surfaces. *Computers and Geotechnics* **19**, No. 3, 171–191.

Lekarp, F. & Dawson, A. R. (1998). Modelling permanent deformation behaviour of unbound granular materials. *Construction and Building Materials* **12**, No. 1, 9–18.

Lekarp, F., Isacsson, U. & Dawson, A. (2000). State of the art I: Resilient response of unbound aggregates. *Journal of Transportation Engineering*, ASCE **126**, No. 1, 66–75.

Li, T. & Meissner, H. (2002). Two-surface plasticity model for cyclic undrained behaviour of clays. *Journal of Geotechnical and Geoenvironmental Engineering*, ASCE **128**, No. 7, 613–626.

Little, P. H. (1993). *The design of unsurfaced roads using geosynthetics*. PhD dissertation, University of Nottingham.

Manson, S. M. (1980). An investigation of the strength and consolidation properties of speswhite kaolin. Cambridge University Engineering Tripos, Part II Research Project Report.

Martin, C. M. & Houlsby, G. T. (2000). Combined loading of spudcan foundations on clay: laboratory tests. *Géotechnique* **50**, No. 4, 325–338.

Matsuoka, H. & Nakai, T. (1974). Stress deformation and strength characteristics of soil under three different principal stresses. *Proceedings of Japanese Society of Civil Engineering* **232**, 59–70.

Mayne, P.W. and Kulhawy, F.H. (1982). K_o–OCR relationships in soil. *Journal of the Geotechnical Engineering Division*, ASCE **108**, 851–872.

McDowell, G. R. & Bolton, M. D. (1998). On the micromechanics of crushable aggregates. *Géotechnique* **48**, No. 5, 667–679.

McDowell, G. R. (2000). A family of yield loci based on micro mechanics. *Soils and Foundations* **40**, No. 6, 133–137.

McDowell, G. R. (2002). A simple non-associated flow model for sand. *Granular Matter* **4**, 65–69.

McDowell, G. R. & Hau, K. W. (2003). A simple non-associated three-surface kinematic hardening model. *Géotechnique* **53**, No. 4, 433–437.

Menzies, B. K., (1988). A computer controlled hydraulic triaxial testing system. *Advanced Triaxial Testing of Soil and Rock*, American Society for Testing and Materials, pp. 82–94.

Mróz, Z. (1967). On the description of anisotropic workhardening. *Journal of the Mechanics and Physics of Solids* **15**, 163–175.

Mróz, Z., Norris, V.A. & Zienkiewicz, O. C. (1979). Application of an anisotropic hardening model in the analysis of elasto-plastic deformation of soils. *Géotechnique* **29**, No. 1, 1–37.

Nova, R. (1982). A constitutive model for soil under monotonic and cyclic loading. *Soil Mechanics – Transient and Cyclic Loads*, eds. G. N. Pande & O. C. Zienkiewicz, John Wiley & Sons Ltd, pp. 343–373.

Ohmaki, S. (1982). Stress-strain behaviour of anisotropically, normally consolidated cohesive soil. 1st International Symposium on Numerical Models in Geomechanics, Zurich, pp. 260–269.

Pappin, J. W. (1979). *Characteristics of a granular material for pavement design*. PhD dissertation, University of Nottingham.

Pender, M. J., (1982). A model for the cyclic loading of overconsolidated soil. *Soil Mechanics – Transient and Cyclic Loads*, eds. G. N. Pande & O. C. Zienkiewicz, John Wiley & Sons Ltd, pp. 283–311.

Porter, O.J. (1938). The preparation of subgrades. *Proc. Highway Research Board* **18**, No.2, Washington, DC, 324–331.

Potts, D. M. & Gens, A. (1984). The effect of the plastic potential in boundary value problems involving plane strain deformation. *International Journal of Numerical and Analytical Methods in Geomechanics* **8**, 341–354.

Potts, D. M. & Zdravković, L. (1999). *Finite element analysis in geotechnical engineering: theory*. London: Thomas Telford.

Powell, W. D., Potter, J. F., Mayhew, H. C. & Nunn, M. E. (1984). The structural design of bituminous roads, *Transport and Road Research Laboratory* **1132**.

Prévost, J. H. (1977). Mathematical modelling of monotonic and cyclic undrained clay behaviour. *International Journal for Numerical and Analytical Methods in Geomechanics* **1**, 195–216.

Prévost, J. H. (1978). Anisotropic undrained stress-strain behaviour of clays. *Journal of the Geotechnical Engineering Division*, ASCE **104**, 1075–1090.

Prŭska, M. J. (1973). Efect of initial stress on the stress-strain relation. *Proc. 8th Int. Conf. Soil Mechanics Foundation Engineering*, Moscow **4**, 26–28.

Ramsamooj, D. V. & Alwash, A. J. (1990). Model prediction of cyclic response of soils. *Journal of Geotechnical Engineering*, ASCE **116**, No. 7, 1053–1072.

Ramsamooj, D. V. & Piper, R. (1992). Theoretical prediction of rutting in flexible pavement subgrades. *Canadian Geotechnical Journal* **29**, 795–778.

Roscoe, K. H. & Burland, J. B. (1968). On the generalised stress-strain behaviour of 'wet' clay, In *Engineering Plasticity* (eds J. Heyman & F. A. Leckie), pp. 535–609.

Roscoe, K. H., Schofield, A. N. & Thurairajah, A. (1963). Yielding of clays in states wetter than critical. *Géotechnique* **13**, No. 3, 211–240.

Sangrey, D. A., Henkel, D. J. & Esrig, M. I. (1969). The effective stress response of a saturated clay soil to repeated loading. *Canadian Geotechnical Journal* **6**, 241–252.

Sasitharan, S., Robertson, P. K., Sego, D. C. & Morgenstern, N. R. (1994). State-boundary surface for very loose sand and its practical implications. *Canadian Geotechnical Journal* **31**, 321–334.

Schmidt, B. (1966). Discussion of 'Earth pressures at rest related to stress history' by Brooker and Ireland (1965). *Canadian Geotechnical Journal* **3**, No.4, 239–242.

Schmidt, B. (1983). Discussion of 'K_o-OCR relationships in soil' by Mayne and Kulhawy (1982). *Journal of the Geotechnical Engineering Division*, ASCE **109**, No. 6, 866–867.

Seed, H. B., Chan, C. K. & Lee, C. E. (1962). Resilience characteristics of subgrade soils and their relation to fatigue failures, *Proc. Int. Conf. Structural Design of Asphalt Pavements*, Ann Abor, Michigan, pp. 611–636.

Seed, H. B., Chan, C. K. & Monismith, C. L. (1955). Effects of repeated loading on the strength and deformation of compacted clay, *Proc. Highway Research Board* **34**, Washington, DC, 541–558.

Shell International Petroleum Company (1978). *Shell pavement design manual: asphalt pavements and overlays for road traffic*. London: Shell International Petroleum Company.

Sheng, D., Sloan, S.W. and Yu, H.S. (2000). Aspects of finite element implementation of critical state models. *Computational mechanics* **26**, 185–196.

Simpson, B. (1992). Retaining structures: displacement and design. *Géotechnique* **42**, No. 4, 541–576.

Stallebrass, S. E. & Taylor, R. N. (1997). The development and evaluation of a constitutive model for the prediction of ground movements in overconsolidated clay. *Géotechnique* **47**, No. 2, 235–253.

Stallebrass, S. E. (1990). *The effect of recent stress history on the deformation of overconsolidated soils*. PhD dissertation, City University.

Sweere, G. T. H. (1990). *Unbound granular bases for roads*. PhD dissertation, Delft University of Technology.

Viggiani, G. & Atkinson, J. H. (1995). Stiffness of fine-grained soil at very small strains. *Géotechnique* **45**, No. 2, 249–265.

Wood, D. M. (1990). *Soil behaviour and critical state soil mechanics*. Cambridge University Press.

Wroth, C. P. & Houlsby, G. T. (1985). Soil mechanics – property characterisation and analysis procedures. *XI Int. Conf. Soil Mechanics and Foundation Engineering*, San Francisco, pp. 1–55.

Yu, H. S. (1998). A unified state parameter model for a clay and sand. *International Journal for Numerical and Analytical Methods in Geomechanics* **22**, 621–653.

Yu, H. S. & Khong, C. D. (2002). Application of a unified plasticity model in finite element analysis. *Proceedings of 3rd International Symposium on 3D Finite Element for Pavement Analysis, Design and Research*, Amsterdam, pp. 253–267.